TUM School of
Computation, Information and Technology

Towards a Better Climate: Novel Measurement and Modeling Approaches for Quantifying Greenhouse Gases and Air Pollutants in Cities

Florian Dietrich

Vollständiger Abdruck der von der TUM School of Computation, Information and Technology der Technischen Universität München zur Erlangung des akademischen Grades eines

Doktors der Ingenieurwissenschaften

genehmigten Dissertation.

Vorsitzender:		Prof. Dr.-Ing. Thomas Eibert
Prüfende:	1.	Prof. Dr.-Ing. Jia Chen
	2.	Prof. Frank Keutsch, Ph.D. (Harvard University)

Die Dissertation wurde am 10. Januar 2022 bei der Technischen Universität München eingereicht und durch die TUM School of Computation, Information and Technology am 2. August 2022 angenommen.

Contents

1. Introduction

This work is about the hardware and software development of a sensor system including a modeling framework for automated and permanent quantification of urban greenhouse gas emissions. Together with considerations for the transition of energy sources for end-use appliances, opportunities for saving global carbon emissions are identified. In addition, air quality is also being investigated. This includes the development of a smart and compact sensor system and mobile measurement campaigns.

1.1. Motivation

Hardly any other topic has concerned people around the world and for many years as much as climate change and air pollution. Melting glaciers, rising sea levels, and the accumulation of severe weather events are just some of the visible effects. The overwhelming majority of climate and environmental researchers worldwide agree that without significant reductions in greenhouse gas and pollutant emissions, we can expect more far-reaching consequences for the climate and life on our planet [1]. Among the greenhouse gases released by human activities, carbon dioxide (CO_2) and methane (CH_4) play the largest role. Among air pollutants, nitrogen oxides (NO_X) and particulate matter (PM) are of particular scientific interest, as these pollutants have a very negative impact on human health [2].

In order to improve the current situation, suitable reduction measures must be introduced. To ensure that efficient and at the same time economically reasonable measures are taken, a precise knowledge of the sources of pollutant emissions is essential. Both the localization and the quantification of the emission source are equally relevant. However, these data are currently not available to the necessary extent or are subject to high uncertainties. This is mainly due to the fact that it is very difficult to effectively measure emissions from large area sources, such as cities, or line sources, such as roads. Instead, these data are merely modeled, creating large uncertainties in the results.

1.2. State of the Art

To improve the quantification of greenhouse gas emissions and air pollutant concentrations, many studies around the world have focused on determining these values using various measurement and modeling approaches.

1.2.1. Greenhouse Gas Measurements

Today, national greenhouse gas emission inventories under the UNFCCC (United Nations Framework Convention on Climate Change) are mandatory for governments around the world if they have signed climate treaties such as the Kyoto Protocol or the Paris Agreement. To this end, the IPCC (Intergovernmental Panel on Climate Change) has developed a methodology that must be used for such national greenhouse gas emissions inventories. This methodology was published in 2006 [3] and refined in 2019 [4] and essentially calculates emissions by multiplying activity data by emission factors. The reason for this approach is that it allows the quantification of greenhouse gas emissions anywhere in the world, regardless of the technical conditions of individual countries. Therefore, the IPCC approach guarantees a simple calculation of urban greenhouse gas emissions and theoretically a good comparability between cities, since the calculations are based on the same standard. However, unknown emitters that are not yet included in emission inventories often lead to underestimation of urban emissions [5], [6]. Since there is currently no suitable measurement approach for greenhouse gas emissions from large-scale sources that can be used to calculate emission inventories, it makes scientific sense to develop new measurement approaches for greenhouse gas emissions in order to verify these inventories with real measurements.

In this thesis, two different types of measurement methods for urban greenhouse gas emissions are used for this purpose, namely in-situ measurements and remote sensing methods.

In Situ Measurements

In the so-called in situ measurements, the point concentration of a specific gas is determined by taking an air sample and analyzing it, e.g. in a chamber inside the instrument. For greenhouse gases, these instruments mostly operate optically in the near-infrared spectrum.

In situ studies include mobile surveys, where vehicles are equipped with high-precision in situ instruments, such as cavity ring-down spectrometers, to detect street-level CH_4 concentrations released from leaking natural gas plants and pipelines [7]–[13]. In situ instruments are also used for airborne measurements with research aircraft or helicopters [14]. To quantify methane emissions of natural gas based

facilities, the downwind tracer flux approach is often utilized [15]–[18]. In contrast to these temporary measurements principles that are especially suitable for quantifying natural gas systems, where the location is known, stationary sensor networks are more particularly suitable for monitoring heterogeneous sources, such as entire cities. In recent years, several city networks have been established to improve emission monitoring. These include networks using in situ high-precision instruments [6], [19]–[21] and low-cost sensor networks deploying non-dispersive infrared sensors [22], [23]. In addition, eddy covariance flux tower measurements are used for directly inferring city fluxes [24], [25].

To attribute the source and determine the leakage rate, either isotopic signatures of the gas are measured [26]–[33], the ethane to methane ratio is determined, because ethane is a unique tracer for fossil fuel related methane emissions, or both methods are used simultaneously [13], [34]–[38].

However, all these approaches include some challenges in measuring urban emission fluxes, such as high sensitivity to the boundary layer height dynamics, large variations due to mesoscale transport phenomena or the fact that they can only capture the fluxes of a rather small area. Therefore, this work also focuses on remote sensing methods, which have some advantages over in situ approaches.

Remote Sensing Approaches

To overcome the shortcomings of in situ measurements of greenhouse gas concentrations for emission estimates, remote sensing methods have been used for several years. Here, remote sensing means measuring the concentration of a large column of air between the optical measurement device and a distant light source, rather than just determining a point concentration, as it is usually done with state-of-the-art in situ sensors. This adds an extra dimension to the concentration measurement. By using the sun as a light source, it is even possible to determine the concentration of an entire atmospheric air column. This is done either directly with instruments on the Earth's surface, called ground-based remote sensing, or indirectly by measuring the sunlight reflected from the Earth using satellites such as OCO-2 [39]–[41] or GOSAT [42]–[44]. In both approaches, the solar spectrum is optically analyzed to determine the column-averaged concentrations by analyzing the attenuation of the characteristic wavelengths of the respective gas, which are in the near-infrared range for greenhouse gases. The main difference of spaceborn to ground-based remote sensing are the signal-to-noise ratio (SNR) and spatial coverage. Since ground-based remote sensing uses direct sunlight, the SNR is much higher than that of the spaceborn method, which analyzes only reflected sunlight. This allows more precise measurements for ground-based instruments. In addition, the temporal resolution of this approach is much better, since satellites such as OCO-2 only target the same

location about every 16 days [45]. However, satellites measure concentrations on a global scale, which is not possible with fixed ground-based instruments. Depending on the objective, one approach or the other may be more appropriate.

The Total Carbon Column Observing Network (TCCON, [46]) is a global sensor network that measures column-averaged greenhouse gas concentrations using ground-based remote sensing. For this purpose, TCCON uses IFS 125HR spectrometers from Bruker Optics (resolution: $0.02\,\mathrm{cm}^{-1}$), each housed in a shipping container. While such stations are suitable for monitoring global trends in greenhouse gas concentrations in the atmosphere, they are not very suitable for urban or even mobile applications. For this purpose, the Karlsruhe Institute of Technology (KIT), in collaboration with Bruker Optics, has developed a compact and portable version of the spectrometer, called EM27/SUN. Similar to the IFS 125HR, the EM27/SUN is a Fourier transform infrared (FTIR) spectrometer, but in tabletop size and with a spectral resolution of 0.5 cm^{-1} [47]–[49]. This portable format has led to several new applications, such as city campaigns, mobile deployment, and the Collaborative Carbon Column Observing Network (COCCON, [50], [51]), which is complementary to TCCON but with a larger number of spectrometers resulting in a higher spatial resolution.

Concentration gradients measured between the upwind and downwind of an emission source are particularly suitable for the determination of greenhouse gas emissions with FTIR spectrometers, since the dynamics of the boundary layer and the surface emission fluxes emitted upwind of the source are thereby cancelled out. This so-called differential column measurements (DCM) with EM27/SUN instruments has an accuracy of 0.01% for column-averaged CO_2 and CH_4 when averaged over 10 minutes [52]. Because of its very high accuracy, this method has been widely used for urban and local source emission studies using mass balances or other modeling techniques.

Using measurements from five EM27/SUNs measured in a 2014 campaign in Berlin, emissions of CO_2 and CH_4 were modeled using a simple dispersion model [53], [54]. A similar sensor configuration was used to measure greenhouse gas emissions from the Paris metropolitan area in spring 2015. In combination with the CHIMERE-CAMS model, these measurements show that the measured concentration enhancements are mainly due to fossil fuel emissions [55]. In St. Petersburg, a measurement campaign using two EM27/SUN instruments was conducted in 2019 to determine emissions from the Russian megacity using a mass balance approach [56].

In addition to these urban studies, column measurements are also used to study local sources, such as CH_4 emission fluxes from a dairy farm in Chino, California [52], [57], and to validate CH_4 inventory emissions from the largest gas-fired power plant in Munich, Germany, using a computational fluid dynamics (CFD) model

based on measurements from two EM27/SUNs [58]. Mobile setups have also been used to study volcanic emissions from Mount Etna [59], and column measurements from satellites over the ocean were validated using an EM27/SUN deployed on a research vessel [60].

However, these studies are all based on campaign mode and are not suitable for permanent monitoring of urban greenhouse gas emissions. Therefore, a main objective of this work is to establish a fully automated urban sensor network for permanent measurement of greenhouse gas concentrations.

Emission Modeling

An atmospheric transport model is required to evaluate the emissions based on the measured concentrations. Such transport models are driven either by wind measurements or wind models to simulate the trajectories of gas molecules. Simple models such as the box model, the column model [61], or the Gaussian plume model [62]–[64] work only under steady wind conditions and are therefore suitable mainly for rough emission estimates. More sophisticated models simulate the trajectories either on a statistical basis, such as the Stochastic Time-Inverted Lagrangian Transport (STILT) model [65], [66], or using turbulent flow simulations, such as Reynolds-averaged Navier-Stokes (RANS) or large-eddy simulation (LES) models, to obtain a 3-dimensional wind field.

Based on these modeled wind fields, inverse modeling approaches are used to locate and quantify emission sources. Current approaches for determining greenhouse gas emissions include Bayesian inversion [67], which requires a probability distribution known as a priori. This means that the spatial distribution of emissions must be estimated before the model run can be started. However, this leads to problems if the sources are significantly misquantified or even unknown, as the model will then make a systematic error. In addition to Bayesian inversion, sparse reconstruction is another option for emission quantification [68]. The advantage of sparse reconstruction is that instead of a pre-known emission field, all that is required is that the emissions are sparse. Sparse in this case means that only a few large emitters contribute significantly to the total emissions and all other emitters can be set to zero without making a significant error in the total emissions. This approach has the great advantage of identifying previously unknown emission sources.

1.2.2. Air Quality Measurements

In contrast to greenhouse gases, concentration levels are of greater interest than emissions for air pollutants, since too high concentrations directly affect human health [2]. Therefore, mostly in situ approaches are usually used for air pollutants. Since

governments are obliged to actually measure air quality parameters, such sensor systems are already well established. In fact, each European agglomeration, meaning an urban area with more than 250k inhabitants, needs to assess their air quality according to the European directive 2008/50/EC. In Germany, government air quality monitoring stations must comply with the 39th Federal Immission Control Ordinance ("Bundes-Immissionsschutzverodnung", BImSchV). This ordinance specifies important parameters for air quality monitoring, such as concentration thresholds, the areas in which air quality must be measured, and the type of reference methods permitted for measuring concentrations [69].

Since these official measurement devices must fulfill the precision and accuracy requirements of the 39th BImSchV, they are large, expensive and difficult to maintain. Therefore, only a few stationary air quality stations are needed and operated per city. For example, in Munich there are only five stations, leading to the problem that air quality is only well known at a few hotspots, but there is a lack of information on the spatial distribution [70]. Therefore, it is currently not possible to determine the actual human exposure to these air pollutants, which would be beneficial for setting appropriate thresholds and mitigation measures. In addition, with such low spatial resolution, unknown or falsely quantified emitters cannot be located.

To overcome the problem of low spatial resolution, several researchers have developed novel measurement techniques that can be broadly divided into two groups: high-precision instruments in a mobile configuration and spatially dense, low-cost sensor networks.

In Salt Lake City, Utah, high-precision instruments are mounted on the roof of two electric light rail trains, recording air quality parameters such as NO_2, O_3, and PM2.5, in addition to greenhouse gases such as CO_2 and CH_4. The trains measured over a period of more than two years, resulting in 760 measurement days and covering several different parts of the city [71]. Other air quality sensors attached to public transportation can be found in Karlsruhe, Germany [72] or Zurich, Switzerland [73].

Such mobile setups allow higher spatial resolution, but have the disadvantage of lower temporal resolution because the sensor is constantly moving. Low-cost sensor networks are therefore another approach. Here, a large number of low-cost sensor systems are combined with sophisticated modeling and calibration approaches to obtain both high spatial and temporal resolution of air quality parameters with an accuracy lower than that of high-precision instruments, but high enough to make scientifically sound conclusions. For such sensor networks, it is often necessary to develop a new sensor system, since these low-cost sensors usually require a weatherproof and climate-controlled environment to function properly. Such efforts have been made in Zurich, Switzerland [74], Oslo, Norway [75], London, United Kingdom [76], and San Francisco, California [22], each of which has such a low-cost sensor network.

1.3. Goals

The goal of this thesis is to overcome some of the existing shortcomings in measuring and modeling greenhouse gas emissions and air pollutant concentrations. For that purpose, suitable measurement systems in combination with a modeling framework that can measure greenhouse gas emissions in a scientifically accurate yet economically feasible manner is developed. In particular, this work focuses on measurements in cities, as they account for 70% CO_2 emissions from fossil fuel [77]. Besides CO_2, this work focuses particularly on the greenhouse gas CH_4, which is the second largest anthropogenic driver of global warming, with a global warming potential approximately 86 times larger than that of CO_2 averaged over 20 years [1]. As natural gas is increasingly used as a bridging technology in power generation, because it is considered more climate friendly than coal [78]–[81], CH_4 emissions will increase over-proportionally if natural gas is released into the atmosphere unburned. Thus, it is important to continuously monitor gas leakage both in the pipeline system and in end-use appliances to avoid a final negative carbon footprint due to the increased use of natural gas as an energy source. Since the lifetime of CH_4 is much shorter than that of CO_2, positive effects for the climate can be achieved much faster. Recent studies have shown that the goals set in the Paris Agreement can only be achieved if CH_4 emissions are drastically reduced [82]. Detecting previously unknown CH_4 emissions is the basis for creating appropriate reduction measures and thus represents a fast-acting measure in the fight against global warming.

Therefore, one of the main aspects of this work is the development of appropriate hardware, software, and a modeling framework to locate and quantify urban CH_4 and CO_2 sources. This should drastically reduce the large uncertainties that currently exist in estimates of greenhouse gas emissions. In addition, this work also focuses on whether and to what extent replacing gas-powered cooking and heating appliances with electric ones can reduce global carbon emissions.

Since greenhouse gas emitters often co-emit air pollutants, this thesis also addresses the quantification of air pollutant concentrations. This includes the development of a smart and compact air quality sensor system based on low-cost sensors to dramatically increase the spatial resolution of existing government air quality monitoring networks. Appropriate calibration and modeling approaches should be used to produce a spatially dense yet accurate air quality map. In addition, a dense air quality sensor network can also be used to classify and accurately locate greenhouse gas emission sources, as different emitters emit different types and proportions of air pollutants.

2. Materials and Methods

Since various gases on different scales are investigated in this thesis, several methods have to be applied, which are presented in the following chapter. For greenhouse gases, ground-based and spaceborne remote sensing and in-situ measurements are applied, for air pollutants exclusively in-situ methods are used.

2.1. Ground-Based Remote Sensing

One main focus of this thesis is the determination of greenhouse gas emissions in an urban area. For this purpose, ground-based remote sensing is chosen as the main measurement method due to the aforementioned advantages of this technique. In addition to the development of a fully automated sensor system, measurement campaigns are conducted and a suitable modeling framework for emission quantification is developed.

2.1.1. Sensor Systems

Ground-based remote sensing using EM27/SUN instruments is an established approach for measuring column-averaged greenhouse gas concentrations and has been used for several years in campaign mode. However, the EM27/SUN is not weatherproof and therefore cannot be used for fully automated operation of a permanent network. Instead, human operators are used for each spectrometer to start, monitor, and stop measurements depending on weather conditions. Therefore, an automated enclosure system had to be developed to protect the sensitive spectrometers from harsh weather conditions such as rain, snow, hail, and large temperature variations. Based on initial developments [83], [84], one of the main parts of this thesis is to develop a fully automated enclosure system that can be used to build a permanent urban greenhouse gas sensor network based on ground-based remote sensing (see Figure 2.1, left). This includes the tasks listed in the following paragraphs.

Improving the PLC Control Software

The PLC (Programmable Logic Controller) controls all peripheral devices within the enclosure. As the most fail-safe device, it should ensure that all other devices are

functioning properly. If not, it will start automatic error handling and, if necessary, send a notification to an operator if the error handling fails. The existing PLC software [84] is extended for this purpose.

All devices inside the enclosure that do not send pure binary signals, such as the PLC, the PC, the router, the surveillance camera and the UPS (uninterruptible power supply) are connected either via Ethernet or USB. The PLC checks the connection to all these devices by pinging them periodically. When a device stops responding, the PLC attempts to restart the respective device by briefly disconnecting it using relays.

Furthermore, the algorithm for controlling the position of the rain cover and ensuring fail-safe error handling is improved. For this purpose, a state machine is developed to ensure proper operation, i.e., the cover always closes when necessary, regardless of external circumstances, or at least sends a notification to an operator if this is not possible in situations such as a broken motor or cable. In addition, the values of all relevant sensors are continuously recorded in an ASCII file to allow debugging in case of a failure. [85]

Vision-Based Direct Solar Radiation Sensor

In previous versions of the enclosure [83], [84], one of the main issues to enable fully automated operation was the lack of a sensor to detect suitable weather conditions for measurements. So far, only a rain sensor has been installed. However, additional information is needed whether the sun is shining or not, since the EM27/SUN can only analyze the solar spectrum when direct sunlight hits the detector.

Existing and self-developed global radiation sensors have all had the difficulty of producing a sensor signal that reliably indicates whether direct sunlight is actually present or whether it is just very bright. Since a bright environment alone is not sufficient for EM27/SUN measurements, but direct sunlight is required, a direct sunlight sensor is needed. However, the existing state-of-the-art direct solar radiation detectors are very large and expensive and contain mechanical components that require maintenance. Therefore, a customized detector is to be developed [85] that does not have these disadvantages.

As a basic principle, a differential approach is used, which is based on computer vision. An artificial object partially shades a projection surface on which the camera is focused. Depending on the direct sunlight, the contrast between shaded and unshaded area changes. The hardware is designed in such a way that a CMOS USB camera looks from below onto a translucent projection surface, which is protected from environmental influences by a transparent dome attached to the top. This dome is covered with some opaque strips to create the necessary shadows (see Figure 2.1, right). The contrast threshold above which such contours indicate whether

Figure 2.1.: Photos of the enclosure system: Left: enclosure system at sunrise on the roof of a school in Taufkirchen, Germany. Right: Close-up of the direct solar radiation sensor.

it is sunny enough to measure is determined empirically by comparing the sensor's contrast values for direct sunlight with the results of the retrieval algorithm described in the next section. [85]–[87]

Fully-Automated Data Processing Chain

A fully automated sensor network generates a huge amount of data that needs to be processed. Therefore, it is important that in addition to the automated measurements, the data processing chain is also automated. For this purpose, a workflow is set up that connects all systems required to transmit, process, store and display the measured concentration data.

On each enclosure system, the measured interferograms are stored as binary files on the local hard disk of the Microsoft Windows PC required to control the EM27/SUN. Data of up to 5 GB is stored per day and instrument. At the end of each measurement day, the PC connects to a Linux cloud at the Leibniz Supercomputing Center (LRZ) via an SSH connection to transfer the interferograms measured by the EM27/SUN and the pressure data recorded by the data logger to the computing cloud. To save local storage space and prevent an operator from having to maintain the storage on each enclosure's local hard drive, the local data is deleted after successful transfer. A cronjob on the Linux cloud checks each night to see if new measurements can be processed using the retrieval algorithm based on GGG2014 [88]. It uses the standard TCCON parameters, but the spectral windows for retrieving different gas species are slightly modified according to the EGI setup [89]. After successful retrieval, the raw data are moved to an LRZ DSS (Data Science Storage)

container for long-term data backup. The retrieved raw concentrations are stored centrally in a MySQL database hosted on the same Linux cloud.

For further data analysis, the concentration data are filtered according to a sophisticated algorithm to reduce the noise of the signal and remove outliers that do not represent the actual concentration values measured at that time. Furthermore, inter-instrument deviations are reduced by applying calibration factors determined in side-by-side measurements performed on a regular basis. In addition, data are resampled over time to allow easier analysis and comparison of measured data from different stations [85], [90], [91]. After converting the filtered data into a JSON file and uploading it to a web server, the data can be viewed publicly online at https://atmosphere.ei.tum.de [91].

Pyra - the Software to Automate EM27/SUN Measurements

To start EM27/SUN measurements, two programs, namely OPUS and CamTracker from Bruker Optics, are needed to align the solar tracker, make all necessary spectrometer settings and start the measurements. These programs usually have to be started manually by an operator, which prevents fully automatic operation. As an initial step, a first version of Pyra was developed prior to this work [92], which allows to start and stop these two spectrometer programs via a single interface. Furthermore, a possibility to automatically stop the measurements at a certain point in time was created. However, for full automation, Pyra still needs to be extended by some functions and the error handling needs to be improved, such as automatically continuing the measurements after the solar tracker has lost the sun or a function has crashed [85]–[87].

Since there should be only one control interface, the PLC control interface [84] is included in Pyra. This allows an operator to observe all important signals at the same time. It also makes the automation software more reliable, since the signals do not have to be transferred between different programs, but can be processed internally. In addition, the newly developed sensor for direct sunlight is also included in Pyra. This includes all data processing of this sensor, resulting in a binary output signal indicating whether there is sufficient sun to measure. Finally, Pyra's logging is been improved to allow better troubleshooting in case of failures by logging more events than before and separating log files on a daily basis. [85]–[87]

Special Enclosure Versions

As more and more external researchers and institutes showed interest in using these enclosure systems, the demands on the systems increased. We decided to design and build improved versions of our enclosure systems for two very extreme applications. The first is built for KIT to support measurements in Sodankylä, Finland, which

is located north of the polar circle, resulting in very cold temperatures and very low solar angles [93]. To this end, expanded heating capacities were incorporated and the rain cover design was modified to allow for a wider range of solar azimuth angles. The second enclosure is designed for the University of Leicester to provide the first measurements of CH_4 emissions from wetlands in East Africa in Jinja, Uganda [94]–[96]. There, near the equator, the high relative humidity combined with very large solar elevation angles are challenges to overcome. In addition to tilting the entire enclosure using car jacks to allow measurements when the sun is at its zenith, thermoelectric coolers were installed to lower the temperature inside the enclosure and condense water vapor to reduce system humidity [85].

2.1.2. Measurement Campaigns

Since automated enclosure systems for EM27/SUN instruments did not exist prior to this work, time-limited measurement campaigns have been used to determine greenhouse gas emissions from large-scale sources such as cities [53]–[55], [97]. Therefore, such campaigns are an important part of this thesis to test the enclosure systems and prepare them for fully automated continuous operation. Due to the high cost of the EM27/SUN, such measurement campaigns are usually a collaboration of several international institutes that lend their instruments to each other.

Munich Campaign - August 2018

The campaign in Munich in August 2018 [98] represents the world's first urban greenhouse gas measurement campaign based on ground-based remote sensing, where all spectrometers used are protected in automated enclosure systems [99]. All five systems are connected to the Internet so they can be controlled remotely. Once set up, there is no need for human operators to be at the sensor sites at all times, so the operational effort is limited to one operator starting and monitoring the measurements remotely. This setup allows many more data points to be collected than in previous campaigns, particularly through early morning, late evening, and weekend measurements.

Oktoberfest Campaign 2018

In September and October 2018, investigations on methane emissions are carried out at the Munich Oktoberfest. In addition to in situ measurements (see Section 2.3), two automated EM27/SUN enclosure systems are deployed upwind and downwind of the festival site [100]–[102]. The systems are located on rooftops less than one kilometer from the festival site. By analyzing the concentration gradients of these two devices, the emissions from the festival should be derived. Since wind conditions

are not constant during the 16 days of the festival, the systems are moved several times depending on the weather forecast to allow for an optimal upwind-downwind configuration.

Oktoberfest Campaign 2019

Further improvements to the enclosure systems, such as equipping each system with an in-house developed direct sunlight sensor, result in five fully automated systems ready for permanent operation in Munich. Combined with five institute-owned EM27/SUNs, the 2019 Oktoberfest campaign is also the launch of the permanent Munich greenhouse gas sensor network called MUCCnet (Munich Urban Carbon Column network) [85], [101], [103]–[108]. MUCCnet is the world's first fully automated and permanent greenhouse gas sensor network based on ground-based remote sensing, providing a unique observation of urban greenhouse gas emission trends in Munich.

Hamburg Campaign - August 2021

Although MUCCnet is designed as a permanent and long-term sensor network, it makes sense from a scientific perspective to deploy the unique sensor hardware in other cities to learn about greenhouse gas metabolism in different locations. Therefore, four of the MUCCnet stations are brought to Hamburg in August 2021 to study greenhouse gas emissions there [109], [110]. Especially in terms of developing a modeling framework, such new data is very helpful to build a universal model that can be applied to any city in the world. Therefore, further campaigns are planned in the near future, e.g. in Vienna, Austria, and Upper Silesia, Poland.

2.1.3. Emission Estimate - Inverse Modeling

Since the results from ground-based remote sensing systems are column-averaged concentrations only, an atmospheric modeling framework is needed to convert these measurements into emission fluxes that are the desired end result. In this thesis, two different approaches for inverse modeling are used, namely Bayesian inversion and sparse reconstruction.

Bayesian Inversion

In the Bayesian inversion approach used, a prior emission distribution is assumed and then scaled according to the observations of the EM27/SUNs. For the emission prior, the TNO GHGco v1.1 inventory [111] is used, which is a $1\,\mathrm{km} \times 1\,\mathrm{km}$-gridded inventory of the greenhouse gases CO_2, CH_4, and CO. It is currently available for

Central Europe. The transport model used is the Stochastic Time-Inverted Lagrangian Transport (STILT) model [65], [66] to calculate the sensitivity of the total column observations recorded by the EM27/SUNs for each grid cell modeled. The unique feature of this inversion is that not only the emissions but also the background concentrations are optimized. To calculate the scaling factors for both the emissions and background concentrations, a cost function is minimized that includes the transport model, the concentration measurements, and the prior emission and background distributions. To avoid the inverse problem being underdetermined, emissions are assumed to be constant over a period of time so that concentration measurements from multiple time steps within that period can be used to determine the scaling factors. The inversion framework was originally developed for an EM27/SUN campaign in Indianapolis, USA, [97] and is adapted accordingly to the Munich case [103], [105]. Since the MUCCnet dataset is probably the world's largest urban ground-based remote sensing dataset, it is ideally suited for the development and improvement of such a Bayesian inverse modeling framework.

Particularly for such Bayesian inversion models, the prior background concentrations are very important to obtain a reliable emission number. Otherwise, the results will be biased towards these incorrectly assumed background concentrations. Current approaches either use constant background concentrations based on averaged atmospheric gas concentrations [97], or take measurements from upwind stations [6] as the prior background concentration. However, the latter approach does not take into account the time it takes for the gas to travel between upwind and downwind stations, resulting in an incorrect background assumption. Therefore, a background approach is developed based on the measurements at all five stations. The total background concentrations are thereby divided into two parts, namely the near-surface background and the atmospheric background. In this way, large daily concentration variations affecting all sites simultaneously (atmospheric background) can be subtracted before the inversion run, resulting in a better SNR of the concentration enhancements caused by urban emitters. [85], [90]

Sparse Reconstruction

To avoid the need for a prior emission distribution, which makes finding unknown emission sources difficult, a second inverse modeling approach is developed based on sparse reconstruction. In this approach, no prior emission map is required. Instead, the emission map is assumed to be sparse. Although the real emission signal is not necessarily sparse, this approach offers a variety of new possibilities for emission estimation. Furthermore, emission maps can be made sparse by transforming them to another domain, as is the case with wavelet transformation in image compression [112]. Subsequently, the unknown emitters can be located and quantified using

sparse reconstruction. Several theoretical case studies in European cities are used to investigate the general feasibility of sparse reconstruction for quantifying urban greenhouse gas emissions. [113]

2.2. Satellite Remote Sensing

In addition to ground-based remote sensing, remote sensing from space is also addressed in this thesis. Measurements from MUCCnet are used to validate the concentration gradients measured by NASA's OCO-2 satellite [114]. Furthermore, OCO-2 data recorded over the Nile Delta in Egypt are analyzed in more detail to estimate anthropogenic CO_2 emissions from this large river delta.

Five years of measurement data from the OCO-2 Level 2 Version 9 Lite product are used to determine CO_2 emissions from the Nile Delta. The Nile Delta represents an interesting study region because it is isolated between deserts and the Mediterranean Sea. Therefore, concentrations measured in the delta are not overlaid by signals caused by upwind emission sources, which means that background concentrations can be easily determined. In addition, there are many anthropogenic emissions in the delta caused by agricultural activities and urbanization, which have hardly been quantified so far. [115]

To quantify the emissions, the concentration gradients measured by the OCO-2 satellite between the river delta and the desert are determined and then compared to modeled concentration enhancements. The model used is a forward model that multiplies the gridded emissions inventory (EDGAR v5.0 [116] and ODIAC v2019 [117]) with STILT-generated footprints driven by ERA5 wind model data [65], [66]. By comparing modeled and measured XCO_2 values at specific receptor locations, scaling factors between modeled and measured CO_2 emissions can be determined. [115]

2.3. In Situ Greenhouse Gas Measurements

While remote sensing offers many advantages for quantifying large-scale sources, the coarse wind fields used for the transport model combined with model uncertainties make it very difficult to study smaller sources in detail. Therefore, it makes sense to additionally use in situ measurements to more accurately locate and quantify potential sources found by remote sensing.

After a remote sensing campaign in 2017 determined that Oktoberfest could be a potential, previously unknown source of methane emissions [98], in situ investigations are conducted near the festival site in 2018 and 2019. This accurately quantifies the total CH_4 emissions from Oktoberfest and determines the source type

of emissions, i.e., antropogenic or biogenic. For this purpose, mobile surveys using a portable in situ CH_4 analyzer are combined with air samples taken at potential emitters and subsequently analyzed in the laboratory. [102], [108]

2.3.1. Mobile Backpack Investigations

In these measurement campaigns, portable CH_4 gas analyzers are used as backpack instruments with which people walk or cycle around the Oktoberfest area. Such an approach allows the localization of previously unknown CH_4 emitters, as it is possible to follow the enhanced concentration levels to eventually find the emission source. It also allows generalization of potential emitters, such as tents, crowds, sewage systems, etc., to simplify the modeling framework. Two different instruments are used in the two consecutive study years. In 2018, the Picarro GasScouter G4302 is used, which is based on the cavity ring-down principle, while in 2019, the LI-COR LI-7810 is used, which is based on the optical feedback cavity-enhanced absorption technique. Both devices have a comparably high precision and can therefore be substituted easily. In addition, these concentration measurements are combined with simultaneously recorded GPS data and wind information measured very close to the festival. An atmospheric transport model developed specifically for this application quantifies the emission flux from the entire Oktoberfest site. [102], [108]

2.3.2. Source Attribution

In order to know, which sources are causing the enhanced CH_4 levels, a source attribution is required. In this thesis, two different approaches are used: isotopic analyses and ethane ratio analyses.

Isotopic Analyses

A very commonly used approach to determine the origin of greenhouse gases is isotopic analyses of the sampled gases. Here, the $\delta^{13}C$ method and the δD method are used together to determine whether the CH_4 enhancements are biogenic or antropogenic in origin. In these two approaches, the ratios of ^{13}C to ^{12}C and of CH_3D to CH_4 are determined using mass spectroscopy. The less negative these two ratios are, the more antropogenic is the origin of the gases. Since the mass spectrometer is a very large instrument, sample bags are filled with air from potential emitters and then analyzed in the laboratory [108]. However, these samples always contain an unknown isotopic fingerprint of the background air. Therefore, Keeling plots are used to determine the isotopic fingerprint of the emission sources only [118].

Ethane Ratio Analyses

In addition to isotope analyses, the proportion of ethane (C_2H_6) in the natural gas is a characteristic of whether the gas is biogenic or antropogenic, since only antropogenic gas contains a significant proportion of ethane. During the studies, Munich natural gas contains about 3% ethane [119], while biogenic gases contain very little ethane [6]. Similar to isotope analyses, air samples are taken at Oktoberfest for ethane analyses and then analyzed in the laboratory. A quantum cascade laser (QCL) absorption spectrometer is used for this type of analysis. By least-squares fitting the ethane fractions of all samples and comparing them to the ethane fraction of the natural gas used, the ratio of the antropogenic fractions of the measured CH_4 enhancements can be determined [108].

2.3.3. Emission Modeling

The two emission models used for the in situ measurements at Oktoberfest are based on a Gaussian plume approach and CFD.

Gaussian Plume Approach

The first model is a multiple Gaussian plume approach, assuming that the 16 large beer tents at the festival are the largest CH_4 sources. This assumption is based on previously conducted source attribution analyses and mobile measurements at the festival site. The Gaussian plume model is a steady-state model for simulating the dilution of gases emitted from a point source. It assumes that the plume emitted from a chimney, for example, propagates in a Gaussian shape as a function of wind speed and direction and two dispersion coefficients in the crosswind and vertical directions. The Gaussian plume model is an established approach in atmospheric sciences and is widely used [37], [120]–[123]. However, at Oktoberfest, several adjacent sources emit simultaneously. Therefore, the standard approach is modified to a multiple Gaussian plume model in which 16 point source emissions are superimposed on each other. The resulting modeled concentrations are compared to concentrations measured during walks and bike rides around Oktoberfest. By scaling the linearly weighted emissions from the tents until the correlation between measured and modeled plumes is maximized, the emissions from the tents can be determined. [102]

Computational Fluid Dynamics

To increase the spatial resolution up to one meter, a forward CFD model is also developed for Oktoberfest. For this purpose, [124] constructed a 3D mesh model of

the Oktoberfest area with beer tents and other buildings. A high-resolution wind field at the festival site is simulated using the Reynolds-Averaged Navier-Stokes (RANS) equations, combined with a k-ϵ turbulence model [125]. Subsequently, the CH_4 dispersion is calculated using the unsteady convection-diffusion equation to produce forward-simulated CH_4 enhancements [124]. The subsequent steps to determine emissions are identical to [102].

2.4. In Situ Air Quality Measurements

In addition to greenhouse gases, urban air quality monitoring is another important part of this thesis. By performing mobile measurements and developing a low-cost air quality measurement system, the spatial resolution of existing air quality monitoring can be significantly increased. Combined with suitable modeling approaches, an air quality map of Munich should be created.

2.4.1. Mobile Surveys

One way to increase the spatial resolution of the current five government air quality monitoring stations is through mobile measurements. High-precision instruments such as CE DOAS (Cavity-Enhanced Differential Optical Absorption Spectroscopy) and CAPS (Cavity Attenuated Phase Shift) instruments mounted in a vehicle are used to create an air quality map of Munich [70]. However, such a mobile-collected air quality map cannot be directly compared to the values from government air quality stations because these two different data sets are not based on the same standards. There are two main challenges to overcome: systematically higher concentration measurements in the mobile setup due to the lower distance to emitters and diurnal influences that distort the mobile measurements. The latter influences can be reduced, for example, by additional measurements from a stationary long-pass (LP) DOAS instrument whose daily measurements were used to normalize temporal effects such as diurnal or weekly cycles due to varying traffic volumes and changes in the planetary boundary layer, as described by [70].

The second type of bias is caused by the closer proximity of the measuring gas inlet to the emission sources compared to stationary measuring points, when measuring devices are mounted in a vehicle to perform mobile measurements. While mobile setups measure directly on the road, stationary government air quality measuring stations in Germany have to comply with the 39$^{\text{th}}$ BImSchV. This includes that the inlets of these stations must be at least 25 m from the nearest cross street, but no more than 10 m from the roadside. In addition, the inlet must be between 1.5 and 4 m high [69]. In order to correct the systematically higher values of the mobile measurements, two different approaches are tested.

The first approach is to determine a correction factor between these two types of measurements. For this purpose, a small measurement campaign is carried out near the government air quality measurement station at Stachus in Munich. By varying the inlet position in terms of both distance to the road (2 to 10 m) and height (0.5 to 4 m) in combination with a linear regression approach, a correction factor is calculated that can be applied to the mobile measurements. [70]

The second approach uses a bicycle trailer instead of a vehicle to transport the instruments. In combination with an increased inlet height, the requirements of the 39th BImSchV can be met in most cases when riding on the bike lanes next to the road. Since this regulation requires stationary and non-moving sensors, stops are made at predefined locations to precisely meet the requirements (see Section 2.4.2). [126]

2.4.2. Smart Air Quality Sensor System

While the spatial resolution of a mobile measurement system is much better than that of stationary sensors, the temporal resolution is much lower, since the mobile sensor cannot be at several locations at the same time. In addition, even if these measurements are made comparable to government monitoring station values through calibration, they are not currently certified to 39th BImSchV and therefore cannot be used by state authorities in a legal context. Therefore, a spatially dense stationary sensor network is desirable. To enable such a network, compact and stand-alone sensor systems are needed that can be easily installed at different locations in the urban area. Such a sensor system is developed in this thesis.

Sensing Technology

Today, there are two major sensor technologies for low-cost measurement of gas concentrations of air pollutants, namely metal oxide sensors and electrochemical sensors. While metal oxide sensors change their resistance depending on the concentration of the target gas, electrochemical sensors work similar to a fuel cell. This means that the target gas triggers a chemical reaction, namely oxidation or reduction, at one of the two electrodes. The current between the two electrodes resulting from the electrical charge balance can be measured and converted into a concentration. Due to better sensitivity, better long-term stability, and better linearity, electrochemical sensors are chosen for the smart and compact air quality sensor system, although they are more expensive than metal oxide sensors [127], [128]. Since electrochemical sensors are cross-sensitive to other gases, NO_2, NO, O_3, and CO are measured so that the measurements can be subsequently corrected using an appropriate calibration and modeling approach. In addition, environmental parameters such as

temperature, relative humidity, and air pressure are also measured, as these parameters also affect the performance of the electrochemical sensors. For PM, optical particle counters are used in which air is drawn through a chamber where particles are optically counted with light generated by a laser. [127]–[129]

Electronic Assembly

The electronics are designed for stand-alone operation, i.e. they are equipped with batteries, a solar cell and a mobile communication module (see Figure 2.2). All peripherals are connected to a main board where a microcontroller controls each sensor system. In addition, battery management, a WiFi module for communication with the calibration unit during side-by-side measurements, an SD card for local data storage, a real-time clock, and the GSM (Groupe Special Mobile) communication module for transmitting measurement data to our server are mounted directly on this main board. GSM is chosen for data communication mainly because of its very good coverage and high data transmission rates compared to other options such as LoRaWAN (Long Range Wide Area Network). [127]–[129]

The sensors for measuring the pollutants are each located on a separate printed circuit board (PCB). This allows a modular approach, i.e. a different number and type of sensors can be connected to the main board without having to change the hardware of the main board. Communication between the sensor boards and the main board is done via I^2C (Inter-Integrated Communication). Each sensor board consists of a potentiostatic circuit to operate the electrochemical sensors. In addition, a transimpedance amplifier converts the sensor output signal, which is a current, into a voltage. This very small voltage signal is then amplified by a non-inverting or inverting operational amplifier and finally converted to a digital value by an ADC (analog-to-digital converter). To ensure that each sensor board can be used for both reducing and oxidizing gases, both circuits are already printed on the sensor boards. To switch between the two versions, only a few resistors have to be exchanged. Version A is used for oxidizing gases such as NO_2 and O_3 and version B for reducing gases, such as NO and CO. The PM sensor already has a digital output and does not require a sensor board. It is connected to the main board via SPI (Serial Peripheral Interface). [127]–[129]

Although the sensor system is equipped with a small solar panel and batteries, power consumption must be kept low to enable long-term measurements even at partially shaded measurement locations, at night or in winter. Therefore, energy-intensive devices such as the GSM module, the fan for generating the sample air flow and the PM sensor do not run continuously. Instead, the intervals for taking measurements and uploading data are adjustable, for example, to one measurement per minute and one upload per hour. In the meantime, the components are switched

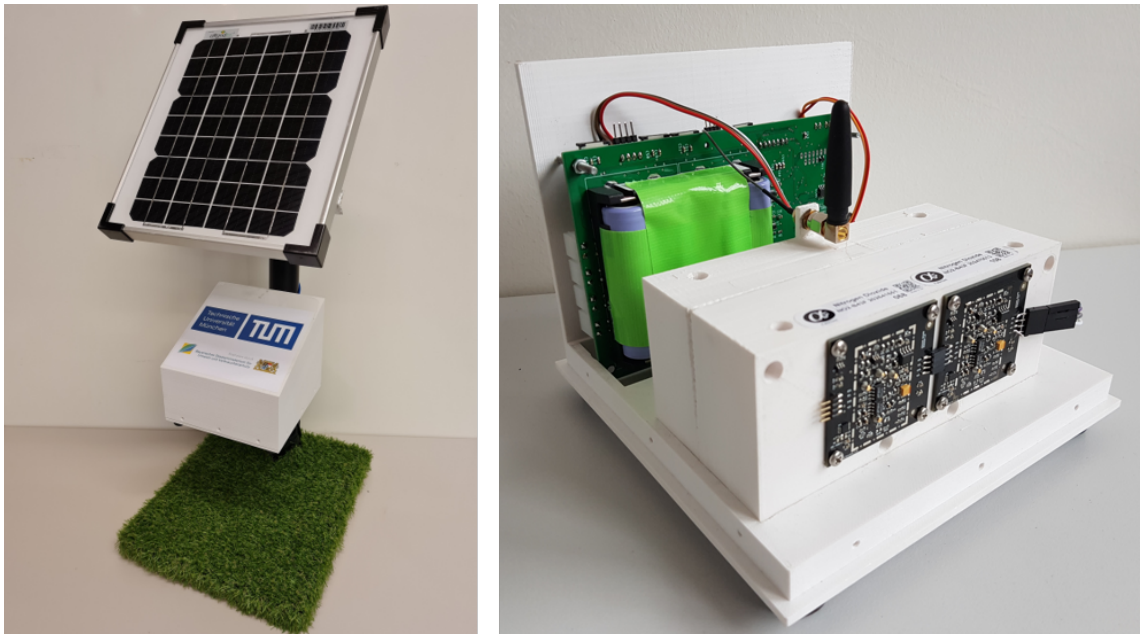

Figure 2.2.: Photos of the low-cost air quality sensor box. Left: Air quality sensor box (white) mounted on a demonstrator including solar panel. Right: Interior view of the air quality sensor box with main board, batteries, air duct, antenna and two sensor boards (front).

off and the microcontroller goes into deep sleep mode to reduce power consumption to a minimum. [127], [129]

Weatherproof Housing

Since the electrical equipment is not weatherproof, a housing is needed to protect it from harsh weather conditions. Such a housing must be waterproof, lightweight and durable. Based on the good experience with the rain covers of the EM27/SUN enclosure systems, this housing is also 3D printed using PETG as material. Since the sensors need to be exposed to ambient air, an inlet is needed. This inlet and all other openings, such as the electrical connectors, are located on the bottom to prevent precipitation from entering the system. In addition, to prevent the gas sensors from being exposed to large fluctuations in air pressure caused by wind, which can cause the sensors to misbehave, the sensors are installed in an air duct. This air duct is supplied with fresh air by a small fan (see Figure 2.2, left). For each measurement, the fan is switched on only briefly, then the system waits until the air in the duct has calmed down before measuring the gases. [127], [129]

Data Processing

The measurement data is stored locally on the SD card until the GSM module is switched on to send the data, e.g. of the last hour, to a web server via an HTTP connection. A PHP (PHP: Hypertext Preprocessor) script runs permanently on the web server, which receives the data, processes it and stores it in a MySQL database. If the transmission is successful, a confirmation with the current server time is sent back to the sensor system to regularly update the real-time clock of the sensor box. [127], [129]

Calibration

Although electrochemical sensors have better performance than, for example, metal oxide sensors, such low-cost sensors need to be calibrated to ensure proper operation. As shown by [74] and [130] in the city of Zurich, side-by-side calibration is an absolutely necessary step before distributing the sensors in the field. Such calibration must also be performed for each of the low-cost sensor boxes presented here to account for production variations that cause significant changes in the output signal. Similar to [74], [130], an individual model should be created for each sensor, including various parameters such as concentrations of cross-sensitive gas species, temperature, relative humidity, etc.

Furthermore, these sensors are subject to drift and aging effects, as shown in [74]. Therefore, calibrations should be performed regularly, e.g., on a weekly basis, to keep such effects to a minimum. Since it would be too complicated to collect all 50 sensor boxes to be installed in the city every week, a different calibration approach is developed. In this approach, a mobile calibration unit with certified high-precision reference instruments will drive by all sensor boxes and take a measurement side-by-side for a short period of time. The results of these calibration measurements shall be used to update the individual data model of each sensor box. The mobile calibration unit is to be installed, for example, on a bicycle trailer or a cargo bicycle so that the calibration unit can get as close as possible to each low-cost sensor box, which would not be possible if the reference sensors were installed in a vehicle. In addition, the use of the bicycle method does not produce any falsifying exhaust gases.

3. Journal Publications - Summaries

The following section lists brief summaries of journal publications in which the author of this dissertation was a lead author. Copies of the journal articles can be found in the Appendix.

3.1. MUCCnet: Munich Urban Carbon Column network

This study is about the Munich Urban Carbon Column network (MUCCnet), the world's first urban sensor network that has been permanently measuring greenhouse gases using the differential column measurement (DCM) principle since summer 2019. In this measurement principle, column-averaged CO_2, CH_4 and CO concentrations are measured with a solar-tracking Fourier transform spectrometer (here: EM27/SUN from Bruker Optics), using the sun as a light source. The advantage of these column measurements is that they are relatively insensitive to vertical redistributions of tracer masses and surface fluxes upwind of the city. This makes such measurements very suitable as inputs to an inversion system and thus ideal for quantifying greenhouse gas emissions.

Because permanent and long-term observations are required to understand the global carbon cycle and to monitor emission reductions, automation is essential. We have therefore developed electronically controlled enclosure systems to be able to set up such a greenhouse gas sensor network for fully automated quantification of large-scale emission sources. In addition to the hardware, this also includes suitable software that independently starts and stops the measurements and provides suitable error handling.

The results of our sensor network MUCCnet and our remote sites in Jinja, Uganda, and Sodankylä, Finland show the advantages of such an automated network, such as a very high data volume, low manpower requirements and high data quality. Due to the very frequent measurements taken regardless of the day of the week or the time of the year, this study shows that such networks can effectively detect both the global increasing trend of CO_2 concentrations and the seasonal cycle. Thanks

to automation, we were able to continue measuring during the COVID-19 lockdown in spring 2020. By correlating the gradients of CO_2 column concentrations with traffic volumes, we show that our network is able to qualitatively detect variations in urban emissions.

Furthermore, the network can be uniquely used to validate greenhouse gas satellites by comparing not only absolute values, but also concentration gradients for the first time. Due to the existence of MUCCnet, NASA's OCO-2 and OCO-3 satellites have been measuring urban CO_2 concentration gradients over Munich since spring 2020. In contrast to the normal operating mode, they use the spatially high-resolution target mode over Munich to compare the satellite measurements with our ground-based measurements. MUCCnet thus provides a globally unique opportunity to validate satellite-based emission estimates.

In the future, we will combine our unique dataset with atmospheric inversion techniques to determine Munich's greenhouse gas emissions for the first time using measurements. In addition, we will use our rich dataset to detect and quantify unknown greenhouse gas emission sources.

With this study, we have thus laid the foundation to be able to determine urban greenhouse gas emissions using column measurements. The characteristics of the hardware presented here - such as high reliability, ease of use, and low operational costs - provide the basis for becoming a new standard for monitoring urban greenhouse gas concentrations.

As indicated in the author contribution section, the author of this dissertation was responsible or co-responsible for conceiving the study, developing the concept, leading the hardware and software development as well as the setup of the sensor network, building the enclosure systems, programming the software, performing the measurements, analyzing the measurement data, and writing the manuscript.

F. Dietrich, J. Chen, B. Voggenreiter, P. Aigner, N. Nachtigall, and B. Reger, "MUCCnet: Munich Urban Carbon Column network", *Atmospheric Measurement Techniques*, vol. 14, no. 2, pp. 1111–1126, Feb. 11, 2021, Publisher: Copernicus GmbH. DOI: 10.5194/amt-14-1111-2021

3.2. Methane emissions from the Munich Oktoberfest

In this study, the Munich Oktoberfest, the largest beer festival in the world, became the first festival to have its CH_4 emissions determined by measurements. Such events are a potential source of fossil CH_4 emissions, as significant amounts of natural gas are used for heating and cooking. Leaks in the supply pipelines as well as incomplete combustion in the gas appliances can accordingly cause unintended CH_4 emissions. We used in situ measurements in combination with a Gaussian dispersion model to determine emissions from the festival. Measurements were made during walking and cycling tours around the perimeter of the Oktoberfest site. Measurements revealed CH_4 enhancements of up to 100 ppb compared to background levels and post-Oktoberfest measurements.

The average emission of Oktoberfest determined with a multiple Gaussian plume model was $(6.7\pm0.6)\,\mu g(m^2s)^{-1}$ (1σ standard deviation). A comparison between emissions during the week ($4.6\,\mu g(m^2s)^{-1}$) with those at the weekend ($8.5\,\mu g(m^2s)^{-1}$) shows that the emission intensity on the weekend was almost twice as high as during the week. From this result, we conclude that a higher number of visitors leads to higher emissions. However, the daily emission cycle exhibits oscillatory behavior that is not correlated with visitor numbers, and thus emissions cannot be explained by visitor numbers alone. In addition, a calculation of the possible biogenic CH_4 enhancements caused by the visitors showed a value that was five times smaller than the measured values. Instead, fossil CH_4, such as that produced by incomplete combustion of natural gas or losses in gas appliances, appears to account for the largest share of Oktoberfest CH_4 emissions. However, it is difficult to provide a final answer as to exactly which sources contributed to the measured overall enhancements with this study. After all, since we were not allowed to enter the Oktoberfest grounds with the measuring device, the distance to the sources was simply too large to precisely locate and quantify the individual CH_4 sources. It is equally difficult to make a statement about how large the proportion of fossil versus biogenic sources is. To improve this in future studies, several additional approaches are conceivable. For example, air samples can be taken at the festival site using sample bags and then analyzed in the laboratory. Such a laboratory analysis also has the advantage of determining isotope ratios, such as $\delta^{13}C$ and δD, or ethane ratios, in addition to measurements of CH_4 concentration. Both methods allow a classification of the measured gas into fossil or biogenic origin.

Overall, the method presented here has the potential to determine emissions from medium sized area sources of all types in a fairly straightforward manner. Potential applications for locating and quantifying overlapping methane sources range from

groups of small cow barns, uncovered heaps in landfills, or wetlands made of groups of ponds and swamps, etc.

Thus, in this study, we have developed a generally applicable method to quantify greenhouse gas emissions from area sources. Furthermore, using Oktoberfest as an example, this study shows that large festivals can be significant CH_4 emitters and should therefore be included in future emission inventories. Only if all major sources of greenhouse gases are accurately quantified, the targets for reducing global CH_4 emissions can be met.

As indicated in the author contribution section, the author of this dissertation was responsible or co-responsible for planning the campaign, performing the measurements, analyzing the data, and writing the manuscript.

J. Chen[1], F. Dietrich[1], H. Maazallahi, A. Forstmaier, D. Winkler, M. E. G. Hofmann, H. Denier van der Gon, et al., "Methane emissions from the Munich Oktoberfest", *Atmospheric Chemistry and Physics*, vol. 20, no. 6, pp. 3683–3696, Mar. 27, 2020, Publisher: Copernicus GmbH. DOI:10.5194/ACP-20-3683-2020

[1]These authors contributed equally to this work.

3.3. Climate Impact Comparison of Electric & Gas-Powered End-User Appliances

We conducted a detailed study of methane emissions from gas-powered end-use appliances and then compared their climate impacts with those of electricity-powered appliances. To this end, we used the Munich Oktoberfest, the largest beer festival in the world, as a case study and then applied our findings to 25 countries that contribute significantly to global natural gas consumption. For this purpose, we investigated the source signature of CH_4 enhancements at the festival using a portable CH_4 gas analyzer. We also performed isotopic analyses of air samples ($\delta^{13}C$ and δD ratios) and determined the ethane content of the samples. Both methods are used to determine the source type for the enhanced gas concentrations.

Both the results of the isotopic and ethane analyses of the gas indicated that the CH_4 elevations were predominantly caused by natural gas used for cooking and heating at the festival site, rather than biogenic processes caused by visitors. The study further shows that incomplete combustion and leaks in end-use equipment are the likely cause of the emissions, and leaking pipelines are not significant contributors. Since heating and cooking are mainly done in the beer tents, the tents are the main sources of CH_4 enhancement at Oktoberfest. Overall, we estimate the CH_4 leakage rate at the Oktoberfest site to be 1.4%.

We then investigated whether, given the existing CH_4 leakage, carbon emissions could be saved if electric appliances were used instead of gas appliances. To do this, we compared the carbon footprint of these two types of appliances for heating and cooking. Although natural gas is considered a fairly climate-friendly alternative to other fossil fuels, we found that electric appliances at Oktoberfest have had a smaller carbon footprint than natural gas-powered appliances since 2005, due to the extensive use of renewable electricity at the festival and methane emissions not previously included in the calculation of the total carbon footprint. If all natural gas-powered equipment at Oktoberfest had been replaced with electric equipment, approximately 450 tons of CO_2 equivalents could have been saved in 2019, representing 87% of the total carbon emissions caused by energy use at the festival.

Since carbon emissions from Oktoberfest contribute very little to the global carbon budget, emission reductions at Oktoberfest are not a solution to global climate problems. However, gas appliances are not only used at Oktoberfest, but in many households around the world. Therefore, we extended our study to estimate in which countries replacing gas-powered appliances with electric ones could save carbon emissions. To do this, we analyzed carbon emissions from energy demand in the household sector for 25 major natural gas-consuming countries around the world. Because the carbon footprint of electricity generation differs significantly

among these countries, it is not possible to make a general statement about whether electric or gas-powered end-use appliances are more climate-friendly. Rather, each country must be considered individually. We found that currently electricity is the more climate-friendly energy source than natural gas for domestic cooking and heating in only seven of these 25 countries. However, as carbon emissions in electricity supply will continue to decrease in most countries, mainly due to the growing share of renewable energy, electricity could become a more climate-friendly energy source than natural gas for end-use appliances in these countries in the near future.

Even though we are aware that it is not possible to replace all gas appliances in the world with electric appliances, as often the electrical infrastructure is simply missing or electricity is the significantly more expensive energy source than natural gas in many countries, we nevertheless demonstrate with this study a possibility with which people all over the world and in a relatively simple way, can contribute significantly to the reduction of global carbon emissions.

As indicated in the author contribution section, the author of this dissertation was responsible or co-responsible for conceptualization, data curation, formal analysis, funding acquisition, investigation, methodology, project administration, software, supervision, visualization, and writing the original draft of the manuscript.

F. Dietrich, J. Chen, A. Shekhar, S. Lober, K. Krämer, G. Leggett, C. van der Veen, *et al.*, "Climate Impact Comparison of Electric and Gas-Powered End-User Appliances", *Earth's Future*, vol. 11, no. 2, e2022EF002877, 2023. DOI: 10.1029/2022EF002877

4. Discussion and Conclusion

The results of this thesis include the development of hardware, software and modeling approaches for the quantification of greenhouse gases and air pollutants. For this purpose, the hardware and software of an enclosure system for EM27/SUN spectrometers was further developed to enable fully automated operation [85]. These systems have been tested in six successful measurement campaigns to determine urban greenhouse gas emissions in Munich [85], [98], [100], [102]–[107] and Hamburg, Germany [109], [110] and for measurements in Jinja, Uganda [94]–[96] and Sodankylä, Finland [93]. The extensive testing of the enclosure system shows that the hardware and software are suitable for long-term operation even at sites with extreme weather conditions. In combination with an automated data processing chain, such enclosure systems were the basis for building MUCCnet, the world's first permanent urban greenhouse gas sensor network based on ground-based remote sensing [85]. MUCCnet demonstrates that ground-based remote sensing can be used not only to permanently monitor the global atmospheric carbon concentration trend, as is done primarily with TCCON instruments [88], but also to permanently measure urban greenhouse gas concentration gradients [85]. These concentration gradients are the prerequisite for quantifying urban emissions using atmospheric modeling approaches that were further developed and adapted to the Munich case in this thesis, including Bayesian inverse modeling [97], computational fluid dynamics modeling [124], and sparse reconstruction [113].

In addition to remote sensing, this thesis involves the first methane studies at a large festival using mobile in situ measurements at Oktoberfest 2018 [102] and 2019 [108]. These studies identified Oktoberfest as a previously unknown yet significant source of anthropogenic methane emissions, primarily due to incompletely burned natural gas from cooking and heating appliances. Furthermore, the Oktoberfest study shows that electric appliances at the festival have a much smaller carbon footprint than natural gas-powered appliances due to the intensive use of electricity from renewable energy sources. Comparing these two energy sources on a global scale shows that replacing natural gas-powered cooking and heating appliances with electric appliances could save carbon emissions worldwide [108].

Besides the quantification of greenhouse gases, air pollutants are also investigated in this thesis. For air pollutants, the spatial representativeness of government air quality monitoring stations was determined and a first prototype of a compact and

stand-alone sensor box was developed and built [127].

These results provide significant added value to global greenhouse gas and air quality research. For example, the global EM27/SUN sensor network COCCON [50], [51] requires fully automated enclosure systems for long-term operation similar to TCCON [88]. Therefore, the development in this thesis is a great benefit to the global EM27/SUN community as it can be used to automate ground-based remote sensing measurements around the world. This significantly reduces manpower requirements and maximizes the amount of data [85]. Based on the automated measurements, it is possible to focus more on scientific questions, e.g. where are still unknown or wrongly quantified emitters or how are greenhouse gas emissions evolving over the years? In addition, MUCCnet's unique dataset can be used for many new applications, such as validating urban concentration gradients using satellites. Until now, only absolute concentration values could be validated using instruments from TCCON [131], COCCON [51], or mobile setups [60]. With MUCCnet, it is possible for the first time to additionally validate concentration gradients permanently with a spatially dense EM27/SUN sensor network [114], which is an essential step towards emission quantification with remote sensing data from space.

The emission quantification model determined for Oktoberfest can be used in the future to quantify all types of medium sized area sources of methane where multiple point sources are superimposed, such as landfills, wetlands, etc [102]. This study also suggests that temporary events should be included in future emission inventories. Although they last only a short time, they can contribute significantly to annual emission levels [102] and should therefore be included in emission inventory products such as TNO GHGco v1.1, which currently does not include time-limited events [111]. In addition to these local improvement opportunities, this study can also help reduce global carbon emissions. While previous research primarily suggests switching from coal to natural gas as a bridging technology for energy transition [78]–[81], the results of this study show that switching from natural gas to electricity for residential cooking and heating appliances may be an even better option for reducing global GHG emissions now or in the near future.

The development of the low-cost air quality sensor system lays the foundation for the establishment of a spatially dense sensor network similar to the networks in Zurich, Switzerland [74], Oslo, Norway [75], London, United Kingdom [76] and San Francisco, California [22]. In contrast to these sensor networks, the planned regular calibration will bring added scientific value to the Munich sensor network, as the measurement will be more trustworthy after being calibrated on a weekly basis [126].

Although the approaches developed in this thesis offer great benefits, there are still some limitations that could be improved in future work. Regarding the enclosure

systems, the hardware is already very reliable. However, the software can still be improved. The two main challenges are the enclosure PCs running Microsoft Windows operating system and the moderate long-term stability of Pyra, which currently requires occasional manual restarts. To overcome these problems, a switch to a Linux-based operating system can be made in combination with various bug fixes of Pyra. In addition, the two mesoscale emission models studied in this work still have quite large uncertainties that make it difficult to determine emission numbers accurately and with high spatial resolution. The main reason for this behavior is the coarse ERA5 wind model used with a temporal resolution of one hour and a spatial resolution of $0.1\,^{\circ} \times 0.1^{\circ}$. Therefore, actual 3D wind measurements with wind lidar instruments comparable to the approach presented in [132], or spatially higher-resolution transport models created using computational fluid dynamics, for example, are feasible solutions. In addition, the unknown background concentration also contributes to the uncertainty of the final emission number. These currently only modeled background concentrations could be measured in the future, e.g. with mobile measurement devices upwind of the city or by satellite measurements.

Regarding the low-cost air quality sensor box, several future improvements are possible. Currently, it is a prototype that shows feasibility. To build up a sensor network, 50 slightly improved sensor boxes are to be built. The same applies to the calibration unit, which is only theoretically planned. However, this is not the subject of this thesis anymore and will be continued by [126].

Overall, this thesis contains several new and innovative approaches to quantify urban greenhouse gases and air pollutants through measurements combined with modeling. The approaches shown have been intensively tested and have proven to be practicable. Some of these approaches are even part of an international best practice guideline for observing urban greenhouse gas emissions [133] and can therefore make an important contribution to improving the global climate in the near future.

A. Copy of "MUCCnet: Munich Urban Carbon Column network"

Atmos. Meas. Tech., 14, 1111–1126, 2021
https://doi.org/10.5194/amt-14-1111-2021

Atmospheric Measurement Techniques
Open Access
EGU

MUCCnet: Munich Urban Carbon Column network

Florian Dietrich, Jia Chen, Benno Voggenreiter, Patrick Aigner, Nico Nachtigall, and Björn Reger

Environmental Sensing and Modeling, Technical University of Munich (TUM), Munich, Germany

Correspondence: Florian Dietrich (flo.dietrich@tum.de) and Jia Chen (jia.chen@tum.de)

Received: 24 July 2020 – Discussion started: 12 August 2020
Revised: 2 December 2020 – Accepted: 25 December 2020 – Published: 11 February 2021

Abstract. In order to mitigate climate change, it is crucial to understand urban greenhouse gas (GHG) emissions precisely, as more than two-thirds of the anthropogenic GHG emissions worldwide originate from cities. Nowadays, urban emission estimates are mainly based on bottom-up calculation approaches with high uncertainties. A reliable and long-term top-down measurement approach could reduce the uncertainty of these emission inventories significantly.

We present the Munich Urban Carbon Column network (MUCCnet), the world's first urban sensor network, which has been permanently measuring GHGs, based on the principle of differential column measurements (DCMs), since summer 2019. These column measurements and column concentration differences are relatively insensitive to vertical redistribution of tracer masses and surface fluxes upwind of the city, making them a favorable input for an inversion framework and, therefore, a well-suited candidate for the quantification of GHG emissions.

However, setting up such a stationary sensor network requires an automated measurement principle. We developed our own fully automated enclosure systems for measuring column-averaged CO_2, CH_4 and CO concentrations with a solar-tracking Fourier transform spectrometer (EM27/SUN) in a fully automated and long-term manner. This also includes software that starts and stops the measurements autonomously and can be used independently from the enclosure system.

Furthermore, we demonstrate the novel applications of such a sensor network by presenting the measurement results of our five sensor systems that are deployed in and around Munich. These results include the seasonal cycle of CO_2 since 2015, as well as concentration gradients between sites upwind and downwind of the city. Thanks to the automation, we were also able to continue taking measurements during the COVID-19 lockdown in spring 2020. By correlating the CO_2 column concentration gradients to the traffic amount, we demonstrate that our network is capable of detecting variations in urban emissions.

The measurements from our unique sensor network will be combined with an inverse modeling framework that we are currently developing in order to monitor urban GHG emissions over years, identify unknown emission sources and assess how effective the current mitigation strategies are. In summary, our achievements in automating column measurements of GHGs will allow researchers all over the world to establish this approach for long-term greenhouse gas monitoring in urban areas.

1 Introduction

Climate change is one of the defining issues of our time, and one that affects the entire planet. To reduce greenhouse gas (GHG) emissions effectively, accurate and continuous monitoring systems for local- and regional-scale emissions are a prerequisite.

Especially for urban areas, which contribute to more than 70 % of global fossil fuel CO_2 emissions (Gurney et al., 2015) and are therefore hotspots, there is a shortage of accurate emissions assessments. The city emission inventories often underestimate emissions due to unknown emission sources that are not yet included in the inventories (Chen et al., 2020; Plant et al., 2019; McKain et al., 2015).

In recent years, several city networks have been established to improve emission monitoring. These include networks using in situ high-precision instruments (McKain et al., 2015; Bréon et al., 2015; Xueref-Remy et al., 2018; Lamb et al., 2016) and low-cost sensor networks deploying non-dispersive infrared sensors (Kim et al., 2018; Shusterman et al., 2016). In addition, eddy covariance flux tower

measurements are used for directly inferring city fluxes (Feigenwinter et al., 2012; Helfter et al., 2011). However, all these approaches involve some challenges when it comes to measuring urban emission fluxes, such as high sensitivity to the boundary layer height dynamics, large variations due to mesoscale transport phenomena or the fact that they can only capture the fluxes of a rather small area.

Column measurements have proven to be a powerful tool for assessing GHG emissions from cities and local sources, because they are relatively insensitive to the dynamics of the boundary layer height and surface fluxes upwind of the city if a differential approach is used (Chen et al., 2016). Therefore, this method has recently been widely deployed for emission studies of cities and local sources using mass balance or other modeling techniques. In St. Petersburg, Makarova et al. (2020) deployed two compact solar-tracking Fourier transform infrared (FTIR) spectrometers (EM27/SUN) and a mass balance approach to study the emissions from the fourth-largest European city. The EM27/SUN spectrometer has been developed by the Karlsruhe Institute of Technology (KIT) in collaboration with Bruker and has been commercially available since 2014 (Gisi et al., 2011, 2012; Hase et al., 2016). Hase et al. (2015) and Zhao et al. (2019) used the measurements of five EM27/SUNs to measure emissions of CO_2 and CH_4 in Berlin. With a similar sensor configuration, Vogel et al. (2019) studied the Paris metropolitan area and applied the CHIMERE-CAMS model to show that the measured concentration enhancements are mainly due to fossil fuel emissions. Jones et al. (2021) combined measurements from Indianapolis (five EM27/SUNs) with an adapted inverse modeling technique to determine the urban GHG emissions.

Besides these urban studies, column measurements are also used to investigate local sources: Chen et al. (2016) and Viatte et al. (2017) determined the source strength of dairy farms in Chino, California. By combining column measurements with a computational fluid dynamics (CFD) model, Toja-Silva et al. (2017) verified the emission inventory of the largest gas-fired power plant in Munich. With mobile setups, Butz et al. (2017) studied emissions from the volcano Mt. Etna, Luther et al. (2019) quantified the coal mine emissions from upper Silesia and Klappenbach et al. (2015) utilized column measurements on a research vessel for satellite validations above the ocean. However, these studies are all based on the campaign mode and not suited for monitoring the urban emissions permanently. Only TCCON (Total Carbon Column Observing Network; Wunch et al. (2011)) and COCCON (Collaborative Carbon Column Observing Network; Frey et al., 2019; Sha et al., 2020) are measuring the global GHG column concentrations permanently. For this purpose, TCCON uses IFS 125HR spectrometers (resolution: $0.02\,cm^{-1}$), while COCCON uses calibrated EM27/SUN spectrometers (resolution: $0.5\,cm^{-1}$). However, both networks focus on detecting GHG background concentrations and are not primarily designed to study urban emissions.

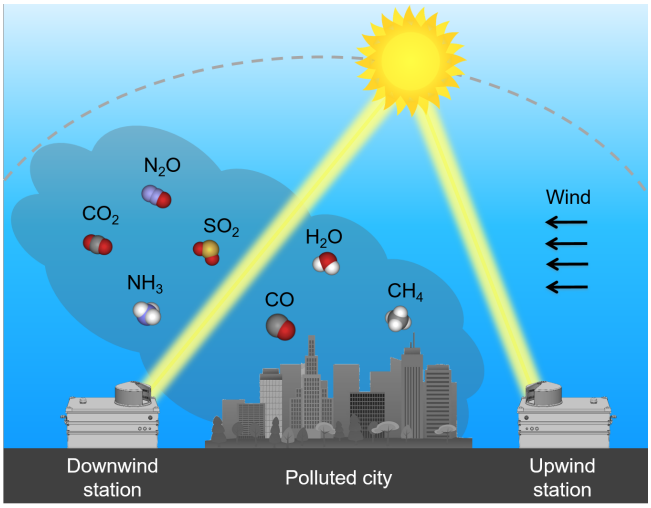

Figure 1. Basic principle of the differential column measurements: with the help of an upwind and at least one downwind station, the column-averaged GHG concentrations are measured. The differences between the two stations are representative for the emissions generated in the city.

In this paper, we present the Munich Urban Carbon Column network (MUCCnet), the permanent urban GHG network in Munich, which is based on the differential column measurement (DCM) principle and consists of five fully automated FTIR spectrometers. The combination of our sensor network with a suitable modeling framework will build the basis for monitoring urban GHG emissions over years, identifying unknown emission sources, validating satellite-based GHG measurements and assessing the effectiveness of the current mitigation strategies.

2 Measurement principle

As a measurement principle, the DCM method is used (Chen et al., 2016). DCM is an effective approach for determining the emissions of large-area sources using just a small number of stationary ground-based instruments. The basic principle of DCM is illustrated in Fig. 1. The column-averaged concentrations of a gas in the atmosphere are measured upwind and downwind of an emission source, utilizing ground-based FTIR spectrometers that use the sun as a light source. The concentration enhancements between the two stations are caused by the urban emissions. Chen et al. (2016) have shown that the differences between the upwind and downwind column concentrations are relatively insensitive to the boundary layer height and upstream influences. Therefore, DCM in combination with a wind-driven atmospheric transport model can be used to determine emissions.

3 Measurement system

In order to use the DCM principle for long-term monitoring of the urban GHG emissions, a fully automated measurement system is needed. For this, we developed an electronically controlled enclosure system that includes the related software.

3.1 Hardware

The enclosure system protects the spectrometer inside against harsh weather conditions and other harmful events, such as power or sensor failures. Furthermore, it enables communication between the devices inside the system and allows the host to remotely control the measurements over the internet. Under suitable measuring conditions, such as sunny weather and valid sun elevations, the system automatically starts the measurement process. During the day, the measurements are checked regularly by the enclosure software to detect and solve malfunctions autonomously. When the measuring conditions are no longer suitable, the system stops taking measurements and closes the cover to secure the spectrometer. An operator is informed about any unexpected behavior by email.

3.1.1 Standard edition

The described enclosure is based on our first prototype system, presented in Heinle and Chen (2018), which has been continuously running on the rooftop of the Technical University of Munich (TUM) in Munich's inner city since 2016. This system was developed to semi-automate the measurement process using an EM27/SUN spectrometer over the years. For the permanent urban GHG network, we improved this system to make it more reliable, easier to transport and fully autonomous.

Our new enclosure system is based on a lightweight yet robust aluminum housing (Zarges K470 box, waterproof according to IP54) that we modified for our purposes. The CAD model of this system is shown in Fig. 2. A rotating cover at the top of the housing allows the sunrays to hit the mirrors of the solar tracker at arbitrary azimuth and elevation angles. Every 10°, a magnet is fixed in the outer cover (see Fig. 3). Reed sensors in the inner cover count these signals so that the relative position of the cover can be computed. Before the cover is opened and after every full rotation, two additional reed sensors indicate the absolute zero position. The target position of the cover is computed automatically depending on the coordinates of the site and the time. Optical rain and direct solar radiation sensors indicate whether the current environmental conditions are suited for measurements.

Signal lamps, push buttons and an emergency stop button can be used to control the basic functions of the enclosure directly at the site. Full control can only be achieved by remote access to the enclosure computer, which is an industrial embedded box PC. In addition to the remote access, the computer is also responsible for controlling the spectrometer and the solar tracker and for storing the interferograms before they are transferred to our retrieval cloud via the internet.

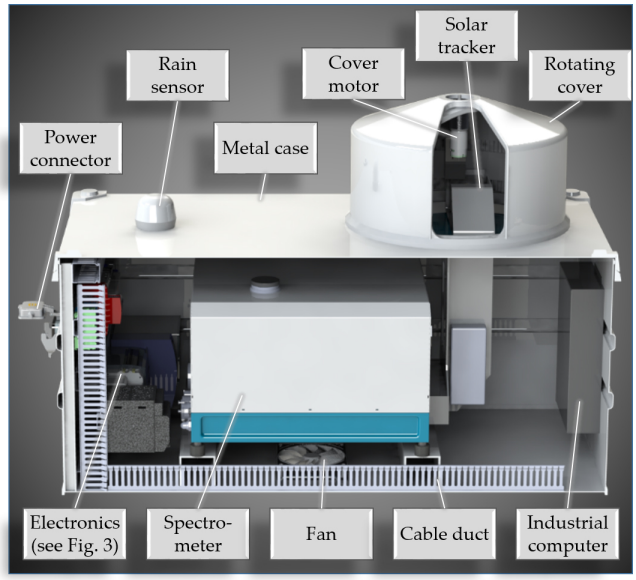

Figure 2. Side view of the enclosure system (CAD model).

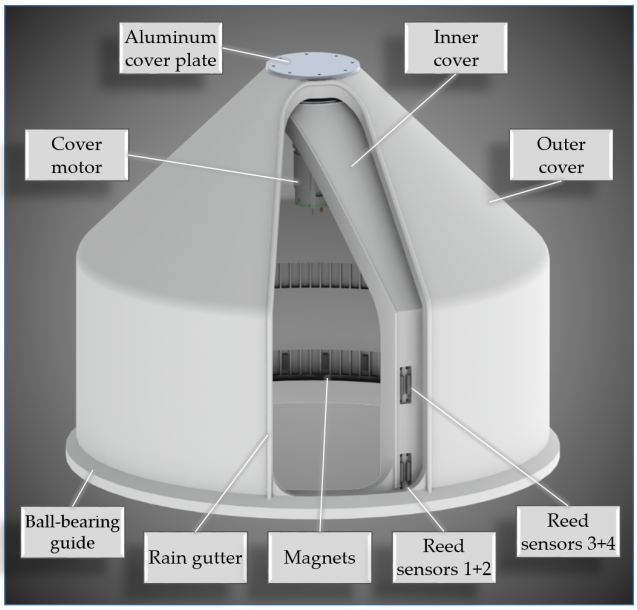

Figure 3. CAD model of the newly designed cover (outer and inner one) with a small opening and a steeper slope compared to the first version in Heinle and Chen (2018). With the help of the reed sensors 1 and 2, the relative position of the cover is calculated (in 10° steps). The second sensor indicates the direction. The reed sensors 3 and 4 are used to determine the absolute zero position each time before the cover opens.

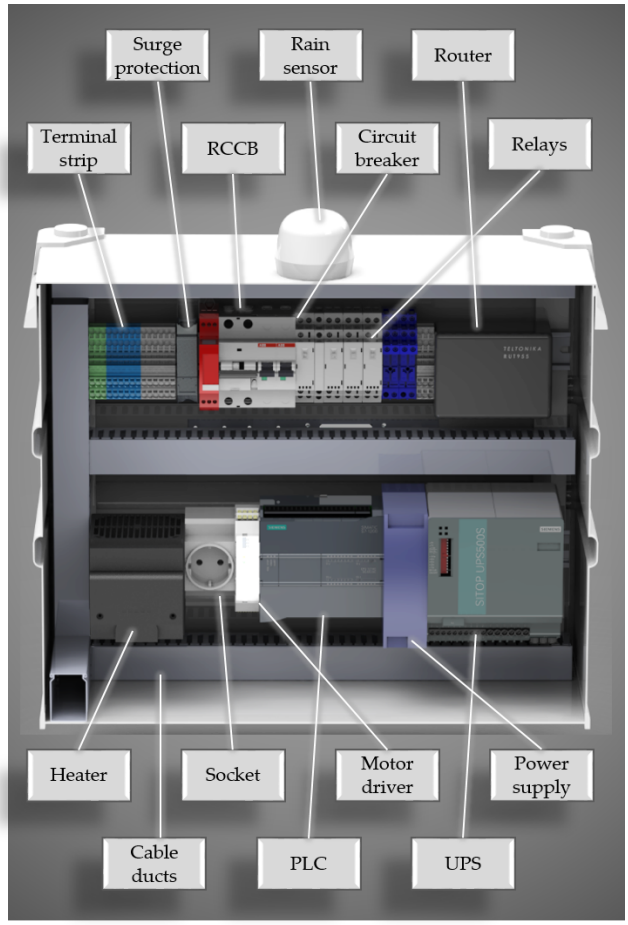

Figure 4. CAD model of the electrical components inside the enclosure.

The enclosure system itself is controlled by a Siemens S7-1200 PLC (programmable logic controller) and not by the enclosure computer that runs on a Microsoft Windows operating system. This approach ensures that the safety features – such as rain or power failure detection, cover motor control and temperature control – are separated from the Windows operating system, making the enclosure less error-prone and more fail-safe.

All the additional electronics are placed in the rear part of the enclosure systems and are shown in Fig. 4 in detail. Besides the PLC, we installed an LTE router, a heater, the motor driver, two circuit breakers, surge protection devices and an RCCB (residual current circuit breaker). In addition, new relays were added to the system to be able to reset all error-prone devices – such as the computer, router or PLC – remotely. In order to make the system as lightweight as possible, we replaced the large and heavy thermoelectrical cooler by a cooling fan and a heater, and replaced the lead–acid battery of the UPS (uninterruptible power supply) by capacitor-based energy storage. All the devices inside the system communicate via the two standard protocols TCP/IP and USB.

Figure 5. Image of the new enclosure system on the roof of a school at our southern site, Taufkirchen. The systems includes, inter alia, the newly designed rotating cover, the lightweight aluminum case, the solar radiation sensor and a surveillance camera attached to a post.

A photo of one of the four newly developed enclosure systems for the Munich network can be seen in Fig. 5. It shows the measurement setup at our southern site on top of a flat rooftop.

3.1.2 Universal editions

Our enclosure system was originally developed to measure the GHG concentrations in Munich at a latitude of 48.15° N. Therefore, the rotating cover that protects the solar tracker from bad weather was designed to enable measurements for all possible solar angles at such a latitude. However, if the enclosure system is used somewhere else in the world, these limitations need to be considered. That is why we designed our new cover so that it can measure solar elevation angles up to about 80° and azimuth angles between 30 and 300° for setups in the Northern Hemisphere. The asymmetric azimuth angle range is due to the non-centered first mirror of the solar tracker. If the system is used in the Southern Hemisphere, it must be rotated by 180° and a setting must be changed in the software. These solar angles cover most places in the world. Furthermore, we adapted some features to overcome challenges such as extreme temperatures and high relative humidity. We developed two of these special editions and tested them at both very low and very high latitudes: one in Uganda next to the Equator and one in Finland next to the polar circle.

As part of the NERC MOYA project, the University of Leicester has been using our enclosure system to measure CH_4 emissions from the wetlands north of Jinja, Uganda (latitude: 0.4° N), since the beginning of 2020 (Humpage et al., 2019). Quite apart from the significantly higher temperatures and

Figure 6. Setup of the tropical version of our enclosure in Jinja, Uganda (Latitude: 0.4° N). With the help of car jacks the whole system is tilted in order to enable measurements at high elevation levels close to 90°. Furthermore, the system is equipped with two 150 W thermoelectrical coolers (attached at the two sides of the system) that keep the temperature inside the enclosure constant at 25 °C. Photo by Neil Humpage, University of Leicester.

relative humidity than in Munich, the very high solar elevation angles (up to 90°) are challenging. These high angles are a problem both for the cover of the enclosure as it blocks the sun in such cases and for the solar tracker of the spectrometer. The solar tracker of the EM27/SUN can only measure up to elevation angles of about 85°. At higher elevations, the control algorithm is no longer stable. Therefore, both the spectrometer and the cover cannot work properly at such high elevation angles.

To overcome this challenge, we tilted the whole enclosure system by a few degrees to simulate the instrument being located at a site with a higher latitude than it actually is. This is done using two state-of-the-art car jacks (see Fig. 6), which can elevate the side of the enclosure that points towards the Equator up to 15°. As a result, the very low elevation angles can no longer be measured, as the sun is then blocked by the lid of the enclosure, although this is not an issue. This is because the air mass dependency of the slant column cannot be reliably handled by the GFIT retrieval algorithm at these high solar zenith angles (Wunch et al., 2011). Using this unique approach, both the solar tracker and the rotating cover work properly at high elevation angles, which makes this approach suited for locations at low latitudes.

Since the temperature and relative humidity are much higher than in central Europe, the fan and heater normally used are replaced by two 150 W thermoelectrical coolers. They can keep the temperature at a constant level of 25 °C under normal weather conditions in Uganda, as well as being able to condense water vapor to reduce the relative humidity inside the system.

Our enclosure is, however, suited to work not only at very low latitudes but also at high ones. To test the system under such conditions, we built another enclosure system for the COCCON site next to the TCCON station in Sodankylä at a latitude of 67.4° N (Tu et al., 2020). There, the system has been measuring continuously since 2018, which shows that our system can not only withstand cold winters but is also suitable to measure a large azimuth angle range.

Overall, we developed a system that is universally applicable and can be used for a wide latitude range to enable ground-based GHG measurements worldwide with minimum effort and maximum measurement data.

3.2 Software

For controlling and automating the enclosure system, we developed two independent software programs: ECon and Pyra. The purpose of ECon is to control all safety and enclosure features that are monitored by the PLC, whereas Pyra is used to control the spectrometer and take measurements automatically. Pyra also includes a user interface (UI) through which the operator can set all parameters and observe the current state of the system.

3.2.1 Enclosure control (ECon)

The enclosure control software ECon was already a part of the first enclosure version (Heinle and Chen, 2018). There, a microcontroller program is used to control the enclosure features, such as opening and closing the rotating cover, analyzing the rain sensor data, powering the spectrometer and monitoring the UPS. For the new version, we separated these safety operations from the measurement-related software that is running on a Windows computer to make these features fail-safe. As the microcontroller is replaced by a PLC in the new version, the ECon software needed to be renewed as well.

ECon is structured as a sequence control that loops through the main program, which is grouped into several functions, over and over again. These functions include, for example, the detection of any alarm caused by the UPS, encoder or power failures; the request of the current solar azimuth angle and the control of the cover motor; and other outputs such as relays or signal lamps.

The most safety-relevant function is the control of the cover motor. The program is structured in such a way that closing the cover is prioritized in any condition. Even in the event of a reed sensor failure, the program will make sure that the cover closes correctly by evaluating the sensor signals, which are implemented redundantly.

Furthermore, ECon monitors whether the ethernet connections to the computer, spectrometer and internet are working properly. If any malfunction is detected, the program automatically restarts the spectrometer, computer or router, depending on the kind of failure, by briefly interrupting the power supply to the respective device using relays. This approach ensures a minimum requirement of human interactions if malfunctions occur, which is particularly beneficial for operating very remote sites.

To keep the temperature within a predefined range, ECon also controls the temperature inside the enclosure by powering either the heater or the fan, depending on the actual and the given nominal temperature.

3.2.2 Automation software (Pyra)

In order to control the measurements of the spectrometers automatically, it was necessary to develop software that covers all the tasks that a human operator normally does to perform the measurements. We decided to use Python as the programming language to develop both the automation software and a user interface that allows an operator to set all necessary parameters and observe the current state of the system. The program runs all the time on each enclosure computer and serves as a juncture between the spectrometer, enclosure system and operator. Since the measurements are based on the spectral analysis of the sun, we have named the program Pyra, which is a combination of the programming language Python and the name of the Egyptian sun god Ra.

The manufacturer Bruker provides the EM27/SUN spectrometers with the two independent software components OPUS and CamTracker, to control both the spectrometer itself and the camera-based solar tracker that is attached to the spectrometer. Pyra does not replace these two software elements but provides the possibility to start, stop and control them automatically. Besides these necessary tasks, Pyra also monitors the operating system and the spectrometer to detect malfunctions such as insufficient disk space or non-working connections. Furthermore, it evaluates whether the environmental conditions are suited for measurements and logs each event to a file.

Pyra has four different operating modes: the manual one, in which the operator can start and stop the measurements with just one click; two semi-automated modes, in which Pyra starts and stops the measurements based on either a defined time or the solar zenith angle (SZA) range; and the fully automated mode. In the latter, Pyra evaluates the direct solar radiation sensor data and combines them with the SZA information calculated online to start and stop the measurements whenever the environmental conditions are suitable.

A more detailed description about the features of Pyra can be found in Appendix A.

Although Pyra was developed to automate the process of EM27/SUN spectrometers that are operated in our enclosure system, it can also be used without this system or in a different shelter. In this case, only the fully automated mode no longer works, as the information from the direct solar radiation sensor is not available. However, all the other modes work, which leads to less human effort and more reliable measurements.

All the aforementioned features of Pyra are combined in a common user interface (see Fig. 7). It is a clear and handy interface that allows any operator to make all the necessary settings for performing automated measurements using EM27/SUN spectrometers. In total, there are three Pyra tabs (measurement, configuration and log) and one ECon tab, which we also included in this user interface. The ECon tab allows us to control the PLC that operates the enclosure system (for details, see Sect. 3.2.1). Thus, the program itself runs not on the enclosure computer but on the PLC, which makes the safety-related features fail-safe. As the PLC does not provide its own graphical user interface, we decided to include these functions – such as controlling the cover motor, heater, fan, relays etc. – in the Pyra UI as well. For that, the Python library *snap7* is used, which makes it possible to communicate with a Siemens S7 PLC using an ethernet connection.

3.2.3 Automated retrieval process

For a fully automated greenhouse gas observation network, not only the measurements need to be autonomous; the data processing also needs to be autonomous. Therefore, we automated the data processing chain as well.

At the end of a measurement day, each enclosure computer automatically uploads all the interferograms and weather data via an SSH connection to our Linux cloud server at the Leibniz Supercomputing Center in Garching. After about 5 d, when the a priori vertical pressure profiles from NCEP (National Centers for Environmental Prediction) are available, the retrieval algorithm converts the information from the interferograms into concentrations. The retrieval algorithm used is GGG2014 (Wunch et al., 2015), which is also used to retrieve all the TCCON data. We applied the standard TCCON parameters, including the air-mass-independent correction factors. The spectral windows for retrieving diverse gas species are slightly modified according to the EGI setup (Hedelius et al., 2016).

4 Network setup

We tested the automated network consisting of five spectrometers in a measurement campaign in August 2018 (Dietrich et al., 2019), before the permanent network was installed in September 2019. In addition, our first enclosure system has been permanently measuring on the university rooftop since 2016.

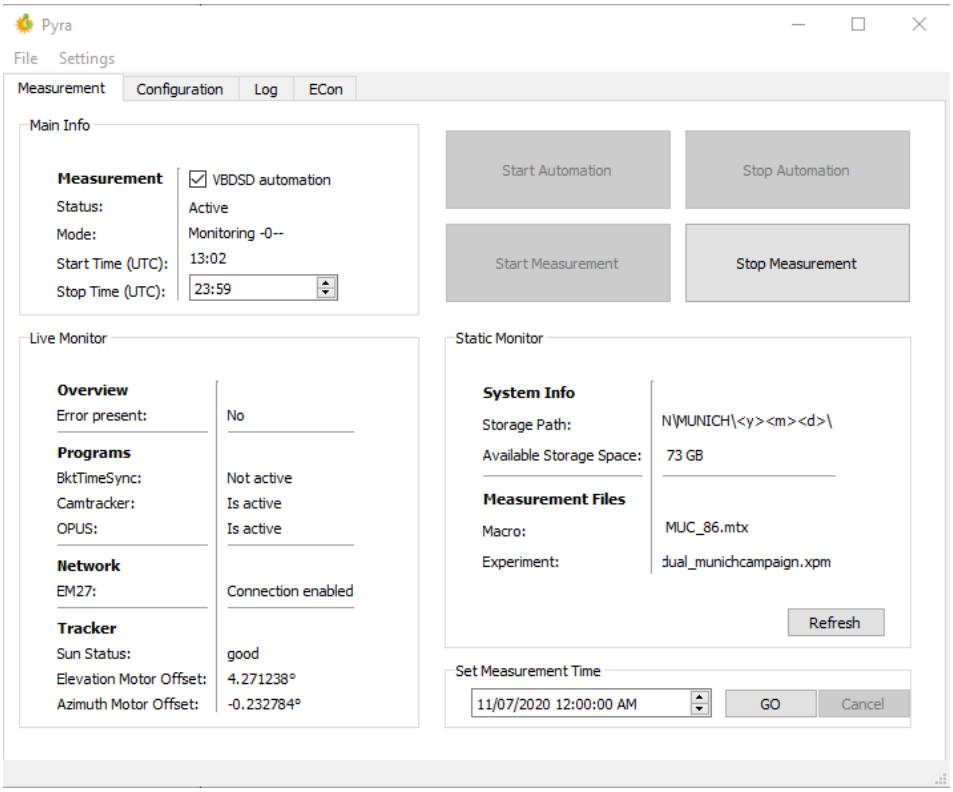

Figure 7. User interface for the control software, Pyra. In total there are four different tabs (*Measurement, Configuration, Log* and *Enclosure control*) that can be selected. In this image, the measurement tab is shown.

4.1 Test campaign – Munich, August 2018

After building a total of five enclosure systems, we established the first fully automated GHG sensor network based on the differential column measurement principle (Chen et al., 2016) in a 1-month measurement campaign in Munich.

To test our enclosure systems and the network configuration, we borrowed spectrometers from KIT and the German Aerospace Center (DLR). In addition to our long-term operating station in the inner city, we set up a system in each compass direction (see red shaded enclosure systems in Fig. 8). A distance of approximately 20 km was selected between the downtown station and each outer station, to ensure that the outer stations are not directly affected by the city emissions if they are located upwind.

Thanks to the automation, we were able to take measurements on each of the 25 sunny days in August, both weekdays and weekends, mostly from very early in the morning to late evening (approx. 07:00 to 20:00 CEST). This kept human interactions to a minimum and restricted them mostly to setting up and disassembling the enclosure systems on the rooftops that we used as measurement sites. Therefore, this campaign was characterized by a very small effort as well as a very high data volume. These results are the desired outcomes of such campaigns and are also the foundation for using this kind of setup for a permanent urban GHG observation network.

4.2 Permanent Munich GHG network setup

Although the configuration of the outer stations in the August 2018 campaign was well suited for capturing the background concentrations, this setup cannot be used to determine the emissions of the city center of Munich separately from its outer surroundings. Instead, the greater Munich area emissions are captured as well. As our focus is emissions from the city itself, we decided to go closer to the city boundaries for our permanent sensor network. The distance between the downtown station and each outer station was halved to 10 km (see green enclosure systems in Fig. 8). Thus, the outer stations are located approximately at the city boundaries of Munich. The second benefit of such a dense sensor setup is that it can be better used for validating concentration gradients measured by satellites. Due to the unique dataset of our sensor network, the NASA satellites OCO-2 (Crisp et al., 2017) and OCO-3 (Eldering et al., 2019) have been measuring CO_2 concentrations over Munich in the target mode since spring 2020. The area OCO-2 can cover over Munich in this mode is approximately 21 km × 13 km. As the satellite trajectory is not exactly aligned on the north–south axis, the distance

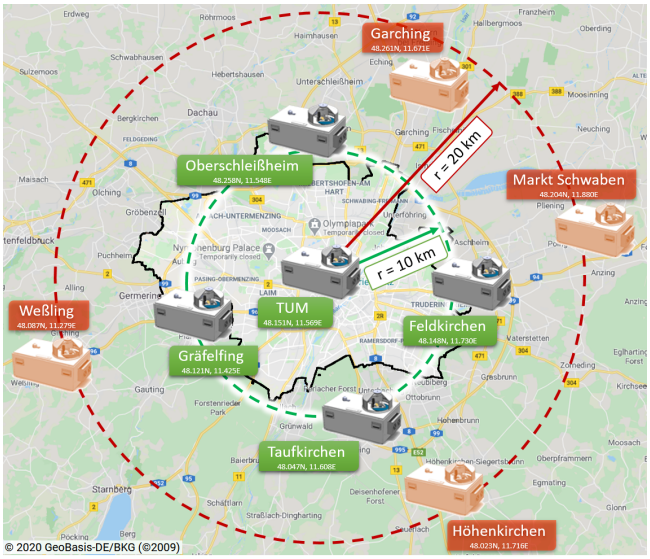

Figure 8. Map of the greater Munich area together with the two different sensor network setups that have been implemented. The urban area itself (indicated by the black border) is largely contained within the inner green dashed circle in the center, which represents the current setup of the stationary network. The light red shaded sensor systems, together with the center station, represent the setup during our 2018 summer campaign. Both setups are characterized by a center station and a station in each compass direction to measure the inflow and outflow of GHG concentrations under arbitrary wind conditions. Map data are from © Google Maps.

of 10 km between the inner and outer stations is optimal for capturing the urban concentration gradients.

In addition to the relocation, the enclosure systems were slightly improved based on the experiences from the August 2018 campaign. In particular, this includes the addition of a direct solar radiation sensor in order to start and stop the measurements depending on the actual weather conditions. Furthermore, we replaced the three borrowed spectrometers with our own ones so that all five instruments can measure long-term.

All in all, we were able to set up MUCCnet, the first permanent urban column concentration network for GHGs, in September 2019 using our own five spectrometers. Since this date, we have been measuring not only the absolute GHG concentration trend of Munich but also the city gradients, which will be used to determine the urban GHG emissions in Munich over the years, as well as to find unknown emission sources.

5 Results

Since 2015, we have been continuously measuring the GHG concentrations in Munich with at least one instrument. Over time, the amount of data has increased as we have improved our automation and used more and more instruments.

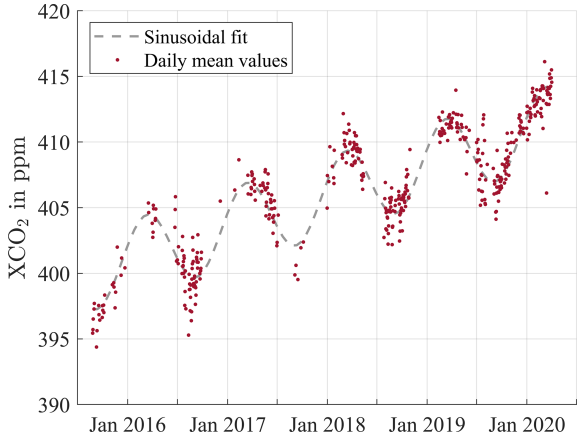

Figure 9. Daily mean values of the CO_2 measurements from the downtown station in Munich. The concentrations follow the globally rising trend. Furthermore, the seasonal cycle with lower concentrations in summer and higher concentrations in winter is clearly visible for the 5-year period shown.

5.1 Seasonal cycle

In Fig. 9, we show the measurement curve of our downtown station over the first 5 years of measurements. In order to display the seasonal cycle, we use a sinusoidal function of the form

$$c_{CO_2}(t) = a \cdot \left(\sin\left(\frac{2\pi(t-b)}{365}\right)\right) + ct + d \quad (1)$$

with the parameters a to d to be fitted. One can clearly see the globally rising trend in CO_2 (about 2.4 ppm yr^{-1}), as well as the seasonal cycle over the 5-year period.

Although the entire period from fall 2015 to summer 2020 is covered, some times within this range yield a much greater volume of data than others. These high-density data clusters represent our campaigns in summer 2017 and 2018. A further hot spot can be detected in fall 2016, when the first version of our enclosure system (Heinle and Chen, 2018) was established and intensively tested in the semi-automated mode. Since summer 2019, the fully automated enclosure system has been measuring whenever the weather conditions are suitable, which results in a very high and dense data volume.

In total, we have measured on 498 d throughout the last 5 years. Of these, only days with continuous measurements of at least 1 h are taken into account. The ratio of measurement days compared to non-measurement days is about 17 % for the time period before summer 2019. Once full automation was established, this ratio increased to about 52 %, which shows the great benefit of our fully automated sensor network approach. In this calculation all days are taken into account, regardless of whether the measuring conditions were good or bad.

Figure 10. Calibration measurements of all our five sensor systems on the roof of our institute's building. One can see four slightly different versions of our enclosure systems.

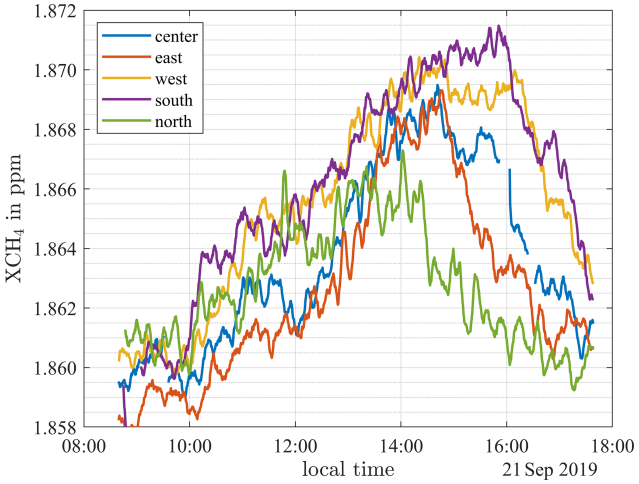

Figure 11. CH_4 measurement values (5 min average) from all five stations during our Oktoberfest 2019 campaign on 21 September 2019. The concentration gradients between the single stations are clearly visible, which indicates the presence of strong CH_4 sources in the city.

5.2 Side-by-side and urban gradient comparison

The results in the previous section show that our automation works and that we are able to gather a lot of GHG measurement data. The final goal of our network is, however, to quantify the urban emissions. For that, the gradients between the single stations need to be analyzed. As the concentration enhancements of column-averaged dry-air mole fractions are quite small for an urban emission source, it is absolutely necessary to calibrate the instruments regularly. In addition to the calibration of absolute concentration values during measurements next to the TCCON station in Karlsruhe, the relative comparison between the single instrument is even more decisive. Therefore, we calibrate all instruments regularly with respect to our defined standard represented by the instrument ma61. Figure 10 shows the setup of this kind of side-by-side measurement day, where five automated sensor systems measure next to each other on our university roof.

For each instrument and gas species, a constant correction factor f (see Table B1) is determined to convert the raw concentration value c_{raw} to the corrected concentration value c_{corr} using linear scaling:

$$c_{\mathrm{corr}} = \frac{c_{\mathrm{raw}}}{f}. \tag{2}$$

As an absolute reference value, we will use the instrument that was calibrated at a TCCON station most recently. So far, the most recent correction value determined by Frey et al. (2019) before shipping the instruments from Bruker to Munich has been used (see Table B2).

Figure 11 shows the CH_4 gradients of a standard measurement day on a Saturday during Oktoberfest 2019. It indicates that our sensor network can detect the differences in CH_4 concentrations well, which allows us to determine the urban emissions using these measurements as an input. Furthermore, one can see that our automated network allows us to measure not only on weekdays but also on weekends from early morning to evening, without the need for human resources.

In Fig. 12, we show the CO_2 concentration enhancements above the background concentration for the four outer-city stations depending on the wind direction. For this purpose, we use an ultrasonic wind sensor (Gill WindObserver II) on a roof in the inner city of Munich (48.148° N, 11.573° E, 24 m a.g.l.). To determine the background concentration, we use the data from all of our measurement stations and determine the lowest measurement point for each time step. Afterwards, a moving average with a window size of 4 h is used to smooth the curve as we assume that the background concentration must not change rapidly. For each station, a polar histogram shows where the concentration enhancements originate and how frequent they are. In contrast to a standard wind rose, the different colors indicate the strength of the concentration enhancement; yellow means low and red high enhancement. The wind speed is displayed by the distance of the respective cell to the center point of each circle.

One can see clearly that for all four stations the enhancements are higher towards the city. For the eastern station, for example, the highest enhancements, indicated by the reddish color, are located in the west. These results indicate that the captured GHGs are mainly generated in the city and that our network is able to detect and quantify such urban emitters. Due to technical issues, not all stations started their measurements at the same time. Therefore, the data volume collected at the southern station, which started no earlier than May 2020, is much smaller. An overview of when each station

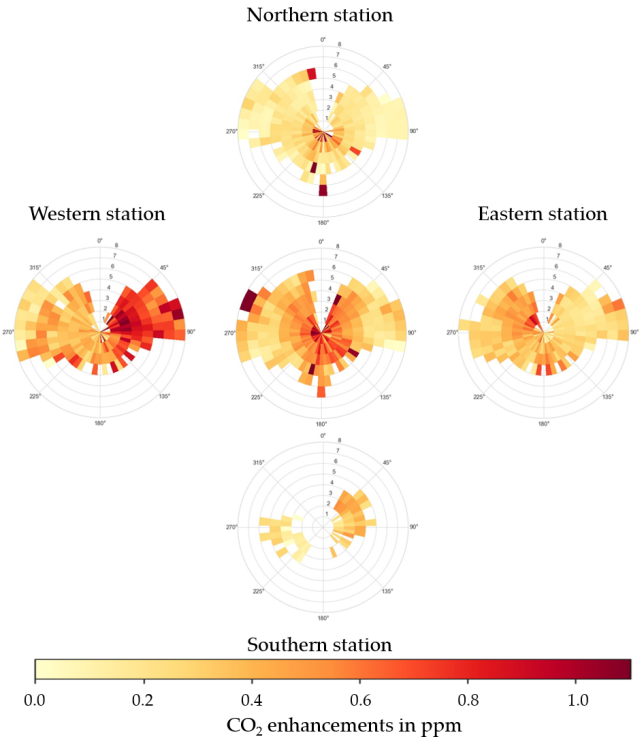

Figure 12. Concentration enhancements over the background for each of the five stations displayed as a polar histogram. The CO_2 enhancements are represented by the different colors (low (yellow) to red (high)). The wind direction is indicated by the location of the respective cells in the circle, and the wind speed by the distance of the cells to the center point.

Table 1. Start of operation including the number of measurements taken by each station so far (until 12 August 2020).

Instrument	Location	Start date	Data points
ma61	Center	September 2015	1550k
mb86	East	August 2018	850k
mc15	West	September 2019	310k
md16	North	December 2019	270k
me17	South	May 2020	16k

started its measurements in the permanent network, including the data collected so far, is shown in Table 1.

5.3 Influences of the COVID-19 lockdown on urban concentration gradients

Thanks to the automation, we took measurements throughout the COVID-19 lockdown in spring 2020, which resulted in a unique dataset showing the influence of such a drastic event on the urban GHG gradients of a city like Munich. Figure 13 displays the gradients between the measurements of the inner-city station and the background concentrations (cf. Sect. 5.2).

All concentration gradients are clustered into biweekly bins. In Fig. 13, the median of these bins is displayed as the blue curve. The error bars indicate the 1σ standard deviation of these biweekly distributions. In addition, volume of traffic in Munich is displayed in red using the congestion rate provided by TomTom International BV. Furthermore, the COVID-19 lockdown period is shown as the grey shaded area.

The plot demonstrates that the lockdown had a significant impact on traffic flow. The CO_2 enhancements show a similar pattern throughout the first half of the year 2020. Based on the regression plot, there seems to be a correlation between the reduced traffic volume and the lower CO_2 enhancements ($R^2 = 0.63$). Both curves first decrease and then increase again after the strict restrictions were gradually loosened.

However, our statistical approach, which uses about 100 000 measurement points, shows large variations in the CO_2 enhancements for the single bins. Such high variations are, however, not concerning as the approach does not take into account wind speed and direction, for example. Furthermore, the assumption of homogeneously distributed emissions sources does not reflect the truth, and photosynthetic effects are not considered. Therefore, it can only serve as a first indication of how the emissions were reduced during the lockdown period. In the future, we will apply more sophisticated modeling approaches to quantify the emissions.

6 Conclusion

We present the world's first permanent urban GHG column network consisting of five compact solar-tracking spectrometer systems distributed in and around Munich (MUCCnet). We developed the hardware and software to establish this kind of a fully automated GHG sensor network for quantifying large-area emission sources, such as cities. Both the enclosure system and the related Python program for automating the measurement process can be used by the community to build up similar sensor networks in cities worldwide. Also, COCCON would benefit greatly from this kind of automated system, as the current approach of operating EM27/SUN spectrometers in this network still requires man power on site to start up measurements and to protect the spectrometer from adverse meteorological conditions. Permanent and long-term observations will help to improve the understanding of the global carbon cycle.

With our sensor systems, we carried out several test campaigns between 2016 and 2019 and finally set up the permanent urban GHG sensor network based on the differential column methodology in fall 2019. The results show the advantages of this kind of automated network, such as very high data volume, low personnel effort and high data quality. Due to the very frequent measurements that were taken independent of the day of the week or the season, this study shows

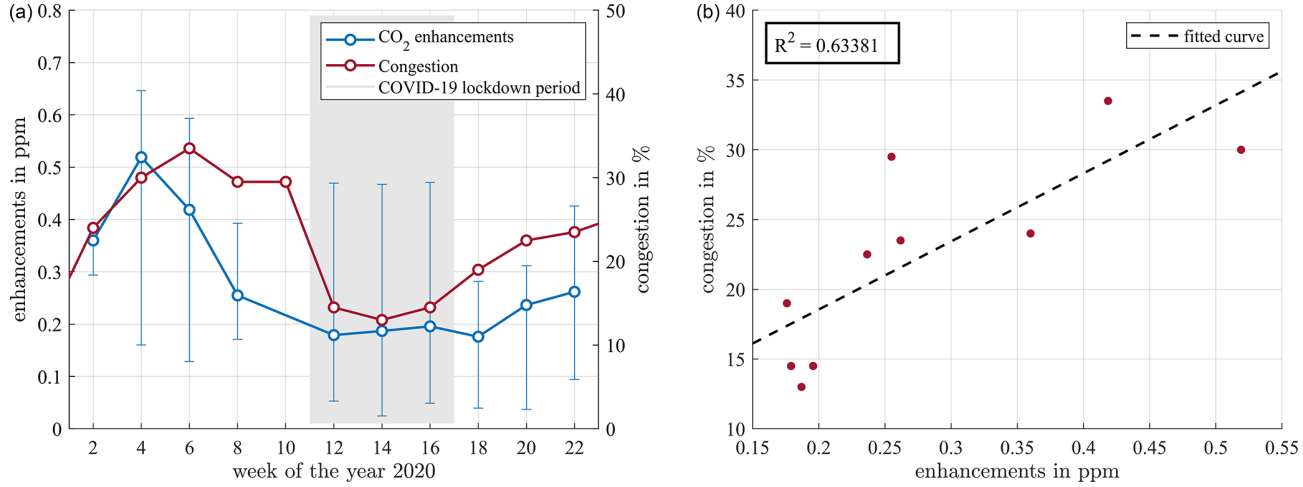

Figure 13. Correlations between the CO_2 enhancements over the background measured at our inner-city station in Munich and the traffic amount represented by the congestion rate (**a**: time series; **b**: regression plot). The time period includes the COVID-19 lockdown in spring 2020. We show the median trend of all column concentration gradients clustered into biweekly bins. The error bars show the 1σ standard deviation of all enhancements within the respective 2-week period. Traffic data are from © 2020 TomTom International BV.

that our network can effectively detect both the globally rising trend of CO_2 concentrations and the seasonal cycle.

The final goal of this kind of network is the quantification of urban GHG emissions. For that, the concentration gradients between the downwind and upwind stations are decisive, as they represent the anthropogenic emissions superimposed with biological processes. Our results indicate that these gradients can be captured clearly with our sensor setup. Additional analyses, including wind information, show that the city causes these enhancements.

Furthermore, the network can be used to validate GHG satellites in a unique way, as not only absolute values but also concentration gradients can be compared. Since spring 2020, the NASA OCO-2 and OCO-3 satellites have been measuring urban CO_2 concentration gradients in Munich using the spatially highly resolved target mode in a recurring pattern to compare the satellite measurements with our ground-based ones.

With the benefit of full automation, we were also able to measure concentration gradients during the COVID-19 lockdown period in spring 2020. The results show a possible correlation between the CO_2 column concentration gradients and the traffic amount, both of which appear to be drastically affected by the lockdown.

In order to quantify the Munich GHG emissions, we are currently developing an atmospheric transport model based on Bayesian inversion. This kind of modeling framework will help us quantify Munich's GHG emissions in the future and find correlations with parameters such as time of the day, season and weather conditions. Furthermore, we will use our rich dataset to detect and quantify unknown GHG emission sources.

In summary, this study provides the framework for establishing a permanent GHG sensor network to determine urban concentration gradients using column measurements over a wide range of latitudes. The characteristics of the hardware presented here – such as high reliability, ease of use and low operating costs – form the basis for it to become a new standard for monitoring urban GHG concentrations.

Appendix A: Pyra – software features

To control the spectrometer program OPUS, we use the Microsoft Windows technology *dynamic data exchange* (DDE), which is also supported by OPUS. It is a protocol for exchanging data based on the client–server model and allows us to send requests, such as starting a measurement or loading a specific setting file, to OPUS. With the help of DDE, combined with an MTX macro file for OPUS, Pyra can start recurring measurements of the spectrometer. The necessary settings are stored in an XPM experiment file and are loaded into the program in the same way.

Communication with the solar tracker program CamTracker is simpler, as this program's settings no longer need to be changed after the initialization. Therefore, we asked the manufacturer Bruker to implement an autostart option for the tracker. Whenever CamTracker is called with this option, the solar tracker automatically aligns its two mirrors with the calculated live position of the sun and enables the tracking of the sun. Once the program has been terminated, the tracker automatically moves back to its parking position.

In order to detect malfunctions, Pyra is equipped with several live monitoring functions. It monitors whether the two programs OPUS and CamTracker are still running correctly every 0.2 s. If they are not, it automatically restarts the non-working program to proceed with the measurements. Furthermore, the log files of CamTracker are read continuously, which allows us to detect automatically if the solar tracker is not tracking the sun correctly anymore, for example. Such a behavior is quite common as the solar tracker uses a camera-based approach to follow the sun over the course of the day. In cloudy conditions, the algorithm sometimes mistakenly detects objects other than the sun, resulting in incorrect tracking. In such a case, the tracking is restarted using the calculated position of the sun at the given coordinates and time. In addition to trying to solve the error automatically, Pyra also sends an error notification email to an operator, whose email address can be defined in the settings.

Appendix B: EM27/SUN calibration factors

Table B1. Scaling factors of the side-by-side measurements with reference to our standard instrument ma61 for CO_2 and CH_4.

No.	Date	Species	ma61	mb86	mc15	md16	me17
1	August 2018	CO_2 (R^2)	1 (1.00)	0.99998 (0.99)	–	–	–
		CH_4 (R^2)	1 (1.00)	0.99966 (0.99)	–	–	–
2	February 2019	CO_2 (R^2)	1 (1.00)	0.99960 (0.99)	–	–	–
		CH_4 (R^2)	1 (1.00)	0.99996 (0.99)	–	–	–
3	September 2019	CO_2 (R^2)	1 (1.00)	–	0.99922 (0.96)	–	–
		CH_4 (R^2)	1 (1.00)	–	0.99946 (0.99)	–	–
4	December 2019	CO_2 (R^2)	1 (1.00)	0.99995 (0.98)	–	1.00034 (0.97)	–
		CH_4 (R^2)	1 (1.00)	0.99999 (0.86)	–	1.00041 (0.90)	–
5	November 2020	CO_2 (R^2)	1 (1.00)	–	–	–	0.99989 (0.98)
		CH_4 (R^2)	1 (1.00)	–	–	–	1.00175 (0.99)

Table B2. Scaling factors according to Frey et al. (2019) of our five EM27/SUN instruments with respect to the reference EM27/SUN (S/N 037) at KIT.

Instrument	S/N	Date (yyyymmdd)	CO_2	CH_4	CO
ma61	61	20170713	0.9993	0.9996	1.0000
mb86	86	20180214	0.9986	1.0002	0.9975
mc15	115	20190725	0.9998	1.0005	1.0272
md16	116	20191014	0.9998	0.9996	1.0055
me17	117	20191031	1.0015	1.0004	1.0058

Code and data availability. The Python software Pyra and the measurement data can be provided by the authors upon request.

The measurement data are also available at http://atmosphere.ei.tum.de/ (Dietrich et al., 2021).

Author contributions. FD and JC conceived the study and developed the concept; FD led the hardware and software development as well as the setup of the sensor network. FD, BV and BR built the enclosure systems. PA, BV and FD developed the software Pyra. FD and JC performed the measurements. FD, JC and NN analyzed the measurement data. FD and JC wrote the manuscript.

Competing interests. The authors declare that they have no conflict of interest.

Acknowledgements. We thank Ludwig Heinle for developing the first version of a semi-automated enclosure system; Frank Hase for testing and calibrating the instruments prior to the delivery and for providing us with two spectrometers each for our August 2018 and Oktoberfest 2019 campaign; André Butz for providing us with his EM27/SUN in our August 2018 campaign; Jacob Hedelius for his support in all matters concerning the GFIT retrieval algorithm; Stephan Hachinger for helping us regarding the automated retrieval process on the Linux cloud; Jonathan Franklin, Taylor Jones, Andreas Luther and Ralph Kleinscheck for their support during our measurement campaigns; Neil Humpage and Harmut Boesch for testing our enclosure system in Uganda; Martin Wild, Norbert Tuschl, Abdurahim Bingöl, Sebastian Zunterer and Bernhard Obermaier for manufacturing the enclosure systems; Markus Garhammer and Mark Wenig for providing us with meteorological data; First Mayor Andreas Janson (Feldkirchen) and the municipalities of Gräfelfing, Markt Schwaben, Oberschleißheim and Taufkirchen as well as Lothar Lauterbach from the ARCONE Technology Center Höhenkirchen, who allowed us to use their rooftops as measurement sites; and our students Andreas Forstmaier, Adrian Wenzel, Nikolas Hars, Jared Matzke, Yiming Zhao, Xu Hang, Dingcong Lu, Xiao Bi and Michal Wedrat for their help during the campaigns and the network setup as well as programming helpful automation scripts and supporting the CAD model. TUM is grateful to Stefan Schwietzke and Daniel Zavala-Araiza for helpful conversation in their role as part of the Office of the Chief Scientist of the Climate and Clean Air Coalition Methane Science Studies (MSS), which are funded by the Environmental Defense Fund, the European Commission, the companies of the Oil and Gas Climate Initiative, and the United Nations Environment Programme. TUM is additionally grateful for invitations to participate in workshops hosted by UNEP in the context of the Methane Science Studies.

Financial support. This research has been supported by the Deutsche Forschungsgemeinschaft (DFG, German Research Foundation) (grant nos. CH 1792/2-1, INST 95/1544). Jia Chen is supported by the Technical University of Munich – Institute for Advanced Study, funded by the German Excellence Initiative and the European Union Seventh Framework Programme under grant agreement number 291763.

This work was supported by the German Research Foundation (DFG) and the Technical University of Munich (TUM) in the framework of the Open Access Publishing Program.

Review statement. This paper was edited by Markus Rapp and reviewed by David Griffith and one anonymous referee.

References

Bréon, F. M., Broquet, G., Puygrenier, V., Chevallier, F., Xueref-Remy, I., Ramonet, M., Dieudonné, E., Lopez, M., Schmidt, M., Perrussel, O., and Ciais, P.: An attempt at estimating Paris area CO_2 emissions from atmospheric concentration measurements, Atmos. Chem. Phys., 15, 1707–1724, https://doi.org/10.5194/acp-15-1707-2015, 2015.

Butz, A., Dinger, A. S., Bobrowski, N., Kostinek, J., Fieber, L., Fischerkeller, C., Giuffrida, G. B., Hase, F., Klappenbach, F., Kuhn, J., Lübcke, P., Tirpitz, L., and Tu, Q.: Remote sensing of volcanic CO_2, HF, HCl, SO_2, and BrO in the downwind plume of Mt. Etna, Atmos. Meas. Tech., 10, 1–14, https://doi.org/10.5194/amt-10-1-2017, 2017.

Chen, J., Viatte, C., Hedelius, J. K., Jones, T., Franklin, J. E., Parker, H., Gottlieb, E. W., Wennberg, P. O., Dubey, M. K., and Wofsy, S. C.: Differential column measurements using compact solar-tracking spectrometers, Atmos. Chem. Phys., 16, 8479–8498, https://doi.org/10.5194/acp-16-8479-2016, 2016.

Chen, J., Dietrich, F., Maazallahi, H., Forstmaier, A., Winkler, D., Hofmann, M. E. G., Denier van der Gon, H., and Röckmann, T.: Methane emissions from the Munich Oktoberfest, Atmos. Chem. Phys., 20, 3683–3696, https://doi.org/10.5194/acp-20-3683-2020, 2020.

Crisp, D., Pollock, H. R., Rosenberg, R., Chapsky, L., Lee, R. A. M., Oyafuso, F. A., Frankenberg, C., O'Dell, C. W., Bruegge, C. J., Doran, G. B., Eldering, A., Fisher, B. M., Fu, D., Gunson, M. R., Mandrake, L., Osterman, G. B., Schwandner, F. M., Sun, K., Taylor, T. E., Wennberg, P. O., and Wunch, D.: The on-orbit performance of the Orbiting Carbon Observatory-2 (OCO-2) instrument and its radiometrically calibrated products, Atmos. Meas. Tech., 10, 59–81, https://doi.org/10.5194/amt-10-59-2017, 2017.

Dietrich, F., Chen, J., Reger, B., Matzke, J., Forstmaier, A., Bi, X., Luther A., Frey, M., Hase, F., and Butz, A.: First fully-automated differential column network for measuring GHG emissions tested in Munich, EGU General Assembly 2019, Vienna, Austria, 7–12 April 2019, EGU2019–13327, https://doi.org/10.13140/RG.2.2.26867.17441, 2019.

Dietrich, F., Rissmann, M., Makowski, M., and Chen, J.: Column Greenhouse Gas Concentrations, available at: http://atmosphere.ei.tum.de, last access: 8 February 2021.

Eldering, A., Taylor, T. E., O'Dell, C. W., and Pavlick, R.: The OCO-3 mission: measurement objectives and expected performance based on 1 year of simulated data, Atmos. Meas. Tech., 12, 2341–2370, https://doi.org/10.5194/amt-12-2341-2019, 2019.

Feigenwinter, C., Vogt, R., and Christen, A.: Eddy Covariance Measurements Over Urban Areas, in: Eddy Covariance: A Practical Guide to Measurement and Data Analysis, edited by Aubinet,

M., Vesala, T., and Papale, D., Springer Atmospheric Sciences, Springer Netherlands, Dordrecht, https://doi.org/10.1007/978-94-007-2351-1_16, 377–397, 2012.

Frey, M., Sha, M. K., Hase, F., Kiel, M., Blumenstock, T., Harig, R., Surawicz, G., Deutscher, N. M., Shiomi, K., Franklin, J. E., Bösch, H., Chen, J., Grutter, M., Ohyama, H., Sun, Y., Butz, A., Mengistu Tsidu, G., Ene, D., Wunch, D., Cao, Z., Garcia, O., Ramonet, M., Vogel, F., and Orphal, J.: Building the COllaborative Carbon Column Observing Network (COCCON): long-term stability and ensemble performance of the EM27/SUN Fourier transform spectrometer, Atmos. Meas. Tech., 12, 1513–1530, https://doi.org/10.5194/amt-12-1513-2019, 2019.

Gisi, M., Hase, F., Dohe, S., and Blumenstock, T.: Camtracker: a new camera controlled high precision solar tracker system for FTIR-spectrometers, Atmos. Meas. Tech., 4, 47–54, https://doi.org/10.5194/amt-4-47-2011, 2011.

Gisi, M., Hase, F., Dohe, S., Blumenstock, T., Simon, A., and Keens, A.: XCO$_2$-measurements with a tabletop FTS using solar absorption spectroscopy, Atmos. Meas. Tech., 5, 2969–2980, https://doi.org/10.5194/amt-5-2969-2012, 2012.

Gurney, K. R., Romero-Lankao, P., Seto, K. C., Hutyra, L. R., Duren, R., Kennedy, C., Grimm, N. B., Ehleringer, J. R., Marcotullio, P., Hughes, S., Pincetl, S., Chester, M. V., Runfola, D. M., Feddema, J. J., and Sperling, J.: Climate change: Track urban emissions on a human scale, Nature, 525, 179–181, https://doi.org/10.1038/525179a, 2015.

Hase, F., Frey, M., Blumenstock, T., Groß, J., Kiel, M., Kohlhepp, R., Mengistu Tsidu, G., Schäfer, K., Sha, M. K., and Orphal, J.: Application of portable FTIR spectrometers for detecting greenhouse gas emissions of the major city Berlin, Atmos. Meas. Tech., 8, 3059–3068, https://doi.org/10.5194/amt-8-3059-2015, 2015.

Hase, F., Frey, M., Kiel, M., Blumenstock, T., Harig, R., Keens, A., and Orphal, J.: Addition of a channel for XCO observations to a portable FTIR spectrometer for greenhouse gas measurements, Atmos. Meas. Tech., 9, 2303–2313, https://doi.org/10.5194/amt-9-2303-2016, 2016.

Hedelius, J. K., Viatte, C., Wunch, D., Roehl, C. M., Toon, G. C., Chen, J., Jones, T., Wofsy, S. C., Franklin, J. E., Parker, H., Dubey, M. K., and Wennberg, P. O.: Assessment of errors and biases in retrievals of X_{CO_2}, X_{CH_4}, X_{CO}, and X_{N_2O} from a $0.5\,cm^{-1}$ resolution solar-viewing spectrometer, Atmos. Meas. Tech., 9, 3527–3546, https://doi.org/10.5194/amt-9-3527-2016, 2016.

Heinle, L. and Chen, J.: Automated enclosure and protection system for compact solar-tracking spectrometers, Atmos. Meas. Tech., 11, 2173–2185, https://doi.org/10.5194/amt-11-2173-2018, 2018.

Helfter, C., Famulari, D., Phillips, G. J., Barlow, J. F., Wood, C. R., Grimmond, C. S. B., and Nemitz, E.: Controls of carbon dioxide concentrations and fluxes above central London, Atmos. Chem. Phys., 11, 1913–1928, https://doi.org/10.5194/acp-11-1913-2011, 2011.

Humpage, N., Boesch, H., Dietrich, F., and Chen, J.: Testing an automated enclosure system for a ground-based greenhouse gas remote sensing spectrometer; application to the validation of Sentinel-5 Precursor carbon monoxide and methane, in: Copernicus Sentinel-5 Precursor Validation Team Workshop, 11–14 November 2019, Frascati (Rome), Italy, https://doi.org/10.13140/RG.2.2.18535.80808, 2019.

Jones, T. S., Franklin, J. E., Chen, J., Dietrich, F., Hajny, K. D., Paetzold, J. C., Wenzel, A., Gately, C., Gottlieb, E., Parker, H., Dubey, M., Hase, F., Shepson, P. B., Mielke, L. H., and Wofsy, S. C.: Assessing Urban Methane Emissions using Column Observing Portable FTIR Spectrometers and a Novel Bayesian Inversion Framework, Atmos. Chem. Phys. Discuss. [preprint], https://doi.org/10.5194/acp-2020-1262, in review, 2021.

Kim, J., Shusterman, A. A., Lieschke, K. J., Newman, C., and Cohen, R. C.: The BErkeley Atmospheric CO2 Observation Network: field calibration and evaluation of low-cost air quality sensors, Atmos. Meas. Tech., 11, 1937–1946, https://doi.org/10.5194/amt-11-1937-2018, 2018.

Klappenbach, F., Bertleff, M., Kostinek, J., Hase, F., Blumenstock, T., Agusti-Panareda, A., Razinger, M., and Butz, A.: Accurate mobile remote sensing of XCO2 and XCH4 latitudinal transects from aboard a research vessel, Atmos. Meas. Tech., 8, 5023–5038, https://doi.org/10.5194/amt-8-5023-2015, 2015.

Lamb, B. K., Cambaliza, M. O. L., Davis, K. J., Edburg, S. L., Ferrara, T. W., Floerchinger, C., Heimburger, A. M. F., Herndon, S., Lauvaux, T., Lavoie, T., Lyon, D. R., Miles, N., Prasad, K. R., Richardson, S., Roscioli, J. R., Salmon, O. E., Shepson, P. B., Stirm, B. H., and Whetstone, J.: Direct and Indirect Measurements and Modeling of Methane Emissions in Indianapolis, Indiana, Environ. Sci. Technol., 50, 8910–8917, https://doi.org/10.1021/acs.est.6b01198, 2016.

Luther, A., Kleinschek, R., Scheidweiler, L., Defratyka, S., Stanisavljevic, M., Forstmaier, A., Dandocsi, A., Wolff, S., Dubravica, D., Wildmann, N., Kostinek, J., Jöckel, P., Nickl, A.-L., Klausner, T., Hase, F., Frey, M., Chen, J., Dietrich, F., Nęcki, J., Swolkień, J., Fix, A., Roiger, A., and Butz, A.: Quantifying CH4 emissions from hard coal mines using mobile sun-viewing Fourier transform spectrometry, Atmos. Meas. Tech., 12, 5217–5230, https://doi.org/10.5194/amt-12-5217-2019, 2019.

Makarova, M. V., Alberti, C., Ionov, D. V., Hase, F., Foka, S. C., Blumenstock, T., Warneke, T., Virolainen, Y., Kostsov, V., Frey, M., Poberovskii, A. V., Timofeyev, Y. M., Paramonova, N., Volkova, K. A., Zaitsev, N. A., Biryukov, E. Y., Osipov, S. I., Makarov, B. K., Polyakov, A. V., Ivakhov, V. M., Imhasin, H. Kh., and Mikhailov, E. F.: Emission Monitoring Mobile Experiment (EMME): an overview and first results of the St. Petersburg megacity campaign-2019, Atmos. Meas. Tech. Discuss. [preprint], https://doi.org/10.5194/amt-2020-87, in review, 2020.

McKain, K., Down, A., Raciti, S. M., Budney, J., Hutyra, L. R., Floerchinger, C., Herndon, S. C., Nehrkorn, T., Zahniser, M. S., Jackson, R. B., Phillips, N., and Wofsy, S. C.: Methane emissions from natural gas infrastructure and use in the urban region of Boston, Massachusetts, P. Natl. Acad. Sci. USA, 112, 1941–1946, https://doi.org/10.1073/pnas.1416261112, 2015.

Plant, G., Kort, E. A., Floerchinger, C., Gvakharia, A., Vimont, I., and Sweeney, C.: Large Fugitive Methane Emissions From Urban Centers Along the U.S. East Coast, Geophys. Res. Lett., 46, 8500–8507, https://doi.org/10.1029/2019GL082635, 2019.

Sha, M. K., De Mazière, M., Notholt, J., Blumenstock, T., Chen, H., Dehn, A., Griffith, D. W. T., Hase, F., Heikkinen, P., Hermans, C., Hoffmann, A., Huebner, M., Jones, N., Kivi, R., Langerock, B., Petri, C., Scolas, F., Tu, Q., and Weidmann, D.: Intercomparison of low- and high-resolution infrared spectrometers for ground-

based solar remote sensing measurements of total column concentrations of CO_2, CH_4, and CO, Atmos. Meas. Tech., 13, 4791–4839, https://doi.org/10.5194/amt-13-4791-2020, 2020.

Shusterman, A. A., Teige, V. E., Turner, A. J., Newman, C., Kim, J., and Cohen, R. C.: The BErkeley Atmospheric CO_2 Observation Network: initial evaluation, Atmos. Chem. Phys., 16, 13449–13463, https://doi.org/10.5194/acp-16-13449-2016, 2016.

Toja-Silva, F., Chen, J., Hachinger, S., and Hase, F.: CFD simulation of CO_2 dispersion from urban thermal power plant: Analysis of turbulent Schmidt number and comparison with Gaussian plume model and measurements, J. Wind Eng. Ind. Aerod., 169, 177–193, https://doi.org/10.1016/j.jweia.2017.07.015, 2017.

Tu, Q., Hase, F., Blumenstock, T., Kivi, R., Heikkinen, P., Sha, M. K., Raffalski, U., Landgraf, J., Lorente, A., Borsdorff, T., Chen, H., Dietrich, F., and Chen, J.: Intercomparison of atmospheric CO_2 and CH_4 abundances on regional scales in boreal areas using Copernicus Atmosphere Monitoring Service (CAMS) analysis, COllaborative Carbon Column Observing Network (COCCON) spectrometers, and Sentinel-5 Precursor satellite observations, Atmos. Meas. Tech., 13, 4751–4771, https://doi.org/10.5194/amt-13-4751-2020, 2020.

Viatte, C., Lauvaux, T., Hedelius, J. K., Parker, H., Chen, J., Jones, T., Franklin, J. E., Deng, A. J., Gaudet, B., Verhulst, K., Duren, R., Wunch, D., Roehl, C., Dubey, M. K., Wofsy, S., and Wennberg, P. O.: Methane emissions from dairies in the Los Angeles Basin, Atmos. Chem. Phys., 17, 7509–7528, https://doi.org/10.5194/acp-17-7509-2017, 2017.

Vogel, F. R., Frey, M., Staufer, J., Hase, F., Broquet, G., Xueref-Remy, I., Chevallier, F., Ciais, P., Sha, M. K., Chelin, P., Jeseck, P., Janssen, C., Té, Y., Groß, J., Blumenstock, T., Tu, Q., and Orphal, J.: XCO_2 in an emission hot-spot region: the COCCON Paris campaign 2015, Atmos. Chem. Phys., 19, 3271–3285, https://doi.org/10.5194/acp-19-3271-2019, 2019.

Wunch, D., Toon, G. C., Blavier, J. F., Washenfelder, R. A., Notholt, J., Connor, B. J., Griffith, D. W., Sherlock, V., and Wennberg, P. O.: The total carbon column observing network, Philos. T. R. Soc. A, 369, 2087–112, 2011.

Wunch, D., Toon, G. C., Sherlock, V., Deutscher, N. M., Liu, X., Feist, D. G., and Wennberg, P. O.: Documentation for the 2014 TCCON Data Release, CaltechDATA, https://doi.org/10.14291/tccon.ggg2014.documentation.R0/1221662, 2015.

Xueref-Remy, I., Dieudonné, E., Vuillemin, C., Lopez, M., Lac, C., Schmidt, M., Delmotte, M., Chevallier, F., Ravetta, F., Perrussel, O., Ciais, P., Bréon, F.-M., Broquet, G., Ramonet, M., Spain, T. G., and Ampe, C.: Diurnal, synoptic and seasonal variability of atmospheric CO2 in the Paris megacity area, Atmos. Chem. Phys., 18, 3335–3362, https://doi.org/10.5194/acp-18-3335-2018, 2018.

Zhao, X., Marshall, J., Hachinger, S., Gerbig, C., Frey, M., Hase, F., and Chen, J.: Analysis of total column CO_2 and CH_4 measurements in Berlin with WRF-GHG, Atmos. Chem. Phys., 19, 11279–11302, https://doi.org/10.5194/acp-19-11279-2019, 2019.

B. Copy of "Methane emissions from the Munich Oktoberfest"

The following publication "Methane emissions from the Munich Oktoberfest" by Jia Chen[1], Florian Dietrich[1], Hossein Maazallahi, Andreas Forstmaier, Dominik Winkler, Magdalena E. G. Hofmann, Hugo Denier van der Gon, and Thomas Röckmann is published in Atmospheric Chemistry and Physics [102] and is licensed under CC BY 4.0.

[1]These authors contributed equally to this work.

Atmos. Chem. Phys., 20, 3683–3696, 2020
https://doi.org/10.5194/acp-20-3683-2020

Atmospheric Chemistry and Physics
Open Access
EGU

Methane emissions from the Munich Oktoberfest

Jia Chen[1,5,★], **Florian Dietrich**[1,★], **Hossein Maazallahi**[2,4], **Andreas Forstmaier**[1], **Dominik Winkler**[1], **Magdalena E. G. Hofmann**[3], **Hugo Denier van der Gon**[4], **and Thomas Röckmann**[2]

[1]Environmental Sensing and Modeling, Technical University of Munich (TUM), Munich, Germany
[2]Institute for Marine and Atmospheric research Utrecht, Utrecht University, Utrecht, the Netherlands
[3]Picarro B.V., 's-Hertogenbosch, the Netherlands
[4]Climate, Air and Sustainability, TNO, Utrecht, the Netherlands
[5]Institute for Advanced Study, Technical University of Munich, Garching, Germany
★These authors contributed equally to this work.

Correspondence: Jia Chen (jia.chen@tum.de) and Florian Dietrich (flo.dietrich@tum.de)

Received: 11 August 2019 – Discussion started: 22 October 2019
Revised: 15 January 2020 – Accepted: 5 February 2020 – Published: 27 March 2020

Abstract. This study presents the first investigation of the methane (CH_4) emissions of a large festival. Munich Oktoberfest, the world's largest folk festival, is a potential source of CH_4 as a large amount of natural gas for cooking and heating is used.

In 2018 we measured the CH_4 emissions of Oktoberfest using in situ measurements combined with a Gaussian plume dispersion model. Measurements were taken while walking and biking around the perimeter of the Oktoberfest premises (Theresienwiese) at different times of the day, during the week and at the weekend. The measurements showed enhancements of up to 100 ppb compared to background values and measurements after Oktoberfest. The average emission flux of Oktoberfest is determined as $(6.7 \pm 0.6)\,\mu g\,(m^2\,s)^{-1}$. Additional analyses, including the daily emission cycle and comparisons between emissions and the number of visitors, suggest that CH_4 emissions of Oktoberfest are not due solely to the human biogenic emissions. Instead, fossil fuel CH_4 emissions, such as incomplete combustion or loss in the gas appliances, appear to be the major contributors to Oktoberfest emissions.

Our results can help to develop CH_4 reduction policies and measures to reduce emissions at festivals and other major events in cities. Furthermore, events with a limited duration have not yet been included in the state-of-the-art emission inventories, such as TNO-MACC, EDGAR or IER. Our investigations show that these emissions are not negligible. Therefore, these events should be included in future emission inventories.

1 Introduction

Climate change is a global problem that is having a profound impact on living conditions and human societies. The present global warming is very likely due to strong anthropogenic greenhouse gas (GHG) emissions. The Paris Agreement establishes an international effort to limit the temperature increase to well below 2 °C above preindustrial levels. A global stocktake will revisit emission reduction goals every 5 years starting in 2023. The EU aims to cut its GHG emissions by 40 % by 2030 and by 80 % to 100 % by 2050, compared to the 1990 level. The German climate action plan (Klimaschutzplan 2050) contains similar goals, i.e., to cut at least 55 % of German GHG emissions by 2030 and at least 80 % to 95 % by 2050.

Methane (CH_4) is the second-most prevalent GHG emitted by human activities (Allen et al., 2018; Etminan et al., 2016; Myhre et al., 2013). It is estimated to have a global warming potential (GWP) that is 28 to 34 times larger than that of CO_2 over the 100-year horizon (IPCC, 2013). According to Etminan et al. (2016) the GWP is even 14 % higher than the values reported by IPCC. CH_4 has been responsible for around 20 % of the global warming by anthropogenic greenhouse gases since 1750 (Nisbet et al., 2014; Kirschke et al., 2013). Current atmospheric CH_4 concentrations are 2.5 times as high as the preindustrial levels, and since the industrial revolution relative concentration growth of CH_4 has been 3 times faster than that of CO_2. After experiencing a nearly constant CH_4 concentration (total amount of CH_4 in the atmosphere) from

1999 to 2006, CH_4 concentrations have started to increase again (Saunois et al., 2016; Nisbet et al., 2014). The reasons for the renewed growth are not fully understood; fossil fuel methane emissions are largely underestimated (Schwietzke et al., 2016) and could play a major role in the increase (Hausmann et al., 2016; Worden et al., 2017). Natural gas is a growing source of energy, but its unwanted release into the atmosphere is a significant component of anthropogenic CH_4 emissions (Schwietzke et al., 2014; McKain et al., 2015), and its reduction may be essential for attaining the goal of the Paris agreement.

Therefore, recent investigations have concentrated on detecting and quantifying CH_4 emissions from city gas pipelines, power plants, and other gas and oil facilities using various methods. Phillips et al. (2013) mapped CH_4 leaks across all urban roads in the city of Boston using a cavity ring-down mobile analyzer. They identified 3356 leaks with concentrations exceeding up to 15 times the global background level and used their isotopic signatures to show that the leaks are associated with natural gas. Roscioli et al. (2015) described a method using dual-tracer flux ratio measurements complemented by on-site observations to determine CH_4 emissions from natural gas gathering facilities and processing plants. Toja-Silva et al. (2017) used differential column measurements (Chen et al., 2016) and a computational fluid dynamics (CFD) model to quantify emissions from a natural-gas-based power plant in Munich. Atherton et al. (2017) conducted mobile surveys of CH_4 emissions from oil and gas infrastructures in northeastern British Columbia, Canada, and used the CO_2/CH_4 ratios to identify these emissions. Weller et al. (2018) evaluated the ability of mobile survey methodology (von Fischer et al., 2017) to find natural gas leaks and quantified their emissions. Yacovitch et al. (2015) measured CH_4 and ethane (C_2H_6) concentrations downwind of natural gas facilities in the Barnett Shale region using a mobile laboratory. A couple of years later, Yacovitch et al. (2018) investigated the Groningen natural gas field, one of Europe's major gas fields, using their mobile laboratory in combination with airborne measurements. Luther et al. (2019) deployed a mobile sun-viewing Fourier transform spectrometer to quantify CH_4 emissions from hard coal mines. Other studies laid a special focus on city and regional emissions of fossil fuel CH_4. McKain et al. (2015) determined natural gas emission rates for the Boston urban area using a network of in situ measurements of CH_4 and C_2H_6 and a high-resolution modeling framework. Lamb et al. (2016) quantified the total CH_4 emissions from Indianapolis using the aircraft mass balance method and inverse modeling of tower observations, and they distinguished the fossil fuel component using C_2H_6/CH_4 tower data. Wunch et al. (2016) used total column measurements of CH_4 and C_2H_6 recorded since the late 1980s to quantify the loss of natural gas within California's South Coast Air Basin. Most recently, Plant et al. (2019) reported aircraft observations of CH_4, CO_2, C_2H_6, and carbon monoxide (CO) of six old and leak-prone major cities along the East Coast of the United States. They found emissions attributed to natural gas are about a factor of 10 larger than the values provided by the EPA inventory.

Large folk festivals are also likely sources of anthropogenic emissions of air pollutants, such as nitrogen oxides (NO_x), CO, particulate matter ($PM_{2.5}$, PM_{10}), sulfur dioxide (SO_2), etc. Huang et al. (2012) investigated the impact of human activity on air quality before, during, and after the Chinese Spring Festival, the most important festival in China. They used potential source contribution function analysis to illustrate the possible source for air pollutants in Shanghai. Shi et al. (2014) measured concentrations of particulate matter and polycyclic aromatic hydrocarbons (PAHs) during the Chinese New Year's Festival 2013 and estimated the source attributions from cooking, vehicles, and biomass and coal combustion. Kuo et al. (2006) investigated PAH and lead emissions from cooking during the Chinese mid-autumn festival. Nishanth et al. (2012) reported elevated concentrations of various air pollutants such as ozone (O_3), NO_x, and PM_{10} after the traditional Vishu festival in southern India. Nevertheless, up to now, festivals have not been considered a significant source of CH_4 emissions and accordingly, to the best of our knowledge, CH_4 emissions from large festivals have not yet been studied.

Oktoberfest, the world's largest folk festival with over 6 million visitors annually, is held in Munich. In 2018, during the 16 d of Oktoberfest, approximately 8 million L of beer was consumed. For cleaning, dish washing, toilet flushing, etc., 107 million L of water was needed. The use of energy added up to 2.9 million kWh of electricity and 200 937 m^3 of natural gas, 79 % of which is used for cooking and 21 % for heating (München, 2018a).

The measurements during our 2017 Munich city campaign indicated Oktoberfest as a possible source for CH_4 for the first time (Chen et al., 2018). For a better source attribution and a quantitative emission assessment, we have investigated the CH_4 emissions from Oktoberfest 2018 by carrying out mobile in situ measurements and incorporating a Gaussian plume dispersion model. These measurements and modeling approaches are described in Sect. 2. The results of these investigations show that Oktoberfest is an anthropogenic source of CH_4 that has not been accounted for until now. We have compared the determined total emission flux with bottom-up estimates of biogenic emissions from humans, and we also present the daily cycle of the emissions. In addition, the week and weekend variations are shown. From these findings we can draw conclusions about the origins of the Oktoberfest CH_4 emissions, which are presented in Sect. 3.

2 Method

We conducted a mobile survey around the perimeter of Oktoberfest to obtain the CH_4 concentration values around the

festival area (Theresienwiese) and incorporated a Gaussian plume model consisting of 16 different point sources to determine the CH_4 emission strength.

2.1 Measurement approach and instrumentation

The measurements include both CH_4 and wind measurements. The sensors and the way they are used are described in the following.

2.1.1 Concentration measurements

Mobile in situ measurements were conducted to quantify CH_4 enhancements. To this end, two portable Picarro GasScouter G4302 instruments for measuring CH_4 and C_2H_6 were used. The sensor is based on the cavity ring-down measurement principle (O'Keefe and Deacon, 1988), using a laser as a light source and a high-finesse optical cavity for measuring gas concentrations with high precision, which is 3 ppb for CH_4 mode with 1 s integration time (Picarro, 2017). We applied a moving-average filter with a window size of 10 s and a step size of 5 s to the 1 s raw measurements. Since the data are averaged over 10 s, the precision is improved to 1 ppb. To distinguish between fossil-fuel-related and biogenic emissions, the instrument can be switched to CH_4/C_2H_6 mode and measure C_2H_6 with a precision of 10 ppb for an integration time of 1 s.

Since we were not allowed to enter the festival area due to safety concerns, the measurements were carried out by walking and biking many times around the perimeter of Oktoberfest next to the security fences, wearing the analyzer as a backpack. The measurements were taken on several days during and after the time of the festival to compare the differences in emission strength and distribution. Additionally, to observe the hourly dependency of the emissions, the measurements were distributed over the course of the day. In the end, we covered the period between 08:00 and 19:00 (local time) hourly.

For the study, two identical GasScouter G4302 instruments were deployed. One instrument was provided by TNO and the other by Picarro Inc. The former was used in the first week while the latter was used in the second week of Oktoberfest as well as the time after the festival. Although the measurement approach is based on determining the enhancements and not on comparing absolute concentration values, the two instruments were calibrated at the beginning of the campaign.

2.1.2 Wind measurements

In addition to the gas concentrations, wind measurements are vital for estimating the emissions of Oktoberfest using atmospheric models. To this end, a 2D ultrasonic wind sensor (Gill WindObserver II) was placed on a roof close by (48.148° N, 11.573° E, 24 m a.g.l.). These wind measurements were utilized for the emission estimates.

To assess the uncertainty of the wind measurements, we compared these measurements with the values reported by an official station of Germany's National Meteorological Service (Deutscher Wetterdienst, DWD). The DWD station (48.163° N, 11.543° E, 28.5 m a.g.l.) is located about 2.8 km away. As this distance is about the radius of the Munich inner city, we assumed that the difference between the two stations is representative for the uncertainty of two arbitrary measurement points in the downtown area, which is also home to Oktoberfest.

2.2 Modeling approach

To quantify the emissions of Oktoberfest, we used the measured concentration values as input for an atmospheric transport model.

2.2.1 Selection algorithm

For our modeling approach, the plumes of individual surveys (hereafter referred to as "rounds") around the Theresienwiese were evaluated. In total, we completed 94 rounds (69 during and 25 after Oktoberfest). For every round the individual plumes were determined by analyzing a low-pass-filtered version of the measurement time series. A Kaiser window (Kaiser and Schafer, 1980) was utilized for the low-pass filtering.

Once the signal was filtered, a signal section between two adjacent minima was defined as a plume signal if it had an enhancement of more than 5 ppb. We chose this threshold to be equal to the combined uncertainty of the instrument (3 ppb) and background (4 ppb) (see Sect. 2.2.6). This process is illustrated in Fig. 1.

When the initial plume selection phase was completed, the identified plumes were further analyzed. As the path of a measurement around the Oktoberfest premises was predefined by the security fence, the location of each point on that route can be converted into a fixed angle, which simplifies the comparison between the measurements and the model. For that purpose, a center point of the Theresienwiese was defined (see green dot in Fig. 2, 48.1315° N, 11.5496° E). With the help of this point, an angle was assigned to all measurement and model values. This angle was defined similarly to the wind angles, meaning that 0° is in the north and 90° is in the east.

In order to decide whether a measured plume is attributable to emissions from Oktoberfest, a forward model uses the measured wind direction (with uncertainty) to calculate at which angles a plume from Oktoberfest should occur. As can be seen in Fig. 3, only plume 1 was selected because the angle range of this plume (green) largely overlaps with the accepted angle range (grey) computed by the forward model of this plume. In contrast, plume 2 (red) has no overlap with the range computed by the forward model; hence, plume 2 was discarded.

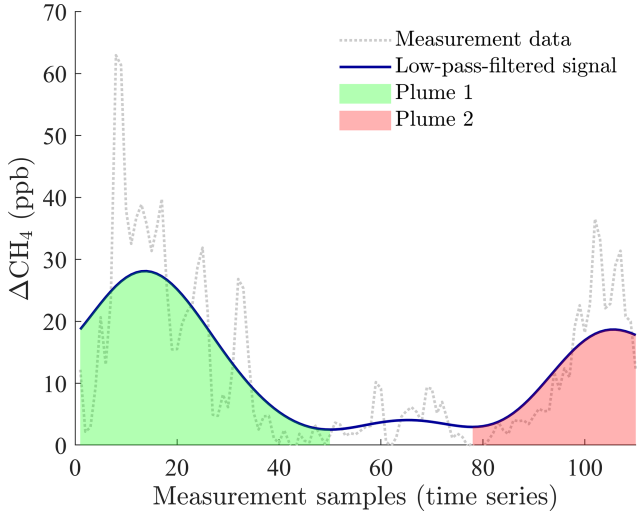

Figure 1. The preprocessed measurement signal (dotted line, moving average with window size of 10 s and step size of 5 s) is shown along with a low-pass-filtered version (blue line), which is used to obtain the single plumes (green and red area). The signal in the center is not detected as a plume, as the enhancement is not high enough. The round shown was recorded by bike and took 550 s (9.2 min).

Additionally, the standard deviation of the wind direction over the time the plume was recorded is taken into account. If the standard deviation is higher than 24°, the plume is not considered, as our approach requires stable wind conditions. Those 24° represent the measurement uncertainty in the wind direction (see Sect. 2.2.6) and are therefore well suited as a lower limit for filtering out too variable wind conditions.

The selection algorithm described above is visually summarized in Fig. 4.

2.2.2 Baseline determination

As one measurement round can take up to 1 h (when walking), the atmospheric conditions can vary during that time period, which will result in a changing background concentration. Therefore, the baseline for determining the concentration enhancements cannot be calculated solely using a constant value.

In our approach, we assume that the baseline during one round is either rising or falling and that there is a linear behavior. Such a straight line is clearly defined by two points. For that reason, the time series for each round was divided into two equally sized bins (first and second half). For each half, we determined the lowest 10 % quantile. Afterwards, the mean values of the smallest 10 % of concentration values of each bin were used to define one straight line, which was used as the background for that specific round (see Fig. 5). The uncertainty of that baseline was determined using the CH_4 concentration deviations of the smallest 10 % of values from the baseline.

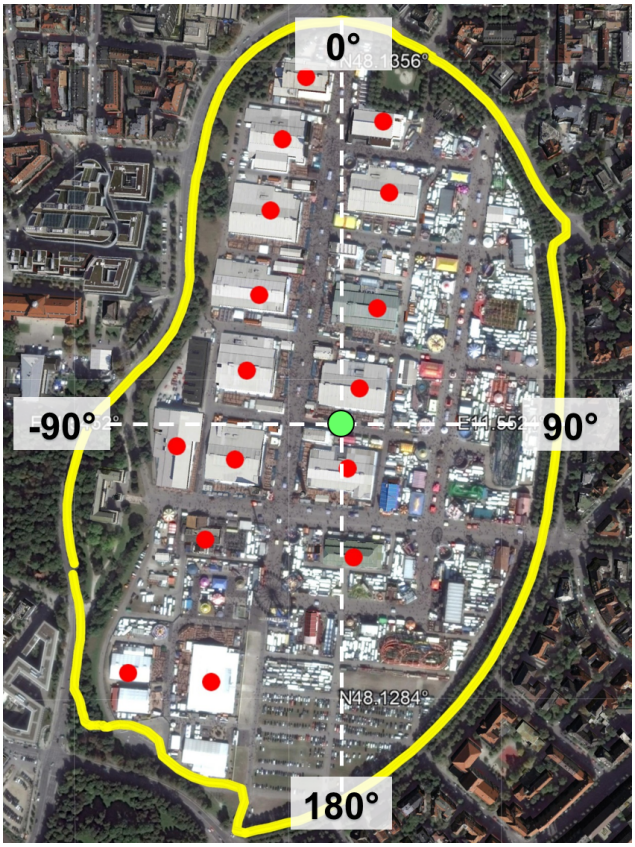

Figure 2. Standard route around Oktoberfest (yellow) including the locations of the 16 tents (red) and the center point (green). Map data are from © Google, DigitalGlobe.

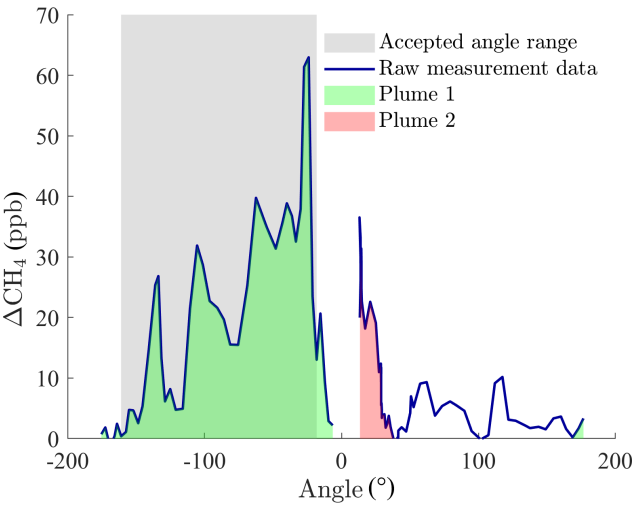

Figure 3. Measurement signal mapped onto the standard route with the angle on the abscissa. Two detected plumes and the accepted angle range computed by the forward model are highlighted. Plume 2 has no overlap with the accepted range and is therefore discarded.

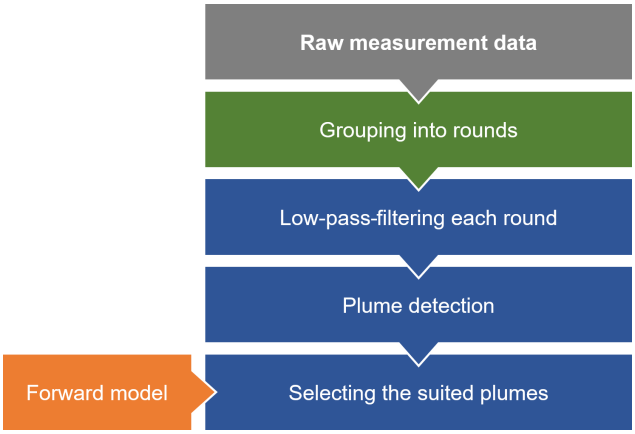

Figure 4. Flowchart visualizing the main steps performed on the raw measurement data in order to obtain an emission estimate.

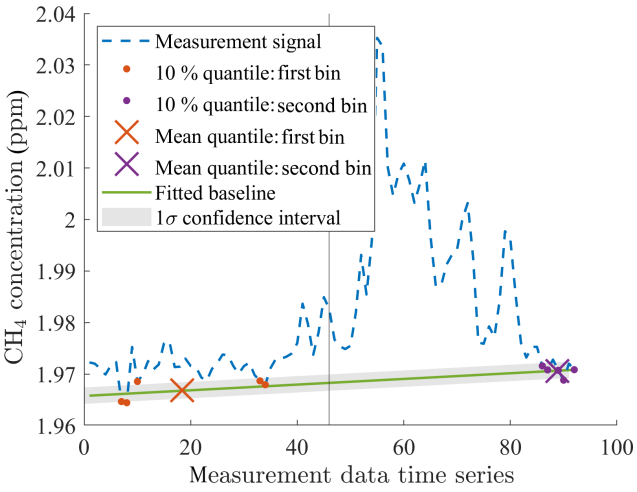

Figure 5. Baseline determination by dividing the measurement signal (blue) into two halves. Afterwards, a line (green) is fitted through the mean values of the lowest 10 % of concentration points of each half. The grey shaded area denotes the 1σ uncertainty range of the baseline.

2.2.3 Gaussian plume model

The framework of our modeling approach is based on a Gaussian plume model described in Sutton (1932), Briggs (1973), and Hanna et al. (1982) and widely used to access local source emissions (Bovensmann et al., 2010; Yacovitch et al., 2015; Atherton et al., 2017; Nassar et al., 2017; Kiemle et al., 2017). It is a steady-state model that simulates the diffusion and the transport of emitted trace gases from a point source. The gas disperses such that its concentration distributions fit well to Gaussian curves in the vertical and horizontal directions.

For a point source emitting continuously with strength Q (mol s^{-1}) at effective height H above the ground and uniform wind speed, the expression for the time-averaged concentration $< c(x,y,z) >$ (mol m^{-3}) is given by the formula below:

$$< c(x,y,z) > = \frac{Q}{2\pi\overline{u}\sigma_y(x)\sigma_z(x)} \exp\left(-\frac{y^2}{2\sigma_y(x)^2}\right) \times \times \left(\exp\left(-\frac{(z-H)^2}{2\sigma_z(x)^2}\right) + \exp\left(-\frac{(z+H)^2}{2\sigma_z(x)^2}\right)\right), \quad (1)$$

with x, y, and z describing the downwind distance, horizontal/cross-wind distance to the x axis, and the height above the ground, respectively. $\overline{u}$ is the time-averaged wind speed, $\sigma_y(x)$ is the standard deviation of the concentration in the cross-wind direction, and $\sigma_z(x)$ is the standard deviation of the concentration in the vertical direction. These dispersion coefficients describe the spreading of a plume increasing with x, which is the downwind distance from the source.

To determine the dependency of σ_y and σ_z on x, diffusion experiments were carried out (Haugen, 1959), which resulted in Pasquill's curves (Pasquill, 1961; Gifford, 1976). Smith (1968) worked out an analytic power-law formula for the relationship between σ_y, σ_z, and x. Briggs (1973) combined the aforementioned curves and used theoretical concepts to produce the widely used formulas presented in Hanna et al. (1982).

During the measurement periods, the surface wind was lower than 4 m s^{-1} and the insolation was strong to moderate. Therefore, stability class A or B was chosen according to the Pasquill turbulence types (Gifford, 1976).

Based on Briggs' recommendations for urban conditions (Briggs, 1973; Hanna et al., 1982), the relationships between the dispersion parameters and the downwind distance are described as

$$\sigma_y(x) = 0.32x(1+0.0004x)^{-1/2}, \quad (2)$$

$$\sigma_z(x) = 0.24x(1+0.001x)^{1/2}. \quad (3)$$

These relationships were used in our study.

2.2.4 Multiple-Gaussian-plume model

The concentration measurements using the backpack instrument were performed close to the festival area (< 500 m), which is why the emissions of Oktoberfest cannot be seen as a single point source. Accordingly, multiple point sources were used, which were modeled as Gaussian plumes before they were superimposed. The spatially superimposed plumes were detected as a continuous plume signal in our measurement. Later on, these plume signals were utilized for the emission assessment.

Since the emission sources of Oktoberfest were unknown, the locations with the highest density of visitors and with the highest energy consumption were chosen as the main sources for the model. Those locations are represented by the 16 biggest beer tents (> 1000 seats) on the festival

premises (see red dots in Fig. 2). To achieve a good correlation between the model and reality, these 16 tents were not treated equally in the final model. Instead, they were linearly weighted according to their maximum number of visitors. Therefore, the largest tent (about 8500 visitors) has, in the end, a greater than 8 times higher influence on the total emission number than the smallest tent (about 1000 visitors).

2.2.5 Forward modeling approach

The multiple Gaussian plume model was used in a forward approach to compare the measured and modeled concentration signals with each other. For this, a predefined route around Oktoberfest was used (see yellow route in Fig. 2) to determine the concentrations for each angle.

The actual shape of the concentration vs. angle graph $c(\alpha)$ for every selected plume i are considered for the determination of the emission of Oktoberfest $E_{\mathrm{Okt},i}$ (see Fig. 6, blue curve). The optimization procedure can be expressed mathematically as follows:

$$E_{\mathrm{Okt},i} = \underset{E_i}{\arg\min} \int_0^{360} |c(\alpha) - M(E_i, \alpha)| \, \mathrm{d}\alpha, \tag{4}$$

where M represents the model. The emission number E_{i} was varied until the areas underneath the modeled and measured curves are the same, and thus the sum of the absolute difference between the model and measurement is minimized.

Specifically, we computed the forward model using the averaged wind information at this time and a prior emission number E_{prior} of 3 µg $(\mathrm{m}^2\,\mathrm{s})^{-1}$ and compared it with the measurement curve. If the shapes look similar (high cross-correlation coefficient), a scaling factor is applied to the prior emission number and varied until the forward model matches the measurements. This procedure is illustrated for one exemplary plume signal in Fig. 6. There, the prior modeled concentrations (orange) are smaller than the measured concentrations (blue). Therefore, the model has to be multiplied with a scaling factor until the areas underneath the modeled and measured curve are the same (yellow). By multiplying the scaling factor $k_{\mathrm{scaling},i}$ with the E_{prior}, the emission number of Oktoberfest $E_{\mathrm{Okt},i}$ for every plume signal i can be determined as

$$E_{\mathrm{Okt},i} = E_{\mathrm{prior}} \cdot k_{\mathrm{scaling},i}. \tag{5}$$

2.2.6 Uncertainty assessment

To determine the uncertainty of the final emission numbers, we considered the uncertainties of our input parameters. These include uncertainties in the wind and concentration measurements as well as uncertainties in the determined baseline. These input parameters were each modeled as a Gaussian distribution. Afterwards, the emission number was determined by running our modeling approach 1000 times using those four parameters (wind speed, wind direction, measured CH_4 concentration, background concentration) as input. In each run, slightly different input values were chosen randomly and independent from each other out of those four distributions.

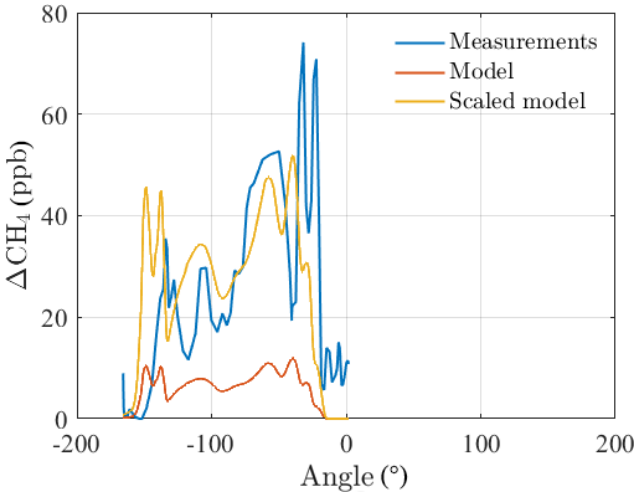

Figure 6. Measurement curve (blue) with the a priori forward model (orange) and the scaled forward model (yellow).

The concentration measurement uncertainty is indicated by the manufacturer Picarro to be about 1 ppb for an integration time of 10 s. This value was used as the standard deviation of the modeled input distribution.

For the wind speed and direction, the instrument uncertainty as well as the spatial variations in the winds were taken into account. For that reason, the uncertainty of the wind measurements was determined by comparing two measurement stations within the inner city of Munich (see Sect. 2.1.2). We determined the differences in wind speed and direction throughout September and October 2018. The differences are representative of the heterogeneity of the wind within the inner city of Munich and, therefore, represent an upper bound for the uncertainty of the wind within the Oktoberfest premises. The comparison of both the wind speed and direction resulted in Gaussian-shaped distributions with mean values each around zero. The standard deviations of the differences between the reported wind directions and speeds of the two stations are 24° and 0.5 m s^{-1} throughout September and October 2018.

The baseline approach described in Sect. 2.2.2 introduces a further error which has to be considered as well. The background concentration was modeled as a linear baseline where the offset follows a Gaussian distribution. Its standard deviation was calculated from the differences between the smallest 10 % of concentration values of each bin and the baseline (see Fig. 5).

Table 1. Mean and standard deviation of the input parameters for the CH_4 plume signal i.

Type	Mean	Standard deviation
Wind speed	$v_{\text{wind,meas},i}$	$0.5\,\text{m}\,\text{s}^{-1}$
Wind direction	$\alpha_{\text{wind,meas},i}$	24°
Instrumentation	$c_{\text{meas},i}$	1 ppb
Background	$c_{\text{backgnd},i}(t)$	$\sigma_{10\,\%\,\text{quantile},i}$

The parameters used for the uncertainty assessment are summarized in Table 1.

3 Results and discussion

3.1 Concentration mapping

The measured CH_4 concentrations were plotted for each round on a map of the Oktoberfest premises to show that there is a clear correlation between the wind directions and the enhancements. As the variations in the boundary layer height should not be taken into account, these plots do not show the absolute concentration values but just the enhancements above the determined background concentrations (see Sect. 2.2.2). Two such plots for two different wind directions are shown in Fig. 7. In addition to the concentration enhancements and the wind direction, the 16 emission sources are shown as black dots on top of each tent. The Gaussian plumes themselves are also represented. These two plots reveal that the highest concentration enhancements can be observed downwind of the Oktoberfest premises.

3.2 Emission number

The average emission of the Oktoberfest 2018 $E_{\text{Okt,avg}}$ is determined by averaging the emission numbers of the N plume signals $E_{\text{Okt},i}$ during the complete Oktoberfest time period (including the weekdays and weekends), accordingly:

$$E_{\text{Okt,avg}} = \frac{1}{N}\sum_{i=1}^{N} E_{\text{Okt},i}. \tag{6}$$

To make the final emission number more robust and to determine an uncertainty, the basic approach of Eq. (6) was improved. Instead of just using the actual measured data, an uncertainty range was applied to the four main input parameters, each using Gaussian distributions (see Sect. 2.2.6).

For every plume signal i, 1000 samples of randomly chosen input datasets from the aforementioned normal distributions of the input parameters were used to determine 1000 slightly different emission numbers $E_{\text{Okt},i,k}$. Using Eq. (6), an average emission number for each realization $E_{\text{Okt,avg},k}$ was calculated:

$$E_{\text{Okt,avg},k} = \frac{1}{N}\sum_{i=1}^{N} E_{\text{Okt},i,k}. \tag{7}$$

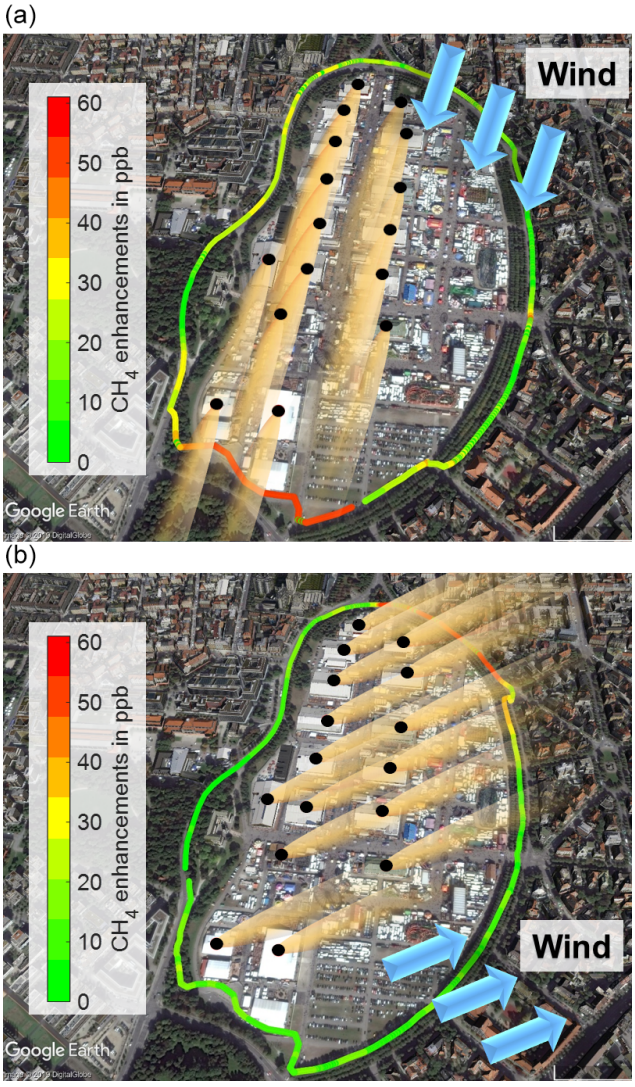

Figure 7. CH_4 concentration enhancements of two measurement rounds including the influence of the 16 Gaussian plumes from the tents (black dots). Wind direction is **(a)** 20° and **(b)** −110°. Map data are from © Google, DigitalGlobe.

The average emission number including an uncertainty assessment can be obtained by determining the mean μ_{Okt} and standard deviation σ_{Okt} of those 1000 realizations:

$$\mu_{\text{Okt}} = \frac{1}{1000}\sum_{k=1}^{1000} E_{\text{Okt,avg},k}, \tag{8}$$

$$\sigma_{\text{Okt}} = \sqrt{\frac{\sum_{k=1}^{1000}(E_{\text{Okt,avg},k} - \mu_{\text{Okt}})^2}{999}}. \tag{9}$$

The result for the total emission number of Oktoberfest 2018 is shown in Fig. 8 and has a value of

$$E_{\text{Okt,total}} = \mu_{\text{Okt}} \pm \sigma_{\text{Okt}} = (6.7 \pm 0.6)\,\mu\text{g}\,(\text{m}^2\,\text{s})^{-1}. \tag{10}$$

To verify whether those emissions were caused by Oktoberfest, Fig. 8 also shows the emissions determined for the time

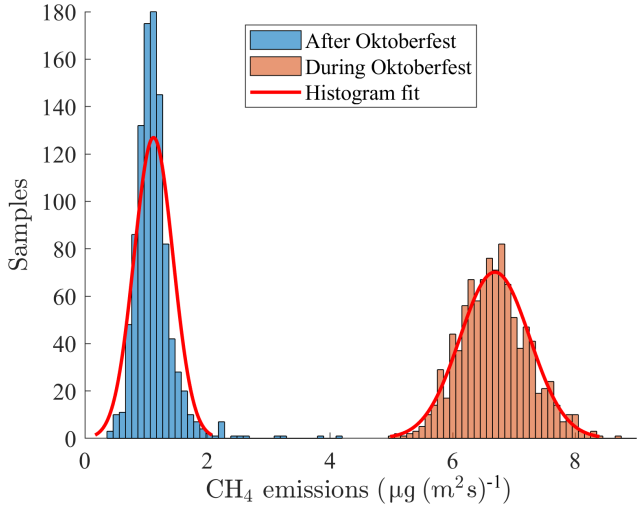

Figure 8. Total CH_4 emission estimates during (light red) and after (blue) the Oktoberfest 2018 including a fitted normal distribution (red line).

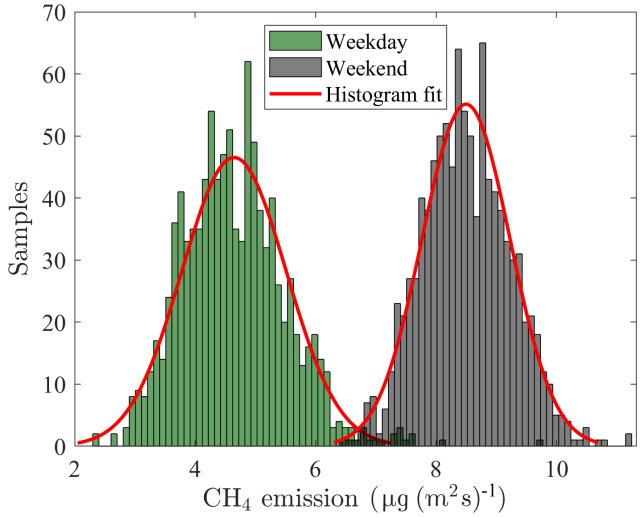

Figure 9. CH_4 emission estimates for a weekday (green) and a weekend day (black) including a fitted normal distribution (red line).

after Oktoberfest (from 8 October through 25 October). This number $(1.1 \pm 0.3)\,\mu g\,(m^2\,s)^{-1}$ is significantly smaller than the one during Oktoberfest but still not zero. It indicates that the emissions are caused by Oktoberfest, and the disassembling of all the facilities, which takes several weeks, still produces emissions after Oktoberfest.

After grouping the emission numbers into the two categories, weekday (in total 47 valid plumes) and weekend (27 valid plumes), two separated distributions are visible in Fig. 9. The average emission for the weekend $(8.5 \pm 0.7)\,\mu g\,(m^2\,s)^{-1}$ is higher than the averaged emission for the weekdays $(4.6 \pm 0.9)\,\mu g\,(m^2\,s)^{-1}$, almost by a factor of 2. To interpret this result, the visitor trend of Oktoberfest was investigated. This trend is based on the officially estimated numbers of visitors (muenchen.de, 2018) and was linearly interpolated (see Fig. 10). Besides the daily trend, it also shows the mean values of the weekdays and weekend days (dotted lines). As the number of visitors at Oktoberfest was also significantly higher on a weekend day than on a weekday (approximately a factor of 2; see Fig. 10), a higher number of visitors results in higher emissions, which indicates the CH_4 emissions are anthropogenic.

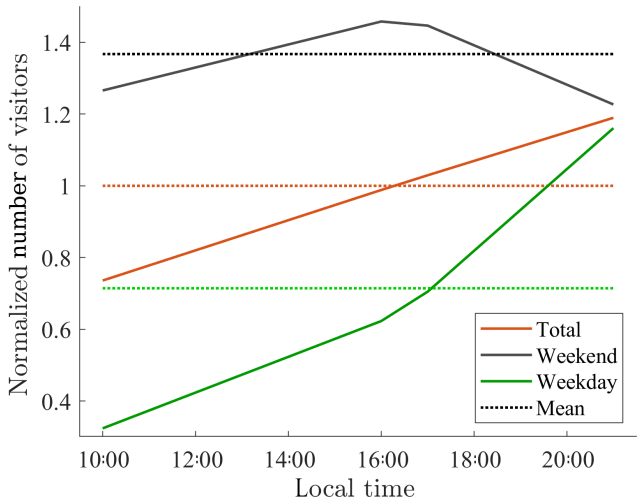

Figure 10. Qualitative daily trend of the number of visitors at Oktoberfest for the weekend (black), weekday (green), and total (red). The dotted line represents the mean value of each trend line.

3.3 Daily emission cycle

To assess the daily cycle of the CH_4 emissions, the emission numbers of the plume signals $E_{\mathrm{Okt},i,k}$ are grouped into hourly bins. Then, for each bin an average emission $E_{\mathrm{Okt,hour},k}$ is calculated. Afterwards, these numbers are averaged for the 1000 realizations to obtain robust results including an uncertainty estimate:

$$\mu_{\mathrm{Okt,hour}} = \frac{1}{1000}\sum_{k=1}^{1000} E_{\mathrm{Okt,hour},k}, \tag{11}$$

$$\sigma_{\mathrm{Okt,hour}} = \sqrt{\frac{\sum_{k=1}^{1000}(E_{\mathrm{Okt,hour},k} - \mu_{\mathrm{Okt,hour}})^2}{999}}. \tag{12}$$

In Fig. 11, the variation in the hourly emission mean $\mu_{\mathrm{Okt,hour}}$ is shown as a blue line. The grey shaded area shows the uncertainty $\sigma_{\mathrm{Okt,hour}}$ of the emission numbers within that hour. The daily emission cycle shows an oscillating behavior overlaid on an increasing trend towards the evening.

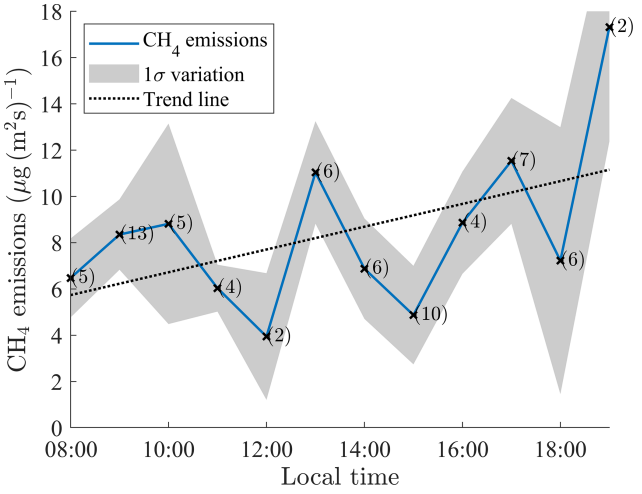

Figure 11. Daily variations in the emissions from Oktoberfest between 08:00 and 19:00 local time. The grey shaded area denotes the uncertainty (1σ standard deviation) within that hour. The numbers in parentheses indicate the number of valid plumes during that hour.

The linear increasing trend is in agreement with Fig. 10, which shows a linearly increasing visitor amount throughout the day, confirming the anthropogenic nature of the emissions. The oscillating behavior indicates that the emissions are related to time-dependent events, such as cooking, heating, and cleaning, which tend to show peaks in the morning, noon, and evening.

3.4 Biogenic human CH_4 emissions

To address the question of whether the people themselves caused the emissions or whether the emissions were caused by processes related to the number of visitors, such as cooking, heating, sewage, etc., we took a closer look at human biogenic emissions.

Most of the previous studies define a methane producer as a person that has a breath CH_4 mixing ratio at least 1 ppm above ambient air (Polag and Keppler, 2019). Keppler et al. (2016), however, used laser absorption spectroscopy to confirm that all humans exhale CH_4. In that study, the mean of the breath CH_4 enhancements above the background from 112 test persons between 1 and 80 years of age is 2316 ppb and the values vary from 26 ppb to 40.9 ppm.

In addition, we have considered the values reported in Polag and Keppler (2019). The authors provided a summary of various studies of human CH_4 emissions in Table 1 and Sect. 3.2, and we used these results to calculate average human CH_4 emissions, which are 2.3 mmol d^{-1} via breath and 7 mmol d^{-1} via flatus. We multiplied these values with the 300 000 persons that visit the Oktoberfest premises ($\approx 3.45 \times 10^5$ m^2) every day. This represents an upper limit of people who are at the Oktoberfest at the same time, as most visitors do not stay all day long. Please note the average emission numbers are not factor weighted by ethnicity, age, and sex, because we do not have those statistics for Oktoberfest. The expected CH_4 emission from the human breath and flatulence in total was calculated as

$$E_{\text{human}} = \frac{(2.3\,\text{mmol}\,\text{d}^{-1} + 7\,\text{mmol}\,\text{d}^{-1}) \cdot 3 \times 10^5 \cdot 16\,\text{g}\,\text{mol}^{-1}}{24 \cdot 3600\,\text{s}\,\text{d}^{-1} \cdot 3.45 \times 10^5\,\text{m}^2} = 1.5\,\mu\text{g}\,(\text{m}^2\,\text{s})^{-1}. \quad (13)$$

Although we assumed the maximum possible number of visitors, the resulting biogenic component is 22 % of the emissions we determined for Oktoberfest. Therefore, the emissions are not solely produced by the humans themselves, but by processes that are related to the number of visitors.

3.5 Emissions from sewage

Besides the direct biogenic human emissions, CH_4 emissions from sewer systems are also possible sources. These emissions are a product of bacterial metabolism within waste water, whose emission strength depends in particular on the hydraulic retention time (Liu et al., 2015; Guisasola et al., 2008) which represents the time the waste water stays in the system. This time decreases with a higher amount of waste water, as the flow increases in such a case.

At Oktoberfest, the amount of waste water is very high as the 107 million L of water and the 8 million L of beer consumed have to flow into the sewer system at some time (München, 2018a). Therefore, the retention time in the sewer system underneath the Theresienwiese is quite low, which makes high CH_4 emissions from sewage unlikely. Furthermore, the waste water consists primarily of dirty water and urine but not feces, which contain many carbon compounds necessary to produce CH_4.

3.6 Fossil fuel CH_4 emissions

The biogenic emissions can likely not fully explain the determined emissions of Oktoberfest. Therefore, fossil-fuel-related emissions, such as leakages and incomplete burning in the gas appliances, have to be considered as well. According to the weekday–weekend emission comparison (see Fig. 9) and the daily emission cycle (see Fig. 11 compared with Fig. 10), there is, in general, a visitor-dependent linear increase in CH_4 emissions throughout the day that is superimposed with time-dependent events such as cooking, cleaning, or heating. These events can cause CH_4 emissions, as about 40 % of the energy used at Oktoberfest is provided by natural gas used for cooking (79 %) and heating (21 %).

C_2H_6 is a tracer of thermogenic CH_4 and therefore can be used to indicate a natural-gas-related source (Yacovitch et al., 2014; McKain et al., 2015). For that reason, we deployed a portable instrument designed to measure CH_4 and C_2H_6. Due to the aforementioned safety reasons, the distance

between the measurements and the closest point source (tent) was 50 to 250 m. Therefore, the CH_4 concentration was relatively low (max. 100 ppb). According to the Munich municipal utilities, the C_2H_6/CH_4 ratio of natural gas used in Munich is about 3 % (München, 2018b), which results in an C_2H_6 concentration lower than 3 ppb, assuming that all of the measured CH_4 is sourced from natural gas. Such a small concentration value is lower than the detection limit of the GasScouter (about 3 ppb with 10 s integration time), which is why we were not able to determine the C_2H_6/CH_4 ratio of the measured gas.

Nevertheless, it is possible to determine an upper bound for the loss rate of natural gas if one assumes that all the emissions are fossil fuel based. The natural gas consumption at Oktoberfest 2018 added up to 200 937 m^3. Therefore, the total weight of the consumed CH_4 at Oktoberfest yields

$$M_{\mathrm{gas,total}} = 0.668\,\mathrm{kg\,m^{-3}} \cdot 200\,937\,\mathrm{m^3} = 1.34 \times 10^5\,\mathrm{kg}. \quad (14)$$

In this study, the CH_4 flux of Oktoberfest has been determined to be 6.7 $\mu g\,(m^2\,s)^{-1}$. If we assume that the emission is continuous throughout the day (about 11 h opening time per day) and homogeneous throughout the entire Oktoberfest premises, the total amount of CH_4 lost to the atmosphere would be

$$M_{\mathrm{CH_4,loss,max}} = 6.7\,\mu g\,(m^2\,s)^{-1} \cdot (16\,d \cdot 11\,h\,d^{-1} \cdot 3600\,s\,h^{-1}) \cdot 3.45 \times 10^5\,m^2 = 1.46 \times 10^3\,kg. \quad (15)$$

The CH_4 share of the natural gas in Munich is on average about 96 % (München, 2018b). If we assume all of the CH_4 emissions are fossil fuel related, the maximum loss rate can be determined as

$$\frac{M_{\mathrm{CH_4,loss,max}}}{M_{\mathrm{CH_4,total}}} = \frac{1.46 \times 10^3\,\mathrm{kg}}{1.34 \times 10^5\,\mathrm{kg} \cdot 96\,\%} = 1.1\,\%. \quad (16)$$

This loss rate of 1.1 % is smaller than the gas leaks reported in the literature, such as a 2.7 % loss rate for the urban region of Boston (McKain et al., 2015) or 2.3 % for the US oil and gas supply chain (Alvarez et al., 2018).

3.7 Comparison with existing CH_4 emission estimates

To the best of our knowledge, there is no comparable CH_4 study dealing with festivals. For a better illustration, we compared the emission flux of the Oktoberfest premises to the emission flux of Boston, which is known as a very leaky city. In the Boston study, McKain et al. (2015) quantified the regional averaged emission flux of CH_4 there as $(18.5 \pm 3.7)\,g\,(m^2\,a)^{-1}$ (95 % confidence interval), which corresponds to $(0.6 \pm 0.1)\,\mu g\,(m^2\,s)^{-1}$ and is less than a tenth of the emissions that we determined for the Oktoberfest premises. Although it is difficult to compare the small and densely populated Oktoberfest premises with the entire city area of Boston, the comparison shows that the emission flux of Oktoberfest is significant.

Table 2. Comparison of the Oktoberfest emission flux to state-of-the-art emission inventory fluxes for the same location.

Description	Year	Flux	Averaging area
Oktoberfest	2018	6.7 $\mu g\,(m^2\,s)^{-1}$	0.3 km^2
TNO-MACC III	2015	0.9 $\mu g\,(m^2\,s)^{-1}$	4.6 km^2
EDGAR v4.3.2	2012	1.0 $\mu g\,(m^2\,s)^{-1}$	82 km^2
IER	2008	0.1 $\mu g\,(m^2\,s)^{-1}$	4.0 km^2

Furthermore, we compared the Oktoberfest emission flux to the state-of-the-art emission inventory fluxes of that quarter of Munich. For that purpose, the annual emission fluxes of TNO-MACC III (2015) (Denier van der Gon et al., 2017; Kuenen et al., 2014), EDGAR v4.3.2 (2012) (Janssens-Maenhout et al., 2019), and IER (2008) (Pregger et al., 2007) are converted to the common unit of micrograms per square meter per second. In Table 2, the converted values are shown. Furthermore, the different inventories have different spatial resolutions. Therefore, the fluxes are averaged over areas that represent not only the Oktoberfest premises but also additional urban districts. Nevertheless, the Oktoberfest emissions are significantly higher than all three inventories considered. Therefore, festivals such as Oktoberfest can be significant CH_4 sources. Although only present for a limited time each year, they should be included in the inventories.

4 Conclusions and outlook

This is the first study that deals with the methane emissions of a big festival. We investigated Oktoberfest as it is the world's largest folk festival and a methane source that had not yet been taken into account in the emission inventories.

Combining the in situ measurements with a Gaussian plume dispersion model, the average emission of Oktoberfest was determined to be $(6.7 \pm 0.6)\,\mu g\,(m^2\,s)^{-1}$ (1σ standard deviation). A comparison between weekdays ($4.6\,\mu g\,(m^2\,s)^{-1}$) and weekend days ($8.5\,\mu g\,(m^2\,s)^{-1}$) shows that the emission strength at the weekend was almost twice as high compared to during the week. It demonstrates that a higher number of visitors results in higher emissions. However, the daily emission cycle has an oscillating behavior that cannot be explained by the number of visitors. These results suggest that CH_4 emissions at Oktoberfest do not come solely from the human biogenic emissions, which were 5 times smaller than the emissions determined for the Oktoberfest according to our calculations. Fossil-fuel-related emissions, such as incomplete combustion or loss in the gas appliances, are more likely the major contributors to Oktoberfest emissions.

Due to safety reasons, we were not allowed to enter the festival premises with the instrument. Therefore, the distance from the measurement points to the suspected sources on

the festival terrain was large, which resulted in low CH_4 and C_2H_6 concentrations. The latter were even below the detection limit of the instrument. This limited the possibilities to attribute the emissions to specific sources. To improve this aspect, several additional approaches are possible for future studies. As we are not aware of a more sensitive portable C_2H_6 analyzer, discrete air sampling using sample bags within the tents for C_2H_6 is an option. Furthermore, the measurement of isotope ratios, such as $\delta^{13}C$ and δD, is a useful option to improve the source attribution. For other festivals, researchers might be allowed to get closer to the sources.

The method introduced in this paper is comparatively straightforward; it can be applied widely to discover and quantify overlapping methane sources: groups of small cow barns, uncovered heaps in landfills, or wetlands made of groups of ponds and swamps, etc.

In summary, this study uses Oktoberfest as an exemplary event to show, for the first time, that large festivals can be significant CH_4 emitters. Therefore, these events should be included in future emission inventories. Furthermore, our results provide the foundation to develop reduction policies for such events and a new pathway to mitigate fossil fuel CH_4 emissions.

Data availability. All raw data can be provided by the corresponding authors upon request.

Author contributions. JC, FD, and HM planned the campaign; JC, FD, HM, AF, and DW performed the measurements; JC, FD, AF, and DW analyzed the data; JC and FD wrote the manuscript draft; AF, MEGH, HDvdG, and TR reviewed and edited the manuscript.

Competing interests. The authors declare that they have no conflict of interest.

Acknowledgements. We thank Peter Swinkels and his colleagues from Picarro Inc. who made it possible for us to borrow the GasScouter; Jörg Ochs (Munich municipal utilities, SWM) for providing us with helpful information about the Munich gas distribution system; Hanns-Erik Endres, Manfred Engl, and colleagues from Fraunhofer EMFT, Martin Christ (LMU), and the colleagues from Klenze Gymnasium Munich for providing access to measurement sites; Markus Garhammer, Matthias Wiegner, and Mark Wenig (LMU) for providing us wind and boundary layer height data; Anna-Leah Nickl and Mariano Mertens (DLR) for running high-resolution wind forecasts; Konrad Koch (TUM) for providing us detailed information about the Munich sewer system and helpful discussions; Rachel Chang and Frank Keppler for fruitful discussions; our students Ankit Shekhar, Xiao Bi, and Homa Ghasemifard for helping with the measurements; the reviewers for their valuable comments; and Stephen Starck, Ankit Shekhar, and Rita von Grafenstein for proofreading a previous version of the paper. Jia Chen and Florian Dietrich are supported by Technische Universität München – Institute for Advanced Study, funded by the German Excellence Initiative and the European Union Seventh Framework Programme under grant agreement no. 291763.

Financial support. This work was supported by the German Research Foundation (DFG) and the Technical University of Munich (TUM) in the framework of the Open Access Publishing Program.

Review statement. This paper was edited by Rolf Müller and reviewed by Euan Nisbet and one anonymous referee.

References

Allen, M. R., Shine, K. P., Fuglestvedt, J. S., Millar, R. J., Cain, M., Frame, D. J., and Macey, A. H.: A solution to the misrepresentations of CO_2-equivalent emissions of short-lived climate pollutants under ambitious mitigation, NPJ Clim. Atmos. Sci., 1, 16, https://doi.org/10.1038/s41612-018-0026-8, 2018.

Alvarez, R. A., Zavala-Araiza, D., Lyon, D. R., Allen, D. T., Barkley, Z. R., Brandt, A. R., Davis, K. J., Herndon, S. C., Jacob, D. J., Karion, A., Kort, E. A., Lamb, B. K., Lauvaux, T., Maasakkers, J. D., Marchese, A. J., Omara, M., Pacala, S. W., Peischl, J., Robinson, A. L., Shepson, P. B., Sweeney, C., Townsend-Small, A., Wofsy, S. C., and Hamburg, S. P.: Assessment of methane emissions from the U.S. oil and gas supply chain, Science, 361, 186–188, https://doi.org/10.1126/science.aar7204, 2018.

Atherton, E., Risk, D., Fougère, C., Lavoie, M., Marshall, A., Werring, J., Williams, J. P., and Minions, C.: Mobile measurement of methane emissions from natural gas developments in northeastern British Columbia, Canada, Atmos. Chem. Phys., 17, 12405–12420, https://doi.org/10.5194/acp-17-12405-2017, 2017.

Bovensmann, H., Buchwitz, M., Burrows, J. P., Reuter, M., Krings, T., Gerilowski, K., Schneising, O., Heymann, J., Tretner, A., and Erzinger, J.: A remote sensing technique for global monitoring of power plant CO_2 emissions from space and related applications, Atmos. Meas. Tech., 3, 781–811, https://doi.org/10.5194/amt-3-781-2010, 2010.

Briggs, G. A.: Diffusion estimation for small emissions. Preliminary report, Tech. Rep. TID-28289, National Oceanic and Atmospheric Administration, Oak Ridge, Tenn. (USA), Atmospheric Turbulence and Diffusion Lab., https://doi.org/10.2172/5118833, 1973.

Chen, J., Viatte, C., Hedelius, J. K., Jones, T., Franklin, J. E., Parker, H., Gottlieb, E. W., Wennberg, P. O., Dubey, M. K., and Wofsy, S. C.: Differential column measurements using compact solar-tracking spectrometers, Atmos. Chem. Phys., 16, 8479–8498, https://doi.org/10.5194/acp-16-8479-2016, 2016.

Chen, J., Dietrich, F., Franklin, J., Jones, T., Butz, A., Luther, A., Kleinschek, R., Hase, F., Wenig, M., Ye, S., Nouri, A., Frey, M., Knote, C., Alberti, C., and Wofsy, S.: Mesoscale Column Network for Assessing GHG and NO_x Emissions in Munich, in: Geophysical Research Abstracts, 20, EGU2018–10192–2, 2018.

Denier van der Gon, H. A. C., Kuenen, J. J. P., Janssens-Maenhout, G., Döring, U., Jonkers, S., and Visschedijk, A.:

TNO_CAMS high resolution European emission inventory 2000–2014 for anthropogenic CO_2 and future years following two different pathways, Earth Syst. Sci. Data Discuss., https://doi.org/10.5194/essd-2017-124, in review, 2017.

Etminan, M., Myhre, G., Highwood, E. J., and Shine, K. P.: Radiative forcing of carbon dioxide, methane, and nitrous oxide: A significant revision of the methane radiative forcing, Geophys. Res. Lett., 43, 12614–12623, https://doi.org/10.1002/2016GL071930, 2016.

Gifford, F. A.: Turbulent diffusion-typing schemes: a review, Nucl. Saf., 17, 68–86, 1976.

Guisasola, A., de Haas, D., Keller, J., and Yuan, Z.: Methane formation in sewer systems, Water Res., 42, 1421–1430, https://doi.org/10.1016/j.watres.2007.10.014, 2008.

Hanna, S. R., Briggs, G. A., and Hosker Jr., R. P.: Handbook on atmospheric diffusion, Tech. Rep. DOE/TIC-11223, National Oceanic and Atmospheric Administration, Oak Ridge, TN (USA), Atmospheric Turbulence and Diffusion Lab., https://doi.org/10.2172/5591108, 1982.

Haugen, D. A.: Project Prairie Grass: A Field Program in Diffusion, Geophysical Research Papers, III, Report AFCRC-TR-58-235, Air Force Cambridge Research Center, 1959.

Hausmann, P., Sussmann, R., and Smale, D.: Contribution of oil and natural gas production to renewed increase in atmospheric methane (2007–2014): top–down estimate from ethane and methane column observations, Atmos. Chem. Phys., 16, 3227–3244, https://doi.org/10.5194/acp-16-3227-2016, 2016.

Huang, K., Zhuang, G., Lin, Y., Wang, Q., Fu, J. S., Zhang, R., Li, J., Deng, C., and Fu, Q.: Impact of anthropogenic emission on air quality over a megacity – revealed from an intensive atmospheric campaign during the Chinese Spring Festival, Atmos. Chem. Phys., 12, 11631–11645, https://doi.org/10.5194/acp-12-11631-2012, 2012.

IPCC: Climate Change 2013: The Physical Science Basis. Contribution of Working Group I to the Fifth Assessment Report of the Intergovernmental Panel on Climate Change, edited by: Stocker, T. F., Qin, D., Plattner, G.-K., Tignor, M., Allen, S. K. Boschung,, J., Nauels, A., Xia, Y., Bex, V., and Midgley, P. M., Cambridge University Press, Cambridge, United Kingdom and New York, NY, USA, 1535 pp., doi:10.1017/CBO9781107415324, 2013.

Janssens-Maenhout, G., Crippa, M., Guizzardi, D., Muntean, M., Schaaf, E., Dentener, F., Bergamaschi, P., Pagliari, V., Olivier, J. G. J., Peters, J. A. H. W., van Aardenne, J. A., Monni, S., Doering, U., Petrescu, A. M. R., Solazzo, E., and Oreggioni, G. D.: EDGAR v4.3.2 Global Atlas of the three major greenhouse gas emissions for the period 1970–2012, Earth Syst. Sci. Data, 11, 959–1002, https://doi.org/10.5194/essd-11-959-2019, 2019.

Kaiser, J. and Schafer, R.: On the use of the I0-sinh window for spectrum analysis, IEEE Transactions on Acoustics, Speech, and Signal Processing, 28, 105–107, https://doi.org/10.1109/TASSP.1980.1163349, 1980.

Keppler, F., Schiller, A., Ehehalt, R., Greule, M., Hartmann, J., and Polag, D.: Stable isotope and high precision concentration measurements confirm that all humans produce and exhale methane, J. Breath Res., 10, 016003, https://doi.org/10.1088/1752-7155/10/1/016003, 2016.

Kiemle, C., Ehret, G., Amediek, A., Fix, A., Quatrevalet, M., and Wirth, M.: Potential of Spaceborne Lidar Measurements of Carbon Dioxide and Methane Emissions from Strong Point Sources, Remote Sens., 9, 1137, https://doi.org/10.3390/rs9111137, 2017.

Kirschke, S., Bousquet, P., Ciais, P., Saunois, M., Canadell, J. G., Dlugokencky, E. J., Bergamaschi, P., Bergmann, D., Blake, D. R., Bruhwiler, L., Cameron-Smith, P., Castaldi, S., Chevallier, F., Feng, L., Fraser, A., Heimann, M., Hodson, E. L., Houweling, S., Josse, B., Fraser, P. J., Krummel, P. B., Lamarque, J.-F., Langenfelds, R. L., Le Quéré, C., Naik, V., O'Doherty, S., Palmer, P. I., Pison, I., Plummer, D., Poulter, B., Prinn, R. G., Rigby, M., Ringeval, B., Santini, M., Schmidt, M., Shindell, D. T., Simpson, I. J., Spahni, R., Steele, L. P., Strode, S. A., Sudo, K., Szopa, S., van der Werf, G. R., Voulgarakis, A., van Weele, M., Weiss, R. F., Williams, J. E., and Zeng, G.: Three decades of global methane sources and sinks, Nat. Geosci., 6, 813–823, https://doi.org/10.1038/ngeo1955, 2013.

Kuenen, J. J. P., Visschedijk, A. J. H., Jozwicka, M., and Denier van der Gon, H. A. C.: TNO-MACC_II emission inventory; a multi-year (2003–2009) consistent high-resolution European emission inventory for air quality modelling, Atmos. Chem. Phys., 14, 10963–10976, https://doi.org/10.5194/acp-14-10963-2014, 2014.

Kuo, C.-Y., Lee, H.-S., and Lai, J.-H.: Emission of polycyclic aromatic hydrocarbons and lead during Chinese mid-autumn festival, Sci. Total Environ., 366, 233–241, https://doi.org/10.1016/j.scitotenv.2005.08.006, 2006.

Lamb, B. K., Cambaliza, M. O. L., Davis, K. J., Edburg, S. L., Ferrara, T. W., Floerchinger, C., Heimburger, A. M. F., Herndon, S., Lauvaux, T., Lavoie, T., Lyon, D. R., Miles, N., Prasad, K. R., Richardson, S., Roscioli, J. R., Salmon, O. E., Shepson, P. B., Stirm, B. H., and Whetstone, J.: Direct and Indirect Measurements and Modeling of Methane Emissions in Indianapolis, Indiana, Environ. Sci. Technol., 50, 8910–8917, https://doi.org/10.1021/acs.est.6b01198, 2016.

Liu, Y., Ni, B.-J., Sharma, K. R., and Yuan, Z.: Methane emission from sewers, Sci. Total Environ., 524–525, 40–51, https://doi.org/10.1016/j.scitotenv.2015.04.029, 2015.

Luther, A., Kleinschek, R., Scheidweiler, L., Defratyka, S., Stanisavljevic, M., Forstmaier, A., Dandocsi, A., Wolff, S., Dubravica, D., Wildmann, N., Kostinek, J., Jöckel, P., Nickl, A.-L., Klausner, T., Hase, F., Frey, M., Chen, J., Dietrich, F., Nęcki, J., Swolkień, J., Fix, A., Roiger, A., and Butz, A.: Quantifying CH_4 emissions from hard coal mines using mobile sun-viewing Fourier transform spectrometry, Atmos. Meas. Tech., 12, 5217–5230, https://doi.org/10.5194/amt-12-5217-2019, 2019.

McKain, K., Down, A., Raciti, S. M., Budney, J., Hutyra, L. R., Floerchinger, C., Herndon, S. C., Nehrkorn, T., Zahniser, M. S., Jackson, R. B., Phillips, N., and Wofsy, S. C.: Methane emissions from natural gas infrastructure and use in the urban region of Boston, Massachusetts, P. Natl. Acad. Sci. USA, 112, 1941–1946, 2015.

muenchen.de: Oktoberfest-Barometer: Die beste Zeit für den Wiesnbesuch, available at: https://www.muenchen.de/veranstaltungen/oktoberfest/besucher-service/wiesnbarometer.html (last access: 9 July 2019), 2018.

München: Oktoberfest 2018 Schlussbericht, available at: https://www.ris-muenchen.de/RII/RII/DOK/SITZUNGSVORLAGE/5440803.pdf (last access: 13 March 2020), 2018a.

München: Erdgasbeschaffenheit: Jahresmittel für 2018, available at: https://www.swm-infrastruktur-region.de/dam/

swm-infrastruktur-region/dokumente/erdgas/netzstrukturdaten/erdgasbeschaffenheit-jahresmittel-2018.pdf (last access: 13 March 2020), 2018b.

Myhre, G., Samset, B. H., Schulz, M., Balkanski, Y., Bauer, S., Berntsen, T. K., Bian, H., Bellouin, N., Chin, M., Diehl, T., Easter, R. C., Feichter, J., Ghan, S. J., Hauglustaine, D., Iversen, T., Kinne, S., Kirkevåg, A., Lamarque, J.-F., Lin, G., Liu, X., Lund, M. T., Luo, G., Ma, X., van Noije, T., Penner, J. E., Rasch, P. J., Ruiz, A., Seland, Ø., Skeie, R. B., Stier, P., Takemura, T., Tsigaridis, K., Wang, P., Wang, Z., Xu, L., Yu, H., Yu, F., Yoon, J.-H., Zhang, K., Zhang, H., and Zhou, C.: Radiative forcing of the direct aerosol effect from AeroCom Phase II simulations, Atmos. Chem. Phys., 13, 1853–1877, https://doi.org/10.5194/acp-13-1853-2013, 2013.

Nassar, R., Hill, T. G., McLinden, C. A., Wunch, D., Jones, D. B. A., and Crisp, D.: Quantifying CO_2 Emissions From Individual Power Plants From Space, Geophys. Res. Lett., 44, 10045–10053, https://doi.org/10.1002/2017GL074702, 2017.

Nisbet, E. G., Dlugokencky, E. J., and Bousquet, P.: Methane on the Rise–Again, Science, 343, 493–495, https://doi.org/10.1126/science.1247828, 2014.

Nishanth, T., Praseed, K. M., Rathnakaran, K., Satheesh Kumar, M. K., Ravi Krishna, R., and Valsaraj, K. T.: Atmospheric pollution in a semi-urban, coastal region in India following festival seasons, Atmos. Environ., 47, 295–306, https://doi.org/10.1016/j.atmosenv.2011.10.062, 2012.

O'Keefe, A. and Deacon, D. A. G.: Cavity ring-down optical spectrometer for absorption measurements using pulsed laser sources, Rev. Sci. Instr., 59, 2544–2551, https://doi.org/10.1063/1.1139895, 1988.

Pasquill, F.: The estimation of the dispersion of windborne material, Meteorol. Mag., 90, 33–49, 1961.

Phillips, N. G., Ackley, R., Crosson, E. R., Down, A., Hutyra, L. R., Brondfield, M., Karr, J. D., Zhao, K., and Jackson, R. B.: Mapping urban pipeline leaks: Methane leaks across Boston, Environ. Pollut., 173, 1–4, https://doi.org/10.1016/j.envpol.2012.11.003, 2013.

Picarro: Datasheet GasScouter G4302 CH_4, C_2H_6 and H_2O Analyzer, available at: https://www.picarro.com/support/library/documents/gasscoutertm_g4302_analyzer_data_sheet (last access: 13 March 2020), 2017.

Plant, G., Kort, E. A., Floerchinger, C., Gvakharia, A., Vimont, I., and Sweeney, C.: Large Fugitive Methane Emissions From Urban Centers Along the U.S. East Coast, Geophys. Res. Lett., 46, 8500–8507, https://doi.org/10.1029/2019GL082635, 2019.

Polag, D. and Keppler, F.: Global methane emissions from the human body: Past, present and future, Atmos. Environ., 214, 116823, https://doi.org/10.1016/j.atmosenv.2019.116823, 2019.

Pregger, T., Scholz, Y., and Friedrich, R.: Documentation of the Anthropogenic GHG Emission Data for Europe Provided in the Frame of CarboEurope GHG and CarboEurope IP, available at: http://carboeurope.org/ceip/products/files/Pregger_IER_Final_Report_Feb2007.pdf (last access: 13 March 2020), 2007.

Roscioli, J. R., Yacovitch, T. I., Floerchinger, C., Mitchell, A. L., Tkacik, D. S., Subramanian, R., Martinez, D. M., Vaughn, T. L., Williams, L., Zimmerle, D., Robinson, A. L., Herndon, S. C., and Marchese, A. J.: Measurements of methane emissions from natural gas gathering facilities and processing plants: measurement methods, Atmos. Meas. Tech., 8, 2017–2035, https://doi.org/10.5194/amt-8-2017-2015, 2015.

Saunois, M., Jackson, R. B., Bousquet, P., Poulter, B., and Canadell, J. G.: The growing role of methane in anthropogenic climate change, Environ. Res. Lett., 11, 120207, https://doi.org/10.1088/1748-9326/11/12/120207, 2016.

Schwietzke, S., Griffin, W. M., Matthews, H. S., and Bruhwiler, L. M. P.: Natural Gas Fugitive Emissions Rates Constrained by Global Atmospheric Methane and Ethane, Environ. Sci. Technol., 48, 7714–7722, https://doi.org/10.1021/es501204c, 2014.

Schwietzke, S., Sherwood, O. A., Bruhwiler, L. M. P., Miller, J. B., Etiope, G., Dlugokencky, E. J., Michel, S. E., Arling, V. A., Vaughn, B. H., White, J. W. C., and Tans, P. P.: Upward revision of global fossil fuel methane emissions based on isotope database, Nature, 538, 88–91, https://doi.org/10.1038/nature19797, 2016.

Shi, G.-L., Liu, G.-R., Tian, Y.-Z., Zhou, X.-Y., Peng, X., and Feng, Y.-C.: Chemical characteristic and toxicity assessment of particle associated PAHs for the short-term anthropogenic activity event: During the Chinese New Year's Festival in 2013, Sci. Total Environ., 482–483, 8–14, https://doi.org/10.1016/j.scitotenv.2014.02.107, 2014.

Smith, M. E.: Recommended Guide for the Prediction of the Dispersion of Airborne Effluents, 1st edition, American Society of Mechanical Engineers, New York, 1968.

Sutton, O. G.: A Theory of Eddy Diffusion in the Atmosphere, P. Roy. Soc. Lond. A, 135, 143–165, https://doi.org/10.1098/rspa.1932.0025, 1932.

Toja-Silva, F., Chen, J., Hachinger, S., and Hase, F.: CFD simulation of CO_2 dispersion from urban thermal power plant: Analysis of turbulent Schmidt number and comparison with Gaussian plume model and measurements, J. Wind Eng. Ind. Aerod., 169, 177–193, https://doi.org/10.1016/j.jweia.2017.07.015, 2017.

von Fischer, J. C., Cooley, D., Chamberlain, S., Gaylord, A., Griebenow, C. J., Hamburg, S. P., Salo, J., Schumacher, R., Theobald, D., and Ham, J.: Rapid, Vehicle-Based Identification of Location and Magnitude of Urban Natural Gas Pipeline Leaks, Environ. Sci. Technol., 51, 4091–4099, https://doi.org/10.1021/acs.est.6b06095, 2017.

Weller, Z. D., Roscioli, J. R., Daube, W. C., Lamb, B. K., Ferrara, T. W., Brewer, P. E., and von Fischer, J. C.: Vehicle-Based Methane Surveys for Finding Natural Gas Leaks and Estimating Their Size: Validation and Uncertainty, Environ. Sci. Technol., 52, 11922–11930, https://doi.org/10.1021/acs.est.8b03135, 2018.

Worden, J. R., Bloom, A. A., Pandey, S., Jiang, Z., Worden, H. M., Walker, T. W., Houweling, S., and Röckmann, T.: Reduced biomass burning emissions reconcile conflicting estimates of the post-2006 atmospheric methane budget, Nat. Commun., 8, 2227, https://doi.org/10.1038/s41467-017-02246-0, 2017.

Wunch, D., Toon, G. C., Hedelius, J. K., Vizenor, N., Roehl, C. M., Saad, K. M., Blavier, J.-F. L., Blake, D. R., and Wennberg, P. O.: Quantifying the loss of processed natural gas within California's South Coast Air Basin using long-term measurements of ethane and methane, Atmos. Chem. Phys., 16, 14091–14105, https://doi.org/10.5194/acp-16-14091-2016, 2016.

Yacovitch, T. I., Herndon, S. C., Roscioli, J. R., Floerchinger, C., McGovern, R. M., Agnese, M., Pétron, G., Kofler, J., Sweeney, C., Karion, A., Conley, S. A., Kort, E. A., Nähle, L., Fischer, M.,

Hildebrandt, L., Koeth, J., McManus, J. B., Nelson, D. D., Zahniser, M. S., and Kolb, C. E.: Demonstration of an ethane spectrometer for methane source identification, Environ. Sci. Technol., 48, 8028–8034, https://doi.org/10.1021/es501475q, 2014.

Yacovitch, T. I., Herndon, S. C., Pétron, G., Kofler, J., Lyon, D., Zahniser, M. S., and Kolb, C. E.: Mobile Laboratory Observations of Methane Emissions in the Barnett Shale Region, Environ. Sci. Technol., 49, 7889–7895, https://doi.org/10.1021/es506352j, 2015.

Yacovitch, T. I., Neininger, B., Herndon, S. C., Denier van der Gon, H., Jonkers, S., Hulskotte, J., Roscioli, J. R., and Zavala-Araiza, D.: Methane emissions in the Netherlands: The Groningen field, Elem. Sci. Anth., 6, 57, https://doi.org/10.1525/elementa.308, 2018.

C. Copy of "Climate Impact Comparison of Electric and Gas-Powered End-User Appliances"

The following publication "Climate Impact Comparison of Electric and Gas-Powered End-User Appliances" by Florian Dietrich, Jia Chen, Ankit Shekhar, Sebastian Lober, Konstantin Krämer, Graham Leggett, Carina van der Veen, Ilona Velzeboer, Hugo Denier van der Gon, and Thomas Röckmann is published in Earth's Future [108] and is licensed under CC BY 4.0.

AGU ADVANCING EARTH AND SPACE SCIENCE

Earth's Future

RESEARCH ARTICLE
10.1029/2022EF002877

Climate Impact Comparison of Electric and Gas-Powered End-User Appliances

Florian Dietrich[1], Jia Chen[1], Ankit Shekhar[2], Sebastian Lober[1], Konstantin Krämer[1], Graham Leggett[3], Carina van der Veen[4], Ilona Velzeboer[5], Hugo Denier van der Gon[6], and Thomas Röckmann[4]

[1]Environmental Sensing and Modeling, Technical University of Munich (TUM), Munich, Germany, [2]Department of Environmental Systems Science, ETH Zurich, Zurich, Switzerland, [3]LI-COR Biosciences, Lincoln, NE, USA, [4]Institute for Marine and Atmospheric research Utrecht, Utrecht University, Utrecht, The Netherlands, [5]Environmental Modelling, Sensing and Analysis (EMSA), TNO, Petten, The Netherlands, [6]Climate, Air and Sustainability, TNO, Utrecht, The Netherlands

Key Points:

- Methane emissions at Oktoberfest are measured and classified as natural gas-based using isotopic analysis and the ratio of ethane to methane
- Oktoberfest could save 87% of total carbon emissions from energy consumption if all gas-powered appliances were replaced with electric ones
- We aim to make people aware how the carbon footprint of electric and natural gas-driven end-user appliances compares and evolves over time

Supporting Information:

Supporting Information may be found in the online version of this article.

Correspondence to:

F. Dietrich and J. Chen,
flo.dietrich@tum.de;
jia.chen@tum.de

Citation:

Dietrich, F., Chen, J., Shekhar, A., Lober, S., Krämer, K., Leggett, G., et al. (2023). Climate impact comparison of electric and gas-powered end-user appliances. *Earth's Future*, *11*, e2022EF002877. https://doi.org/10.1029/2022EF002877

Received 10 JUL 2022
Accepted 19 DEC 2022

Author Contributions:

Conceptualization: Florian Dietrich, Jia Chen
Data curation: Florian Dietrich, Ankit Shekhar
Formal analysis: Florian Dietrich, Jia Chen, Ankit Shekhar, Sebastian Lober, Konstantin Krämer, Carina van der Veen, Ilona Velzeboer
Funding acquisition: Florian Dietrich, Jia Chen, Hugo Denier van der Gon, Thomas Röckmann

Abstract Natural gas is considered a bridging technology in the energy transition because it produces fewer carbon emissions than coal, for example. However, when leaks exist, methane is released into the atmosphere, leading to a dramatic increase in the carbon footprint of natural gas, as methane is a much stronger greenhouse gas than carbon dioxide. Therefore, we conducted a detailed study of methane emissions from gas-powered end-use appliances and then compared their climate impacts with those of electricity-powered appliances. We used the Munich Oktoberfest as a case study and then extended the study to 25 major natural gas consuming countries. This showed that electricity has been the more climate-friendly energy source at Oktoberfest since 2005, due to the extensive use of renewable electricity at the festival and the presence of methane emissions, particularly caused by the incomplete combustion and leakages of natural gas in cooking and heating appliances. By contrast, at the global level, our study shows that natural gas still produces lower carbon emissions for end-user appliances than electricity in 18 of the 25 countries studied. However, as the share of renewable energy in the electricity mix steadily increases in most countries, the carbon footprint of electricity will be lower than that of natural gas in these countries in the near future. These findings from our comparison of the total carbon emissions of electric and gas-powered end-use appliances can help inform the debate on how to effectively address climate change.

Plain Language Summary Although natural gas is considered a relatively climate-friendly energy source compared to coal, leakage of methane, the main component of natural gas, can significantly increase the climate impact of natural gas. This is because methane is a very strong greenhouse gas. In this study, we focused on methane leakage from end-use appliances used for cooking and heating. Using the Munich Oktoberfest as a case study, we found that these end-use appliances produce significant methane emissions. Therefore, we investigated at which leakage rates and which electricity mixes it would be better to use electric appliances for cooking and heating instead to reduce overall carbon emissions. We found that despite leakage rates, natural gas is still more climate-friendly than electricity in most countries around the world. However, as the share of renewable energy in the electricity mix increases in most countries, electricity is becoming a more climate-friendly energy source every year. With this study, we want to make people aware of how the climate friendliness of electricity compares to natural gas over time.

1. Introduction

To reach the goal of net-zero greenhouse gas (GHG) emissions, the usage of natural gas is considered to be a bridge technology in many countries, as it is promoted to be more climate-friendly than burning coal (Ladage et al., 2021). However, methane (CH_4), the main component of natural gas, has a much stronger warming potential (GWP_{20} of 86 with the consideration of climate-carbon feedback) than carbon dioxide (CO_2) and is released when natural gas enters the atmosphere incompletely burned (Myhre et al., 2013). Recent studies have shown that anthropogenic fossil CH_4 emissions are generally underestimated (Alvarez et al., 2018; Hmiel et al., 2020; Schwietzke et al., 2016) and that the targets set in the Paris Agreement can only be met if CH_4 emissions are drastically reduced (Nisbet et al., 2019).

To improve the quantification of CH_4 emissions, many studies around the world have focused on determining these CH_4 emissions using various measurement and modeling approaches including mobile street-level

Investigation: Florian Dietrich, Jia Chen, Ankit Shekhar, Sebastian Lober, Konstantin Krämer, Graham Leggett
Methodology: Florian Dietrich, Jia Chen, Ankit Shekhar
Project Administration: Florian Dietrich, Jia Chen
Resources: Jia Chen, Graham Leggett, Hugo Denier van der Gon, Thomas Röckmann
Software: Florian Dietrich, Jia Chen, Ankit Shekhar, Sebastian Lober, Konstantin Krämer
Supervision: Florian Dietrich, Jia Chen
Visualization: Florian Dietrich, Jia Chen, Ankit Shekhar, Sebastian Lober, Konstantin Krämer
Writing – original draft: Florian Dietrich, Jia Chen, Ankit Shekhar
Writing – review & editing: Hugo Denier van der Gon, Thomas Röckmann

measurements with fast in situ analyzers on vehicles (Gallagher et al., 2015; Jackson et al., 2014; Maazallahi et al., 2020; Phillips et al., 2013; von Fischer et al., 2017; Weller et al., 2018, 2020), interpretation of plume measurements utilizing the downwind tracer flux approach (Mitchell et al., 2015; Omara et al., 2016; Roscioli et al., 2015; Zimmerle et al., 2015), larger scale airborne measurements with analyzers on aircraft (Karion et al., 2013; Lyon et al., 2016), local eddy flux measurements (Gioli et al., 2012; Helfter et al., 2016), or FTIR sensor networks (Chen et al., 2016; Dietrich et al., 2021; Hase et al., 2015; Jones et al., 2021; Klappenbach et al., 2021; Makarova et al., 2021; Vogel et al., 2019; Zhao et al., 2019).

To attribute the source and determine the leakage rate, either isotopic signatures of the gas are measured (Beck et al., 2012; Chamberlain et al., 2016; Fisher et al., 2006; Lu et al., 2021; Menoud et al., 2020, 2021; Röckmann et al., 2016; Zimnoch et al., 2019), the ethane to methane ratio is determined, because ethane is a unique tracer for fossil fuel related methane emissions, or both methods are used simultaneously (Allen et al., 2013; Maazallahi et al., 2020; Yacovitch et al., 2014, 2015, 2018; Zavala-Araiza et al., 2015).

In our study, we focus specifically on total emissions from natural gas compared to electricity in the end-use sector, as these emissions are suspected of contributing considerably to the underestimates in current methane emissions inventories (McKain et al., 2015; Plant et al., 2019). We use the Munich Oktoberfest—a very large festival with more than 6 million visitors per year—as a case study where gas end-user appliances are highly concentrated. Overall, 40% of the energy demand at Oktoberfest is met by natural gas (mainly for heating and cooking). The event has already been identified as a significant source of CH_4 (Chen et al., 2020), but it has not been fully understood what portions of these methane emissions are due to natural gas leakages. Due to the extensive use of gas-powered cooking and heating appliances in a limited space, we believe Oktoberfest is a well-suited experimental setup where the climate impacts of using such appliances can be determined quite easily. In addition, Oktoberfest has an exemplary, steadily increasing share of renewable energy in electricity consumption (Landeshauptstadt München, 2019; Landeshauptstadt München Redaktion, 2020), making it a well-suited event where the climate impacts of gas-powered and electric end-user appliances can be compared in a representative way. Therefore, Oktoberfest is particularly suited for demonstrating the differences in total GHG emissions from natural gas compared to electricity for the case where the share of renewables increases over time.

Since emissions reductions only at Oktoberfest will not have a noticeable impact on a global scale, these findings that electricity could be the more climate-friendly alternative for cooking and heating, depending on the electricity mix and leakage rate, need to be transferred globally to achieve positive climate effects. While previous studies have focused either exclusively on leakage rates from gas-fired end-user appliances (Lebel et al., 2022) or on comparing emissions from coal to those from natural gas combustion (Fulton et al., 2011; Ladage et al., 2021; Qin et al., 2017; Tanaka et al., 2019), little consideration has been given to electricity generated by an ever-growing share of renewable energy. When considering how such end-user appliances can be operated in a climate-friendly way, for example, at other festivals, in restaurants or in private households, such a comparison is the basis for the right decision. That is why we also analyze the climate impact of electric and gas-powered appliances for 25 major natural gas-consuming countries to show where and when it is more climate-friendly to use one or the other energy source.

2. Materials and Methods

In the present study, we first determined the total CH_4 emissions from Oktoberfest based on mobile measurements combined with an atmospheric transport model, then used isotope and ethane analyses to assign emission sources and finally determined the point in time and the break-even share of renewables at which electric appliances are more climate-friendly than gas appliances at Oktoberfest. Afterward, we applied our newly developed methods to a global scale and compared the carbon footprint of natural gas and electricity as an energy source for end-user appliances around the world.

2.1. Mobile In Situ Measurements at Oktoberfest

We carried out mobile in situ measurements at Oktoberfest 2019. For that, we utilized the LI-7810 $CH_4/CO_2/H_2O$ Trace Gas Analyzer from LI-COR, which uses the optical feedback cavity-enhanced absorption technique (OF-CEAS), as a mobile backpack instrument. Simultaneously to the measurements, the current position of each data point was recorded using a GPS application on a smartphone that was time-synchronized to the gas analyzer.

In contrast to our preceding study in 2018 (Chen et al., 2020), we were allowed to perform measurements both outside and inside the festival premises as well as inside the tents. To determine the emission strength, only the measurements around the perimeter of Oktoberfest (hereafter referred to as *outer rounds*) were used to allow for an easy comparison to our 2018 results. The measurements on the site (hereafter referred to as *inner rounds*) were mainly used to find emission hotspots.

To cover different days of the week and times of the day, we completed 56 rounds during Oktoberfest. For a comparison to CH_4 emissions outside the festival period, we also completed 15 measurement rounds after the end of Oktoberfest. We do not have any measurements before the start of the festival because the loaner gas analyzer did not arrive in time. However, we assume that the emissions before and after the Oktoberfest are comparable. The rounds during the festival period were divided into outer and inner rounds. Each inner round was always combined with at least one outer round to obtain background concentrations for CH_4 each time.

For the outer rounds, we chose the shortest possible walking distance around the perimeter of Oktoberfest, which is directly behind the security fences. The walking distance for such a round is about 2.6 km (see Figure S1 in Supporting Information S1) and took us on average about 40 min each. Combined with a gas analyzer sampling rate of 1 Hz, approximately 2,400 measurement points were recorded per round.

During our measurements inside the festival premises, we followed two routes that were predefined by us. Both of them were chosen to capture the emissions caused by the large tents and booths on the streets best. Therefore, they follow the streets between the tents that are mainly located in the northwest quarter (see Figure S1 in Supporting Information S1).

2.2. Modeling the CH_4 Emissions

To quantify the CH_4 emissions of Oktoberfest, we combined the measurements around the perimeter of Oktoberfest with the modeling approach developed in Chen et al. (2020). The model is based on a multiple Gaussian plume approach using the 17 largest beer tents as point sources, linearly weighted according to their size, and superimposed to model a continuous expected concentration signal at the sampling points around the perimeter of Oktoberfest. Since we used only the outer rounds for this approach to determining emissions, the sampling sites are at least 100 m away from the nearest sources, resulting in well-mixed concentrations. Since emissions are represented by the concentration differences between upwind and downwind sites, background concentrations were modeled linearly based on the 10% smallest measured values for each round and then subtracted. The entire model results in one emission number for each round. The final emission number is an averaged value of the emission numbers from the 38 individual outer rounds, taking into account the uncertainties of the four input parameters wind speed, wind direction, background concentration, and measured concentration values. For this purpose, these four input parameters were each modeled as an independent Gaussian distribution and the model was run 1,000 times. The resulting mean and standard deviation of the distribution of these 1,000 emissions represent the final emission number and its uncertainty.

The main differences to the investigations in Chen et al. (2020) were a different CH_4 analyzer (in 2018, the Picarro G4301 gas scouter, which is based on the cavity ring-down principle was used) and wind measurements closer to the festival premises, as the sensitivity study in Chen et al. (2020) indicated a strong influence of the wind measurements to the atmospheric model. Therefore, we established a wind sensor very close to the festival premises on top of a building, which is located approximately 150 m west of Oktoberfest (48.134°N, 11.545°E, 26 m a.g.l.). As a sensor, the Lufft WS200-UMB 2D ultrasonic wind sensor was utilized. The other model parameters such as the number of emitters, plume modeling algorithm, averaging approach, etc. were equal to Chen et al. (2020).

2.3. Air Sampling

In addition to the backpack measurements, we took samples of the environmental air at different locations, such as inside and outside the festival premises, inside the beer tents, next to possible emission hotspots at the festival, and in the subway. For this purpose, Standard FlexFoil air sampling bags from SKC Ltd. with a volume of 3 L were used. In total, we filled 30 bags and shipped them afterward to Utrecht University and TNO in the Netherlands, where they were analyzed in the lab. At Utrecht University, in 12 bags (two of them were background samples) $\delta^{13}C$ and δD were analyzed using Isotope Ratio Mass Spectrometry (IRMS) (Brass & Röckmann, 2010).

The device used was the spectrometer model Delta V Plus/Deltaplus XL from Thermo Fisher Scientific Inc. At TNO, the Δethane to Δmethane ratios of the remaining 18 bags (seven of them were background samples) were measured using the Quantum Cascade Laser (QCL) absorption spectrometer model QCL-TILDAS-76 from Aerodyne Research Inc.

2.4. Isotopic Analyses of Air Samples

To determine, whether the measured methane is anthropogenic or biogenic, analyses of the carbon isotopes were made. We used the $\delta^{13}C$ method, in which the ratio between ^{13}C and ^{12}C of the sample gas is compared to the ratio of a predefined standard. Similar to $\delta^{13}C$, we also looked at the ratio of deuterium to normal hydrogen using the δD method. The mathematical expressions for these two methods are shown in Section S2 in Supporting Information S1.

Since the sampled air also includes the unknown background isotopic signature of the gas, we utilized Keeling plots to determine the isotopic signature of the gas emitted exclusively by Oktoberfest. These plots linearize the relation between the $\delta^{13}C$ (or δD) value of the measured air sample and the methane concentration so that the $\delta^{13}C$ (or δD) portion added by the unknown source can be determined (Keeling, 1958).

2.5. Ethane to Methane Ratio of Air Samples

As a second kind of analysis to determine the origin of the sample gas, we examined the Δethane to Δmethane ratio (Allen et al., 2013; Maazallahi et al., 2020; McKain et al., 2015; Yacovitch et al., 2014, 2015, 2018; Zavala-Araiza et al., 2015). For this purpose, we subtract the background concentrations of methane ($CH_{4,bg}$) and ethane ($C_2H_{6,bg}$) from the measured concentrations ($CH_{4,sample}$ and $C_2H_{6,sample}$) to obtain the ratio of the gas added by the source:

$$\frac{C_2H_{6,source}}{CH_{4,source}} = \frac{\Delta C_2H_6}{\Delta CH_4} = \frac{C_2H_{6,sample}}{CH_{4,sample} - CH_{4,bg}} \quad (1)$$

Thereby, we assumed that the ethane concentration $C_2H_{6,bg}$ of the background can be set to zero, which is supported by our five background air samples that we took during the time of Oktoberfest 2019. For each sampling point, a Δethane to Δmethane ratio was determined and afterward compared with the ratio of the Munich gas network. Since the composition of Munich's natural gas is determined only once a month, a weighted average was calculated for the 16 days of Oktoberfest 2019, which took place 10 days in September and 6 days in October 2019. The uncertainties were calculated using the 99% confidence intervals of all gas samples measured in the tent combined with the minimum ($r_{ethane,\ Sept} = 3.04\%$) and maximum ($r_{ethane,Oct} = 3.07\%$) ethane share in September and October 2019, respectively (SWM Infrastruktur GmbH und Co. KG., 2019a, 2019b).

2.6. Calculation of the Climate Impact

To find out, whether gas or electric appliances for cooking and heating have a better carbon footprint, the total emission factors in CO_2 equivalents (CO_2eq) are calculated for the case of electric and gas use only. In our study, we did not focus only on end-user appliances, but looked at the entire supply chain. To this end, we included emission factors for the various energy sources, including power plant efficiencies and, for natural gas-related processes, methane leakage rates.

For the efficiency of the end-user appliances themselves, we have assumed that it is the same for electric and gas-powered appliances. This seems to be a reasonable assumption in terms of a mean value, as several prior studies have found a wide range of efficiencies, some stating that electric appliances (Hager & Morawicki, 2013) and some stating that gas-powered appliances (Adria & Bethge, 2013) require less energy. This wide range is due to different types of stoves and the time used for comparison. Gas-powered appliances, while generally less efficient, heat up much faster than electric appliances.

To calculate the emission factor $EF_{elect}(t)$, if only electricity would be used as an energy source, Equation 2 is utilized:

$$EF_{elect}(t) = \sum_{n=1}^{8} EF_n \cdot p_{elect,n}(t) \quad (2)$$

These emissions differ for each country and are time-dependent, as the proportions of fuel types used for electricity production $p_{elect,n}(t)$ vary over time. In this study, we considered four different types of non-renewable energy sources (coal, oil, gas, and nuclear power) and four different types of renewable energies (hydro, solar, wind,

and geothermal/biomass power) with different emission factors EF_n obtained from Amponsah et al. (2014) (see Table S1 in Supporting Information S1). These emission factors represent global mean values and may vary from country to country due to technological progress. Therefore, the results for certain countries may be subject to uncertainties and should be examined more closely if a specific country is to be studied.

For the case, where we assumed that only natural gas is used for producing the same amount of energy, the emission factor $EF_{\mathrm{NG,\,total}}$ is calculated by adding the emission factors of combusting natural gas EF_3 (see Table S1 in Supporting Information S1) and leaking CH_4, as shown in Equation 3:

$$EF_{\mathrm{NG,total}} = EF_3 \cdot (1 - r_{\mathrm{leak}}) + \frac{\rho_{\mathrm{CH4}} \cdot \mathrm{GWP}_{20,\mathrm{CH4}}}{E_{\mathrm{d,NG}}} \cdot r_{\mathrm{leak}} \tag{3}$$

Where r_{leak} is the leakage rate of natural gas, ρ_{CH4} is the density of CH_4 (0.668 kg/m^3), $\mathrm{GWP}_{20,\mathrm{CH4}}$ the 20-year global warming potential of methane considering climate-carbon feedback (86 tCO_2eq/t) (Myhre et al., 2013) and $E_{\mathrm{d,NG}}$ the energy density of natural gas ($3.6 \cdot 10^{-5}$ TJ/m^3).

2.7. Country Specific Emission Data

Equations 2 and 3 are applied for different countries and years, resulting in a time-dependent country comparison of the carbon footprint of electrical versus gas-driven appliances. We examined the shares and types of non-renewables and renewables in the electricity mix only for countries that account for at least 0.5% of global natural gas consumption (40 countries in total). However, we excluded countries with a renewable energy share of less than 10% in 2019 (which primarily includes Middle Eastern countries), as we want to focus in this study primarily on how an increasing share of renewable energy can make electricity more climate-friendly compared to natural gas. The chosen 25 countries account for 75% of the world's natural gas consumption, with the United States alone accounting for about 21.7%, followed by Russia and China with 12.4% and 5.4%, respectively (WorldData.info, 2020). Similar to the Oktoberfest investigations, in this country comparison, we focused primarily on the climate impact of appliances at the end-user, namely cooking and heating appliances in the household sector.

The data on the electricity mix was taken from the *BP Statistical Review of World Energy, 69*th *Edition* (bp., 2020). The electricity mix data indicate the type and proportion of energy sources (coal, natural gas, oil, nuclear, and renewables) used to generate electricity from 1965 to 2019 (for some countries only from 2000 to 2019). In this study, we concentrate on the 21st century only. The data on the share of renewable energy was also cross-checked with *Trends in Renewable Energy* provided by the International Renewable Energy Agency (IRENA) (International Renewable Energy Agency, 2020). IRENA provides data from 2000 to 2018.

2.8. Phase Transition Plot

To show how the shares of renewable and non-renewable energy and the respective sources for these energies affect the climate friendliness of electricity and natural gas, we used phase transition diagrams. These 2D heat maps depict the standardized emissions difference between electricity and natural gas as a function of renewable energy shares of electricity generation and methane leakage rates. Red shaded areas indicate that natural gas is the more climate-friendly energy, while blue shaded areas indicate that electricity is more climate-friendly. Such a phase transition diagram is shown in Figure 4 on the left and is explained in more detail in the related results Section 3.3.

We used 2019 energy data for both Oktoberfest and each of the 25 countries to create these charts. To create the phase transition plots, we varied the methane leakage rate from 0% to 15% in 0.1% increments and the renewable energy share from 0% to 100% in 1% increments, and calculated the difference in carbon footprint between CO_2eq emissions from electricity and natural gas for each of these points. Then, the minimum percentage of renewables required to make electricity the more climate-friendly energy source is determined by intersecting the line representing all points at which natural gas and electricity are equally climate-friendly with the actual methane leakage rate. The y-value of this intersection represents the minimum percentage of renewable energy required to make electricity the more climate-friendly energy source, taking leakage into account. We then calculated the difference between this minimum share and the current (2019) share of renewables in each country and plotted the differences as a bar chart in Figure 6. Error bars were determined by using the lower and upper bounds

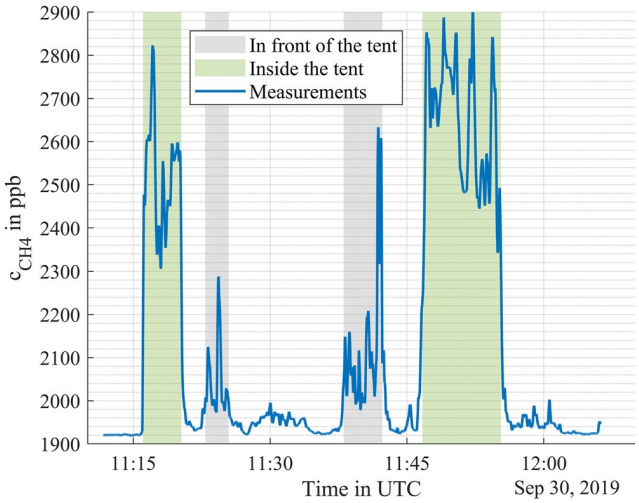

Figure 1. CH_4 mole fractions measured at the Oktoberfest premises. The concentrations measured during a tour at the Oktoberfest premises show a large heterogeneity and are especially enhanced inside (green shaded) and in front of (gray shaded) the beer tents.

of the 90% confidence interval of the leakage rate distribution, which correspond to 0.22% and 5.35%, respectively. The details are further explained in Section 3.4.1.

3. Results

3.1. CH_4 Emission Number

Utilizing all 38 outer rounds during Oktoberfest, we determined an emission number of $(8.5 \pm 0.5)\,\mu g\left(m^2 s\right)^{-1}$. The value is in the same order of magnitude as the one quantified in 2018: $(6.7 \pm 0.6)\,\mu g\left(m^2 s\right)^{-1}$ (Chen et al., 2020). Emissions identified for the period after the end of the festival also have a positive offset in 2019 ($2.5\,\mu g\left(m^2 s\right)^{-1}$ vs. $1.1\,\mu g\left(m^2 s\right)^{-1}$). The distributions of these two emission numbers are shown in Figure S2 in Supporting Information S1. Possible reasons for these slightly higher numbers in 2019 include more accurate wind measurements taken closer to the festival premises or real changes in emissions between the 2 years. Still our 2019 measurements confirm that Oktoberfest is a significant source of CH_4 that can be made more climate friendly if the emission sources can be precisely located and quantified and mitigation measures can thus be developed.

3.2. Source Attribution

To find emission sources on the large festival premises, measurements were made in the vicinity of possible sources and a categorization of the sources into biogenic and anthropogenic origin was carried out. For this purpose, we performed mobile in situ measurements inside the festival premises and determined the isotopic signature and the ethane to methane ratios of air samples taken at Oktoberfest.

3.2.1. Inside Measurements

During our measurements on the festival site, the measurements with our instrument did not detect any CH_4 enhancements in the vicinity of gas control stations and pipelines. This also confirms the statement of Stadtwerke München (SWM) that these stations are already carefully monitored and maintained. Therefore, we did not include these types of emissions in our modeling approach for Oktoberfest. CH_4 concentrations were significantly elevated especially next to the open doors of the beer tents (see Figure 1). In addition, we were allowed to enter one of the large beer tents with our backpack analyzer to verify our assumption further and localize the sources in more detail. Figure 1 shows that the CH_4 mixing ratios of up to 2,900 ppb inside the tents are even higher than in front of the entrance (approximately 2,000–2,600 ppb). Most of the high enhancements were detected when passing the tent kitchen, where cooking is done with gas appliances supplied with natural gas provided by the Munich gas network.

On the streets of the festival grounds, we discovered only two additional hotspots during our 18 tours at the site that were not associated with open tent doors and windows or tent chimneys. The first was close to one of the grilled chicken stalls that run on natural gas and the second was next to a place where fish were grilled over charcoal fires.

We conclude that mostly the 17 large beer tents contribute significantly to the CH_4 emissions of Oktoberfest to the atmosphere. This supports the statement of Chen et al. (2020) that beer tents are the major CH_4 source at Oktoberfest. Therefore, it is a valid approach to model only the large beer tents as sources in order to determine the overall emission strength of Oktoberfest. However, CH_4 is not only emitted by the chimneys but also by open doors and windows of the tents. This should be considered if a spatially higher resolved model is used.

To identify, whether these emissions are of biogenic origin produced by the human bodies or of anthropogenic origin caused by incomplete combustion and leakages of natural gas-driven appliances, air samples were taken and analyzed in the lab afterward.

3.2.2. Isotopic Composition

The results of the isotopic analyses of the samples taken at Oktoberfest are shown in Figure 2 (left and center) as a Keeling plot. The various types of sampling locations, such as in-tent, subway (inside the crowded train

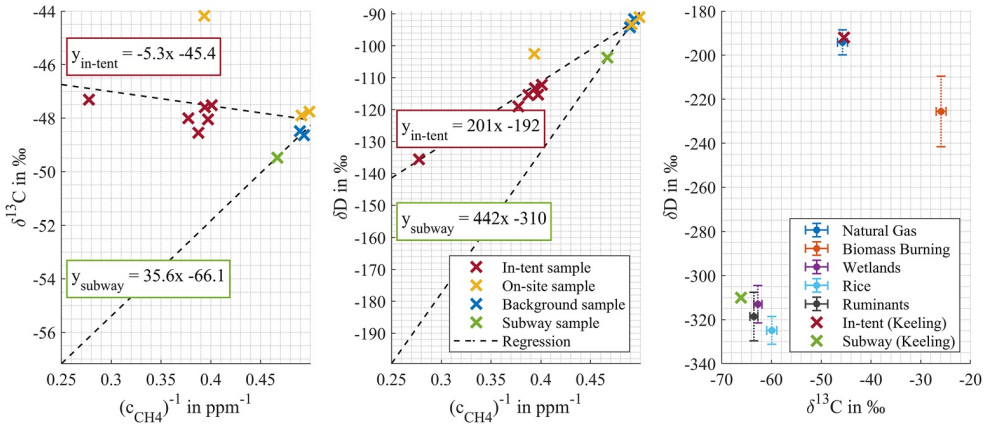

Figure 2. δ^{13}C (left) and δD (center) Keeling plot of the air samples taken at Oktoberfest. In addition, two regression lines are shown in both figures for the Oktoberfest and subway samples, respectively, to determine the isotopic signatures of the sources. Right: Isotopic fingerprint (δ^{13}C vs. δD) off different gas sources (dots with whiskers) based on results of Menoud et al. (2021) including source signatures of Oktoberfest, derived from the Keeling plots (crosses). While the signature of the subway measurement (green cross) is close to biogenic sources, the Oktoberfest measurements (red cross) show a comparable signature to natural gas. These results indicate that Oktoberfest emissions are primarily due to natural gas leakage.

between Oktoberfest and Munich Central Station), and background (outside the Oktoberfest premises) samples, are indicated by different colored crosses. To determine the isotopic signature of each of the two source types, a linear regression line is drawn through all sample points of each source type including the background samples for both δ^{13}C and δD. In this Keeling plot analysis, the intercept of the regression line with the *y*-axis represents the isotopic signature of the gas added by the unknown source. These intercepts are for [δ^{13}C; δD] at [−45.4‰; −192‰] for the in-tent samples and [−66.1‰; −310‰] for the subway sample.

In Figure 2 (right), these isotopic source signatures are compared to typical isotope signatures of different source types, such as natural gas, biomass burning, wetlands, rice, and ruminants. The subway sample (light green cross) shows a clear biogenic signature, which is the expected behavior of a crowd of people. In contrast, the in-tent signature (red cross) is very close to the signature of natural gas, suggesting that the methane emissions of Oktoberfest are primarily caused by fugitive natural gas leakages.

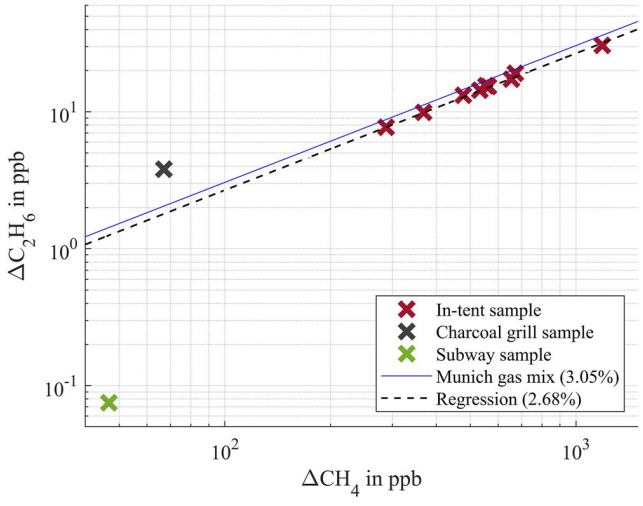

Figure 3. Correlation between Δethane (ΔC_2H_6) and Δmethane (ΔCH_4) of air sampled at various locations at Oktoberfest in a log-log plot. With the exception of the measurements for the subway (green) and the charcoal grill (gray), which show lower and higher ethane enhancement, respectively, all points lie on a line with slope 1, implying a linear relationship between Δethane and Δmethane. Since the slope of this regression line is very close to that of the Munich natural gas mixture, these results indicate that the high methane enhancement inside the tents is caused by natural gas.

3.2.3. Ethane to Methane Ratio

The results of the ethane analyses are shown in Figure 3, where the Δethane to Δmethane correlation is shown as a scatter plot using logarithmic axes. In addition to the two source types *in-tent* and *subway* that we also analyzed with respect to the isotopic fingerprint of the samples in Figure 2, another source type, namely air sampled in front of a large charcoal grill, was analyzed. These three source types exhibit significantly different behavior. The nine samples taken inside the tents (red crosses) show an almost constant Δethane to Δmethane ratio of 2.68% [2.57%, 2.78%] (99% CI). The number is very close to 3.05%, which is the reported averaged ethane to methane ratio of the natural gas used in Munich in September and October 2019 (SWM Infrastruktur GmbH und Co. KG., 2019a, 2019b). Together with the high concentrations measured inside the tents (see Figure 1), this result confirms our hypothesis that the elevated methane levels at Oktoberfest are primarily due to leaking natural gas. A distribution of these ratios is illustrated in Figure S3 in Supporting Information S1. In contrast, the subway sample (light green) has a much lower ethane content and the charcoal grill sample (gray) has a higher ethane content, indicating that small amounts of other methane emissions are present in addition to the natural gas leaks.

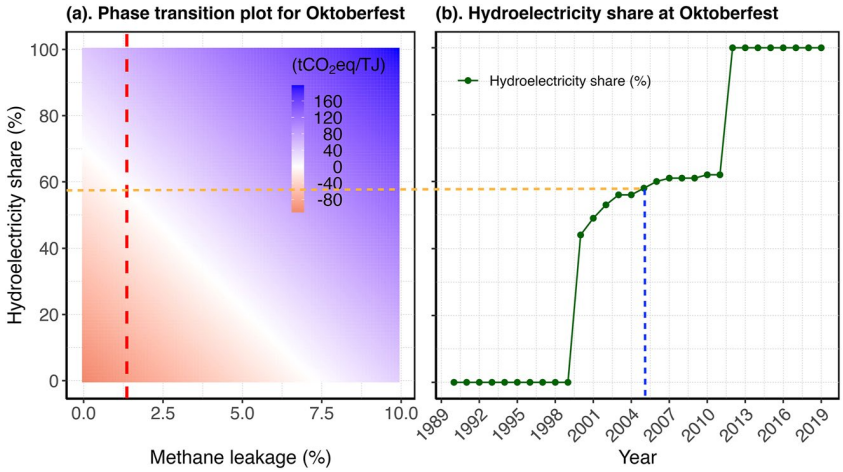

Figure 4. Left: phase transition diagram of hydropower shares in electricity generation versus methane leakage rates. It shows the difference in emissions (in tCO_2eq/TJ) between electricity and natural gas as the energy source for heating and cooking at Oktoberfest. For positive values (blue shaded areas), the use of electricity leads to lower emissions compared to natural gas; for negative values (red shaded areas), the opposite is true. The red vertical dashed line represents the leakage rate of 1.4% measured at Oktoberfest, while the orange horizontal dashed line represents the associated share of renewable energy, where electricity is the more climate-friendly energy source compared to natural gas (58%). Right: share of renewable energies in electricity consumption at Oktoberfest. The dashed orange line shows that the share of renewable energies at Oktoberfest reached the break-even point from 2005 onwards, which means that electricity has been the more climate-friendly energy source than natural gas at the festival ever since.

Dividing the ethane fractions of our Oktoberfest samples ($r_{\text{ethane,Okt}}$) by that of the Munich natural gas mix ($r_{\text{ethane,Muc}}$), we calculate the ratio r_{fugitive} between the ethane shares of these two gases to be

$$r_{\text{fugitive}} = \frac{r_{\text{ethane,Okt}}}{r_{\text{ethane,Muc}}} = \frac{2.68\%\,[2.57\%, 2.78\%]}{3.05\%\,[3.04\%, 3.07\%]} = 88\%\,[84\%, 91\%]. \tag{4}$$

Based on this calculation, we assume that about 88% of the methane emissions in the tents are attributable to fugitive natural gas. The remaining 12% are likely caused by biogenic processes. The values in squared brackets represent the 99% confidence intervals.

In summary, we conclude that the enhanced methane concentrations measured at Oktoberfest 2018 and 2019 are mainly due to natural gas that is either not fully combusted or leaking from natural gas-fueled equipment, such as heaters, grills, and ovens. According to our investigations, gas regulation stations and pipelines at Oktoberfest do not leak significantly and are, therefore, not the reason for the methane enhancements observed.

3.2.4. Leakage Rate

The leakage rate r_{leak} of CH_4 at Oktoberfest is determined as the ratio between the CH_4 loss measured with our instruments ($M_{\text{CH4,loss}}$) and the total CH_4 consumed at Oktoberfest 2019($M_{\text{CH4,total}}$), the calculation of which is explained more in detail in Section S3 in Supporting Information S1:

$$r_{\text{leak}} = \frac{M_{\text{CH}_4,\text{loss}}}{M_{\text{CH}_4,\text{total}}} = \frac{1.635 \cdot 10^3 \text{kg}}{1.186 \cdot 10^5 \text{kg}} = 1.4\% \tag{5}$$

The determined leakage rate is very close to the leakage rate determined by Chen et al. (2020) (1.1%) and lower than the leakage rates determined in the Boston area for all downstream leakage (2.7 ± 0.6%) (McKain et al., 2015) and the entire supply chain (3.3%–4.7%) (Sargent et al., 2021). Alvarez et al. (2018) suggested that methane losses in the U.S. oil and natural gas supply chain are equivalent to 2.3% of gross U.S. natural gas production. However, only end-use equipment was analyzed for Oktoberfest. All leakage in the upstream and midstream natural gas process is not captured by the measurements in this study. We, therefore, conclude that the leakage rate of end-use appliances at Oktoberfest appears to contribute significantly to the overall leakage rate of the natural gas chain. These results suggest that it is relatively easy to achieve a significant improvement in the

carbon footprint of the natural gas chain by simply reducing the leakage rates of end-use appliances. This is likely true not only for Oktoberfest, but for many end-use gas appliances in the world.

3.3. Energy Consideration at Oktoberfest

Although the total energy demand of Oktoberfest has risen within the past 20 years, mainly due to an increase in electricity consumption, total carbon emissions have been drastically reduced. This effect is due to the steadily increasing proportion of renewable electricity used at the festival. Since 2011, only green electricity has been used, 100% of which is generated from hydropower, one of the cleanest renewable energy sources (Amponsah et al., 2014). It should be noted that the hydropower used is only an equivalent for purchased energy and does not represent actual time-of-use statistics. Therefore, emissions caused by electricity use at Oktoberfest could be greater than assumed in our study, depending on which paradigm is used to calculate emissions. We chose this approach of equivalent purchased energy over averaged or marginal emission factors because we believe that purchasing green power at higher rates than conventional power will encourage the expansion of renewable energy over time and should therefore be rewarded. A more detailed analysis of the energy development at Oktoberfest can be found in Section S4 in Supporting Information S1.

We incorporated all energy information determined for Oktoberfest 2019, such as fossil electricity composition, natural gas CO_2eq emissions, renewable energy type, and CH_4 leakage rate, into a phase transition diagram (see Figure 4). This identifies how a changing share of hydropower affects the climate friendliness of electricity compared to natural gas. From the intersection of the white line with the CH_4 leakage rate (red dashed line), it is possible to determine the fraction of hydropower from which electricity is the more climate-friendly energy source than natural gas with consideration of fugitive CH_4 leakages.

Assuming a methane leakage rate of 1.4% determined in our study, electricity with a renewable share greater than 58% is more climate-friendly than natural gas for Oktoberfest as demonstrated in the phase transition plot in Figure 4 (dashed horizontal orange line). Since the share of renewable energy at Oktoberfest exceeded the threshold of 58% in 2005 (see Figure 4, right), it would have been beneficial from a climate change perspective to replace all gas appliances at Oktoberfest with electric appliances starting in this year. In 2019 alone, this could have saved up to 450 tCO_2 emissions.

Such a reduction in emissions for an event that lasts only 2 weeks and is already quite climate-friendly is remarkable and gives us the opportunity to investigate on a larger scale how the type of energy source could help reduce carbon emissions worldwide.

3.4. Comparison of the Climate Impact in Different Countries

The Oktoberfest study showed that whether natural gas or electricity is the more climate-friendly energy source depends very much on the composition of the electricity mix as well as the leakage rate of natural gas. Since each country has its own electricity mix composition, we applied our approach developed for Oktoberfest to 25 major natural gas-consuming countries to understand which of the two energies is more climate-friendly for each of them. For these 25 countries, we studied the climatic impact of electric and natural gas energy sources in two ways. First, using their long-term (2000–2019) temporal trends (shown in Figure 5) and then through a more detailed analysis of the estimated renewable energy gap for the most current year 2019 (shown in Figure 6).

3.4.1. Comparison of Country Emission Over Time

Figure 5 shows the temporal trend of each countries' emission factor for both natural gas (shaded area) and electricity (green solid line). As shown in our Oktoberfest field study, the methane leakage rate has a significant impact on the emission factor of natural gas. Since it is beyond the scope of this paper to determine the leakage rate in each of these countries, we calculated leakage rates based on literature values instead. For this purpose, we calculated the ratio between the sum of all reported fugitive and vented CH_4 emissions of each country and the respective total consumption. Further details on the calculation of the leakage rate can be found in Section S5 in Supporting Information S1. These values only reflect the leakage rates in the respective countries, not the leakage rate in the entire natural gas supply chain. Therefore, upstream and downstream leakage rates are underestimated in countries that mainly consume natural gas and overestimated in countries that mainly produce natural gas. To compensate for these inconsistencies, we determined the distribution of all calculated leakage rates at the country

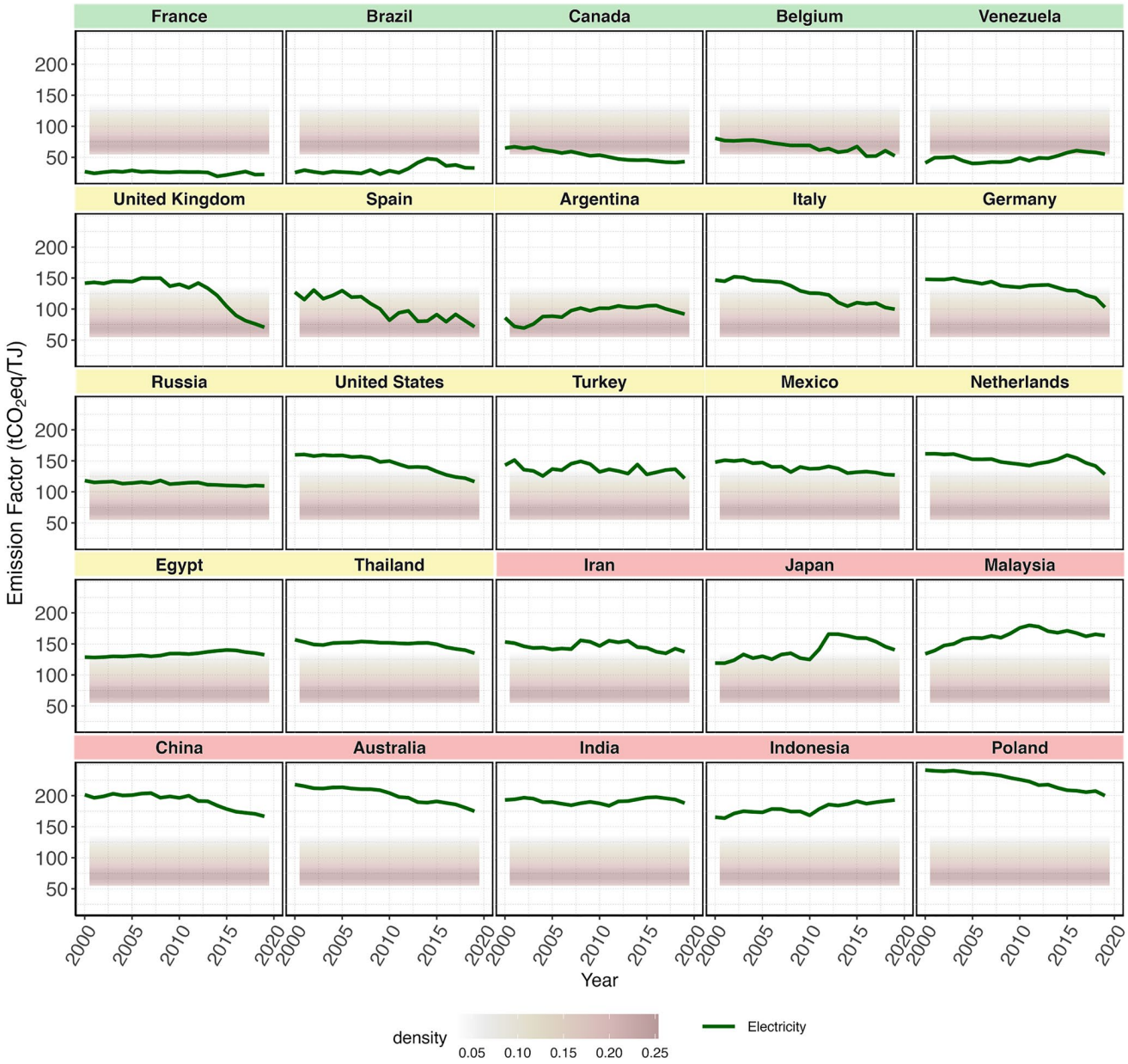

Figure 5. Comparison of CO_2eq emission factors from electricity and natural gas sources over the 20 years from 2000 to 2019 for 25 major natural gas-consuming countries. The emission factor of natural gas is represented by a distribution rather than a distinct line because of the methane leakage rate, which cannot be accurately determined for all countries studied. The countries are colored according to whether their current emission factor for electricity generation is below (green), within (yellow), or above (red) the 90% confidence interval of the distribution of natural gas emission factors.

level. This distribution is presented as a kernel density, with a 90% confidence interval considered, resulting in a lower bound of 0.22% and an upper bound of 5.35% for the leakage rate. This range represents the potential leakage rate throughout the supply chain for all combinations of natural gas producing, transit, and consuming countries. As a result of this leakage rate range, the comparison between the emission factors of electricity and natural gas also only provides upper and lower bounds as of which year electricity could be the more climate-friendly energy source for cooking and heating.

While the carbon footprint of natural gas has remained nearly constant over the years, the carbon emissions of electricity have fluctuated for most countries. This behavior is due to the widely varying emission factors for the different energy sources used to generate electricity (see Table S1 in Supporting Information S1) and is further

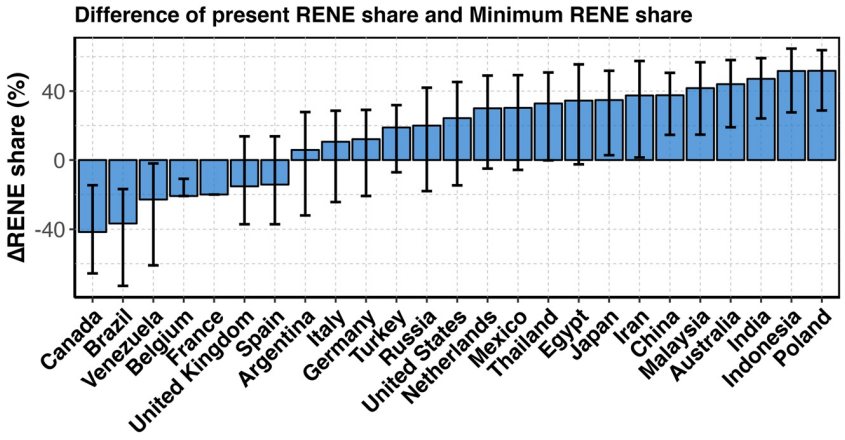

Figure 6. The difference in current renewable energy (RENE) share to reach the break-even point, where natural gas and electricity have the same carbon footprint for 25 countries. Negative values indicate that electricity is already the more climate-friendly energy source compared to natural gas. Values greater than zero represent the increase in RENE share required to make electricity more climate-friendly compared to natural gas. Error bars were determined by using the lower and upper bounds of the 90% confidence interval of the leakage rate distribution, which correspond to 0.22% and 5.35%, respectively.

analyzed in Section S6 in Supporting Information S1. According to the absolute carbon emission factors for electricity generation in 2019, these 25 major natural-gas consuming countries can be classified into three groups (see colored backgrounds in Figure 5).

The first group (green) consists of five countries where the emission factor of electricity in 2019 was below the lower limit of the natural gas emission factor (corresponding to a very small leakage rate of only 0.22%), making electricity very likely the more climate-friendly energy source compared to natural gas. Prominent examples of the first group are Brazil, which has a very high share of renewable energy, and France, which generates its electricity mainly through the extensive use of nuclear power. These results show that not only the share and type of renewable energy, but also the emission factor of non-renewable sources is decisive in determining whether electricity is the more climate-friendly energy source than natural gas.

The second group (yellow) consists of 12 countries where the absolute carbon emissions from electricity intersect the range between the lower and upper limits of the possible natural gas emission levels. These 11 countries have different characteristics that explain why their electricity emission factors are in the same order of magnitude as the natural gas emission factors. These are either the recent increase in the share of renewable energy in electricity generation (e.g., United Kingdom or Germany) or the transition from coal as energy source to electricity generation by natural gas (e.g., United States) (see Figure S7 in Supporting Information S1). More detailed studies are needed for these countries to definitively answer the question of which type of energy source for cooking and heating is the more climate-friendly now and in the near future.

The third group (red) is represented by eight countries where electricity is currently likely to be less climate-friendly than natural gas as the emission factor of electricity is higher than the upper bound of the emission factor of natural gas. These nine countries are characterized primarily by a fairly low share of renewables in electricity generation. Countries that use natural gas as a fossil fuel (e.g., Iran) have lower electricity emission values than countries with extensive use of coal (China, Australia, India, Indonesia, and Poland). For the countries of the third group, natural gas consumption could remain more climate-friendly compared to electricity even in the distant future. In fact, for the five countries with a high proportion of coal as an energy source large amounts of carbon emissions could be saved if natural gas were used as an energy source for end-use appliances instead, since natural gas is, in general, the more climate-friendly energy source compared to coal even if leakages are taken into account (Ladage et al., 2021).

All countries are sorted in ascending order according to their absolute carbon emission factors for electricity generation in 2019.

3.4.2. Country Comparison—Renewable Energy Gap

The results of the phase transition analysis for the 25 countries (see Section S7 in Supporting Information S1) are summarized in Figure 6. There, the 25 countries are sorted in ascending order of the percentage growth in renewable energy share required to reach the break-even point. A negative number means that electricity has a lower emission factor than the mean natural gas emission factor in 2019, so electricity is likely to be the more climate-friendly energy source for household cooking and heating in this country. However, the error bars resulting from the upper and lower bounds of the possible methane leakage rate are quite large, since the leakage rate, which is difficult to determine accurately, has a significant impact on the emission factor of natural gas.

When considering the mean leakage rate, for most of the countries, the share of renewable energy needs to be improved to make electricity a more climate-friendly energy source compared to natural gas. Only Canada, Brazil, Belgium, France, Venezuela, the United Kingdom, and Spain have already reached this point. For the other countries, the share of renewables in the overall electricity mix needs to rise further to make electricity the more climate-friendly alternative to natural gas. It should be noted that the share of renewable energy required to reach the break-even point varies greatly from country to country, depending on the energy mix used for power generation. It ranges from 0% to 67%, depending on the carbon emissions generated by non-renewable electricity generation.

3.4.3. Existing Obstacles for Such Carbon Reductions

Although, replacing natural gas with electric devices could save significant amounts of global carbon emissions, we recognize that it is not possible to immediately run all cooking and heating appliances on electricity instead of natural gas. First of all, there would not be enough electrical energy available or the electricity would have to be generated from non-renewable energy sources, which in turn would increase the carbon footprint. Furthermore, many appliances cannot be easily replaced due to the lack of electrical infrastructure. In addition, natural gas has been in most cases a significantly cheaper energy source than electricity. In Germany, for example, the price per kWh of natural gas in 2019 was only about half that of electricity (see Figure S11 in Supporting Information S1), making it unaffordable for many people to replace gas appliances with electric ones. However, such barriers could be removed by policymakers.

4. Conclusions

In this study, the climate impact of gas appliances used for cooking and heating including the effect of CH_4 leakages was investigated and compared with the carbon footprint of electric appliances. We used the Munich Oktoberfest, the largest beer festival in the world, as a case study and extended our findings to gas appliances around the world. To this end, the source signature of CH_4 enhancements at the festival was investigated utilizing a portable CH_4 gas analyzer combined with isotopic analyses of air samples to determine the $\delta^{13}C$ and δD ratios. In addition, the ethane share of the samples was examined.

Both isotopic and ethane analyses of the gas indicated that the CH_4 enhancements were predominately caused by natural gas used for cooking and heating at the festival premises and not by biogenic processes caused by visitors. Incomplete combustion and leakages in the appliances are much more likely the causes than leaks in pipelines. Since most of the cooking and heating takes place inside the beer tents, these tents are the main sources of CH_4 enhancements at Oktoberfest, which is supported by measurements inside the tents. However, food stalls on the street use natural gas driven appliances as well, so that they contribute to the overall CH_4 enhancements of the festival, too. Overall, the leakage rate at Oktoberfest 2019 is found to be 1.4%, which is slightly higher than the rate of 1.1% determined in 2018 (Chen et al., 2020).

Based on the knowledge of an existing leakage rate, we provide a possible solution to mitigate the climate impact of such large festivals by calculating the carbon footprint of natural gas driven appliances considering the leakage rate. Although, natural gas is considered a fairly climate friendly alternative to other fossil fuels, we found that electrical appliances at Oktoberfest have a much smaller carbon footprint than natural gas driven ones, since Oktoberfest is supplied by renewable electricity only. Replacing all natural gas driven appliances at Oktoberfest with electrical ones could have saved approximately 450 *t* of CO_2eq in 2019, equivalent to 87% of the carbon emissions caused by energy consumption on the festival premises.

Nevertheless, carbon emissions of Oktoberfest contribute only very little to the global carbon budget, making emission reductions at Oktoberfest not a solution to global climate problems. However, gas appliances are used not only at Oktoberfest but in many households around the world. Therefore, we extended our study to estimate whether replacing gas driven appliances with electric ones in specific countries would save global carbon emissions.

Since electricity is generated by different energy sources in each country, the carbon footprint of electricity generation differs significantly between them. To date, only in seven of these countries, electricity is likely the more climate-friendly energy source than natural gas for cooking and heating in the household sector. However, since the share of renewables is steadily increasing in many countries, electricity could become the more climate friendly energy source than natural gas in the near future.

We conclude that from a climate perspective, in countries with low carbon emissions from electricity generation, it would make sense now or in a few years to replace gas appliances for domestic cooking and heating with electric appliances to save overall carbon emissions. Nevertheless, we are aware of the fact that not all gas appliances worldwide can be replaced by electric appliances, especially since there would not be enough electrical energy available or the electricity would have to be generated from non-renewable energy sources, which in turn would increase the CO_2 footprint. Therefore, the share of renewable energies in electricity generation must be further increased. In addition, many countries around the world lack electrical infrastructure, and natural gas is the cheaper energy source compared to electricity in many countries, making it uneconomical for end users to switch from gas to electricity. However, some of these problems are more political in nature and could be solved by governments. In this study, we aim to rise people's awareness of how carbon emissions from electric and gas-powered end-use appliances compare, and identified an option that could reduce a significant amount of carbon emissions in the near future.

Data Availability Statement

The measurement data and scripts used for the Oktoberfest study is preserved at https://doi.org/10.14459/2022mp1663551, available via CC BY 4.0 license and developed openly at https://github.com/ankitshekhar99/Oktoberfest2019Study/tree/main (Dietrich et al., 2022).

Acknowledgments
We thank LI-COR Biosciences for the loan of the mobile gas analyzer; Pim van den Bulk (TNO) for helping with the QCL analyses; our students Xiao Bi and Xinxu Zhao for helping us with the measurements. This research has been supported by the Deutsche Forschungsgemeinschaft (DFG, German Research Foundation) Grant CH 1792/2-1. Jia Chen is partially supported by the Technical University of Munich – Institute for Advanced Study, funded by the German Excellence Initiative and the European Union Seventh Framework Programme under grant agreement number 291763. Ankit Shekhar is supported by ETH Zürich project FEVER ETH-27 19-1. We would also like to thank the reviewers and the editor for their very helpful comments, which helped to improve the paper. Open Access funding enabled and organized by Projekt DEAL.

References

Adria, O., & Bethge, J. (2013). *What users can save with energy-efficient cooking stoves and ovens* (pp. 1–30). bigee.net - Wuppertal Institute for Climate, Environment and Energy. Retrieved from https://energypedia.info/images/2/26/Bigee_cookingstoves_user_savings.pdf

Allen, D. T., Torres, V. M., Thomas, J., Sullivan, D. W., Harrison, M., Hendler, A., et al. (2013). Measurements of methane emissions at natural gas production sites in the United States. *Proceedings of the National Academy of Sciences*, *110*(44), 17768–17773. https://doi.org/10.1073/pnas.1304880110

Alvarez, R. A., Zavala-Araiza, D., Lyon, D. R., Allen, D. T., Barkley, Z. R., Brandt, A. R., et al. (2018). Assessment of methane emissions from the U.S. oil and gas supply chain. *Science*, *361*(6398), 186–188. https://doi.org/10.1126/science.aar7204

Amponsah, N. Y., Troldborg, M., Kington, B., Aalders, I., & Hough, R. L. (2014). Greenhouse gas emissions from renewable energy sources: A review of lifecycle considerations. *Renewable and Sustainable Energy Reviews*, *39*(C), 461–475. https://doi.org/10.1016/j.rser.2014.07.087

Beck, V., Chen, H., Gerbig, C., Bergamaschi, P., Bruhwiler, L., Houweling, S., et al. (2012). Methane airborne measurements and comparison to global models during BARCA. *Journal of Geophysical Research*, *117*(D15). https://doi.org/10.1029/2011JD017345

bp (2020). Statistical review of world energy 2020. *bp Statistical Review of World Energy 2020*, *69*, 68. Retrieved from https://www.bp.com/content/dam/bp/business-sites/en/global/corporate/pdfs/energy-economics/statistical-review/bp-stats-review-2020-full-report.pdf

Brass, M., & Röckmann, T. (2010). Continuous-flow isotope ratio mass spectrometry method for carbon and hydrogen isotope measurements on atmospheric methane. *Atmospheric Measurement Techniques*, *3*(6), 1707–1721. https://doi.org/10.5194/amt-3-1707-2010

Chamberlain, S. D., Ingraffea, A. R., & Sparks, J. P. (2016). Sourcing methane and carbon dioxide emissions from a small city: Influence of natural gas leakage and combustion. *Environmental Pollution*, *218*, 102–110. https://doi.org/10.1016/j.envpol.2016.08.036

Chen, J., Dietrich, F., Maazallahi, H., Forstmaier, A., Winkler, D., Hofmann, M. E. G., et al. (2020). Methane emissions from the Munich Oktoberfest. *Atmospheric Chemistry and Physics*, *20*(6), 3683–3696. https://doi.org/10.5194/acp-20-3683-2020

Chen, J., Viatte, C., Hedelius, J. K., Jones, T., Franklin, J. E., Parker, H., et al. (2016). Differential column measurements using compact solar-tracking spectrometers. *Atmospheric Chemistry and Physics*, *16*(13), 8479–8498. https://doi.org/10.5194/acp-16-8479-2016

Dietrich, F., Chen, J., Shekhar, A., Lober, S., Krämer, K., Leggett, G., et al. (2022). Data sets and modeling software as part of our study titled "Climate impact comparison of electric and gas-powered end-user appliances" [Dataset]. Technical University of Munich. https://doi.org/10.14459/2022MP1663551

Dietrich, F., Chen, J., Voggenreiter, B., Aigner, P., Nachtigall, N., & Reger, B. (2021). MUCCnet: Munich urban carbon column network. *Atmospheric Measurement Techniques*, *14*(2), 1111–1126. https://doi.org/10.5194/amt-14-1111-2021

Fisher, R., Lowry, D., Wilkin, O., Sriskantharajah, S., & Nisbet, E. G. (2006). High-precision, automated stable isotope analysis of atmospheric methane and carbon dioxide using continuous-flow isotope-ratio mass spectrometry. *Rapid Communications in Mass Spectrometry*, *20*(2), 200–208. https://doi.org/10.1002/rcm.2300

Fulton, M., Mellquist, N., & Kitasei, S. (2011). *Comparing life cycle greenhouse gas emissions from natural gas and coal*. Worldwatch Institute.

Gallagher, M. E., Down, A., Ackley, R. C., Zhao, K., Phillips, N., & Jackson, R. B. (2015). Natural gas pipeline replacement programs reduce methane leaks and improve consumer safety. *Environmental Science and Technology Letters*, *2*(10), 286–291. https://doi.org/10.1021/acs.estlett.5b00213

Gioli, B., Toscano, P., Lugato, E., Matese, A., Miglietta, F., Zaldei, A., & Vaccari, F. P. (2012). Methane and carbon dioxide fluxes and source partitioning in urban areas: The case study of Florence, Italy. *Environmental Pollution*, *164*, 125–131. https://doi.org/10.1016/j.envpol.2012.01.019

Hager, T. J., & Morawicki, R. (2013). Energy consumption during cooking in the residential sector of developed nations: A review. *Food Policy*, *40*, 54–63. https://doi.org/10.1016/j.foodpol.2013.02.003

Hase, F., Frey, M., Blumenstock, T., Groß, J., Kiel, M., Kohlhepp, R., et al. (2015). Application of portable FTIR spectrometers for detecting greenhouse gas emissions of the major city Berlin. *Atmospheric Measurement Techniques*, *8*(7), 3059–3068. https://doi.org/10.5194/amt-8-3059-2015

Helfter, C., Tremper, A. H., Halios, C. H., Kotthaus, S., Bjorkegren, A., Grimmond, C. S. B., et al. (2016). Spatial and temporal variability of urban fluxes of methane, carbon monoxide and carbon dioxide above London, UK. *Atmospheric Chemistry and Physics*, *16*(16), 10543–10557. https://doi.org/10.5194/acp-16-10543-2016

Hmiel, B., Petrenko, V. V., Dyonisius, M. N., Buizert, C., Smith, A. M., Place, P. F., et al. (2020). Preindustrial 14 CH_4 indicates greater anthropogenic fossil CH_4 emissions. *Nature*, *578*(7795), 409–412. https://doi.org/10.1038/s41586-020-1991-8

International Renewable Energy Agency. (2020). Statistics time series. Retrieved from https://www.irena.org/Statistics/View-Data-by-Topic/Capacity-and-Generation/Statistics-Time-Series

Jackson, R. B., Down, A., Phillips, N. G., Ackley, R. C., Cook, C. W., Plata, D. L., & Zhao, K. (2014). Natural gas pipeline leaks across Washington, DC. *Environmental Science & Technology*, *48*(3), 2051–2058. https://doi.org/10.1021/es404474x

Jones, T. S., Franklin, J. E., Chen, J., Dietrich, F., Hajny, K. D., Paetzold, J. C., et al. (2021). Assessing urban methane emissions using column-observing portable Fourier transform infrared (FTIR) spectrometers and a novel Bayesian inversion framework. *Atmospheric Chemistry and Physics*, *21*, 13131–13147. https://doi.org/10.5194/acp-21-13131-2021

Karion, A., Sweeney, C., Pétron, G., Frost, G., Hardesty, R. M., Kofler, J., et al. (2013). Methane emissions estimate from airborne measurements over a Western United States natural gas field. *Geophysical Research Letters*, *40*(16), 4393–4397. https://doi.org/10.1002/grl.50811

Keeling, C. D. (1958). The concentration and isotopic abundances of atmospheric carbon dioxide in rural areas. *Geochimica et Cosmochimica Acta*, *13*(4), 322–334. https://doi.org/10.1016/0016-7037(58)90033-4

Klappenbach, F., Chen, J., Wenzel, A., Forstmaier, A., Dietrich, F., Zhao, X., & Fischer, M. (2021). Methane emission estimate using ground based remote sensing in complex terrain (Tech. Rep. No. EGU21-15406). *Copernicus Meetings*. https://doi.org/10.5194/egusphere-egu21-15406

Ladage, S., Blumenberg, M., Franke, D., Bahr, A., Lutz, R., & Schmidt, S. (2021). On the climate benefit of a coal-to-gas shift in Germany's electric power sector. *Scientific Reports*, *11*(1), 11453. https://doi.org/10.1038/s41598-021-90839-7

Landeshauptstadt München. (2019). Ratsinformationssystem der Landeshauptstadt München [text]. Retrieved from https://www.ris-muenchen.de/RII/RII/ris_fulltextsrch.jsp

Landeshauptstadt München Redaktion. (2020). M-Statistik München - Historische Berichte. Retrieved from https://www.mstatistik-muenchen.de/

Lebel, E. D., Finnegan, C. J., Ouyang, Z., & Jackson, R. B. (2022). Methane and nox emissions from natural gas stoves, cooktops, and ovens in residential homes. *Environmental Science & Technology*, *56*(4), 2529–2539. https://doi.org/10.1021/acs.est.1c04707

Lu, X., Harris, S. J., Fisher, R. E., France, J. L., Nisbet, E. G., Lowry, D., et al. (2021). Isotopic signatures of major methane sources in the coal seam gas fields and adjacent agricultural districts, Queensland, Australia. *Atmospheric Chemistry and Physics*, *21*(13), 10527–10555. https://doi.org/10.5194/acp-21-10527-2021

Lyon, D. R., Alvarez, R. A., Zavala-Araiza, D., Brandt, A. R., Jackson, R. B., & Hamburg, S. P. (2016). Aerial surveys of elevated hydrocarbon emissions from oil and gas production sites. *Environmental Science & Technology*, *50*(9), 4877–4886. https://doi.org/10.1021/acs.est.6b00705

Maazallahi, H., Fernandez, J. M., Menoud, M., Zavala-Araiza, D., Weller, Z. D., Schwietzke, S., et al. (2020). Methane mapping, emission quantification, and attribution in two European cities: Utrecht (NL) and Hamburg (DE). *Atmospheric Chemistry and Physics*, *20*(23), 14717–14740. https://doi.org/10.5194/acp-20-14717-2020

Makarova, M. V., Alberti, C., Ionov, D. V., Hase, F., Foka, S. C., Blumenstock, T., et al. (2021). Emission Monitoring Mobile Experiment (EMME): An overview and first results of the St. Petersburg megacity campaign 2019. *Atmospheric Measurement Techniques*, *14*(2), 1047–1073. https://doi.org/10.5194/amt-14-1047-2021

McKain, K., Down, A., Raciti, S. M., Budney, J., Hutyra, L. R., Floerchinger, C., et al. (2015). Methane emissions from natural gas infrastructure and use in the urban region of Boston, Massachusetts. *Proceedings of the National Academy of Sciences*, *112*(7), 1941–1946. https://doi.org/10.1073/pnas.1416261112

Menoud, M., van der Veen, C., Necki, J., Bartyzel, J., Szénási, B., Stanisavljević, M., et al. (2021). Methane (CH_4) sources in Krakow, Poland: Insights from isotope analysis. *Atmospheric Chemistry and Physics*, *21*, 13167–13185. https://doi.org/10.5194/acp-21-13167-2021

Menoud, M., van der Veen, C., Scheeren, B., Chen, H., Szénási, B., Morales, R. P., et al. (2020). Characterisation of methane sources in Lutjewad, The Netherlands, using quasi-continuous isotopic composition measurements. *Tellus B: Chemical and Physical Meteorology*, *72*(1), 1–20. https://doi.org/10.1080/16000889.2020.1823733

Mitchell, A. L., Tkacik, D. S., Roscioli, J. R., Herndon, S. C., Yacovitch, T. I., Martinez, D. M., et al. (2015). Measurements of methane emissions from natural gas gathering facilities and processing plants: Measurement results. *Environmental Science & Technology*, *49*(5), 3219–3227. https://doi.org/10.1021/es5052809

Myhre, G., Shindell, D., Bréon, F.-M., Collins, W., Fuglestvedt, J., Huang, J., et al. (2013). Anthropogenic and natural radiative forcing. In T. F. Stocker, D. Qin, G.-K. Plattner, M. Tignor, S. K. Allen, J. Boschung, A. Nauels, Y. Xia, V. Bex, & P. M. Midgley (Eds.), *Climate change 2013: The physical science basis. Contribution of working group I to the fifth assessment report of the intergovernmental panel on climate change* (pp. 659–740). Cambridge University Press. https://doi.org/10.1017/CBO9781107415324.018

Nisbet, E. G., Manning, M. R., Dlugokencky, E. J., Fisher, R. E., Lowry, D., Michel, S. E., et al. (2019). Very strong atmospheric methane growth in the 4 years 2014–2017: Implications for the Paris agreement. *Global Biogeochemical Cycles*, *33*(3), 318–342. https://doi.org/10.1029/2018GB006009

Omara, M., Sullivan, M. R., Li, X., Subramanian, R., Robinson, A. L., & Presto, A. A. (2016). Methane emissions from conventional and unconventional natural gas production sites in the Marcellus Shale Basin. *Environmental Science & Technology*, *50*(4), 2099–2107. https://doi.org/10.1021/acs.est.5b05503

Phillips, N. G., Ackley, R., Crosson, E. R., Down, A., Hutyra, L. R., Brondfield, M., et al. (2013). Mapping urban pipeline leaks: Methane leaks across Boston. *Environmental Pollution*, *173*, 1–4. https://doi.org/10.1016/j.envpol.2012.11.003

Plant, G., Kort, E. A., Floerchinger, C., Gvakharia, A., Vimont, I., & Sweeney, C. (2019). Large fugitive methane emissions from urban centers along the U.S. East Coast. *Geophysical Research Letters*, *46*(14), 8500–8507. https://doi.org/10.1029/2019GL082635

Qin, Y., Edwards, R., Tong, F., & Mauzerall, D. L. (2017). Can switching from coal to shale gas bring net carbon reductions to China? *Environmental Science & Technology*, *51*(5), 2554–2562. https://doi.org/10.1021/acs.est.6b04072

Röckmann, T., Eyer, S., van der Veen, C., Popa, M. E., Tuzson, B., Monteil, G., et al. (2016). In situ observations of the isotopic composition of methane at the Cabauw tall tower site. *Atmospheric Chemistry and Physics*, *16*(16), 10469–10487. https://doi.org/10.5194/acp-16-10469-2016

Roscioli, J. R., Yacovitch, T. I., Floerchinger, C., Mitchell, A. L., Tkacik, D. S., Subramanian, R., et al. (2015). Measurements of methane emissions from natural gas gathering facilities and processing plants: Measurement methods. *Atmospheric Measurement Techniques*, *8*(5), 2017–2035. https://doi.org/10.5194/amt-8-2017-2015

Sargent, M. R., Floerchinger, C., McKain, K., Budney, J., Gottlieb, E. W., Hutyra, L. R., et al. (2021). Majority of US urban natural gas emissions unaccounted for in inventories. *Proceedings of the National Academy of Sciences*, *118*(44). https://doi.org/10.1073/pnas.2105804118

Schwietzke, S., Sherwood, O. A., Bruhwiler, L. M. P., Miller, J. B., Etiope, G., Dlugokencky, E. J., et al. (2016). Upward revision of global fossil fuel methane emissions based on isotope database. *Nature*, *538*(7623), 88–91. https://doi.org/10.1038/nature19797

SWM Infrastruktur GmbH und Co. KG. (2019a). Erdgasbeschaffenheit: Monatsdurchschnitt Oktober 2019. Retrieved from https://www.swm-infrastruktur.de/dam/swm-infrastruktur/dokumente/gas/netzstrukturdaten/gasanalyse-oktober-2019.pdf

SWM Infrastruktur GmbH und Co. KG. (2019b). Erdgasbeschaffenheit: Monatsdurchschnitt September 2019. Retrieved from https://www.swm-infrastruktur.de/dam/swm-infrastruktur/dokumente/gas/netzstrukturdaten/gasanalyse-september-2019.pdf

Tanaka, K., Cavalett, O., Collins, W. J., & Cherubini, F. (2019). Asserting the climate benefits of the coal-to-gas shift across temporal and spatial scales. *Nature Climate Change*, *9*(5), 389–396. https://doi.org/10.1038/s41558-019-0457-1

Vogel, F. R., Frey, M., Staufer, J., Hase, F., Broquet, G., Xueref-Remy, I., et al. (2019). XCO_2 in an emission hot-spot region: The COCCON Paris campaign 2015. *Atmospheric Chemistry and Physics*, *19*(5), 3271–3285. https://doi.org/10.5194/acp-19-3271-2019

von Fischer, J. C., Cooley, D., Chamberlain, S., Gaylord, A., Griebenow, C. J., Hamburg, S. P., et al. (2017). Rapid, vehicle-based identification of location and magnitude of urban natural gas pipeline leaks. *Environmental Science & Technology*, *51*(7), 4091–4099. https://doi.org/10.1021/acs.est.6b06095

Weller, Z. D., Hamburg, S. P., & von Fischer, J. C. (2020). A national estimate of methane leakage from pipeline mains in natural gas local distribution systems. *Environmental Science & Technology*, *54*(14), 8958–8967. https://doi.org/10.1021/acs.est.0c00437

Weller, Z. D., Roscioli, J. R., Daube, W. C., Lamb, B. K., Ferrara, T. W., Brewer, P. E., & von Fischer, J. C. (2018). Vehicle-based methane surveys for finding natural gas leaks and estimating their size: Validation and uncertainty. *Environmental Science & Technology*, *52*(20), 11922–11930. https://doi.org/10.1021/acs.est.8b03135

WorldData.info. (2020). Energy consumption in Germany. Retrieved from https://www.worlddata.info/europe/germany/energy-consumption.php

Yacovitch, T. I., Herndon, S. C., Pétron, G., Kofler, J., Lyon, D., Zahniser, M. S., & Kolb, C. E. (2015). Mobile laboratory observations of methane emissions in the Barnett Shale region. *Environmental Science & Technology*, *49*(13), 7889–7895. https://doi.org/10.1021/es506352j

Yacovitch, T. I., Herndon, S. C., Roscioli, J. R., Floerchinger, C., McGovern, R. M., Agnese, M., et al. (2014). Demonstration of an ethane spectrometer for methane source identification. *Environmental Science & Technology*, *48*(14), 8028–8034. https://doi.org/10.1021/es501475q

Yacovitch, T. I., Neininger, B., Herndon, S. C., van der Gon, H. D., Jonkers, S., Hulskotte, J., et al. (2018). Methane emissions in The Netherlands: The Groningen field. *Elementa: Science of the Anthropocene*, *6*(57). https://doi.org/10.1525/elementa.308

Zavala-Araiza, D., Lyon, D. R., Alvarez, R. A., Davis, K. J., Harriss, R., Herndon, S. C., et al. (2015). Reconciling divergent estimates of oil and gas methane emissions. *Proceedings of the National Academy of Sciences*, *112*(51), 15597–15602. https://doi.org/10.1073/pnas.1522126112

Zhao, X., Marshall, J., Hachinger, S., Gerbig, C., Frey, M., Hase, F., & Chen, J. (2019). Analysis of total column CO_2 and CH_4 measurements in Berlin with WR_F-GHG. *Atmospheric Chemistry and Physics*, *19*(17), 11279–11302. https://doi.org/10.5194/acp-19-11279-2019

Zimmerle, D. J., Williams, L. L., Vaughn, T. L., Quinn, C., Subramanian, R., Duggan, G. P., et al. (2015). Methane emissions from the natural gas transmission and storage system in the United States. *Environmental Science & Technology*, *49*(15), 9374–9383. https://doi.org/10.1021/acs.est.5b01669

Zimnoch, M., Necki, J., Chmura, L., Jasek, A., Jelen, D., Galkowski, M., et al. (2019). Quantification of carbon dioxide and methane emissions in urban areas: Source apportionment based on atmospheric observations. *Mitigation and Adaptation Strategies for Global Change*, *24*(6), 1051–1071. https://doi.org/10.1007/s11027-018-9821-0

Supporting Information for "Climate impact comparison of electric and gas-powered end-user appliances"

Florian Dietrich[1], Jia Chen[1], Ankit Shekhar[2], Sebastian Lober[1], Konstantin Krämer[1], Graham Leggett[3], Carina van der Veen[4], Ilona Velzeboer[5], Hugo Denier van der Gon[6], Thomas Röckmann[4]

[1]Environmental Sensing and Modeling, Technical University of Munich (TUM), Munich, Germany

[2]Department of Environmental Systems Science, ETH Zurich, 8092 Zurich, Switzerland

[3]LI-COR Biosciences, Lincoln, NE, USA

[4]Institute for Marine and Atmospheric research Utrecht, Utrecht University, Utrecht, the Netherlands

[5] Environmental Modelling, Sensing and Analysis (EMSA), TNO, Petten, the Netherlands

[6]Climate, Air and Sustainability, TNO, Utrecht, the Netherlands

Contents of this file

S1. Introduction

This file includes text, figures and tables to deepen the understanding of the publication entitled 'Climate impact comparison of electric and gas-powered end-user appliances'. All content is referenced in the main manuscript.

S2. Mathematical expressions for δ^{13}C and δD method

In this study, we utilized the Vienna Pee Dee Belemnite (VPDB) standard. Eq. 1 shows the mathematical definition of the δ^{13}C method:

$$\delta^{13}C_{sample} = \left(\frac{\left(\frac{^{13}C}{^{12}C}\right)_{sample}}{\left(\frac{^{13}C}{^{12}C}\right)_{standard}} - 1 \right) \cdot 1000‰ \tag{1}$$

Similar to δ^{13}C, we also looked at the ratio of deuterium to normal hydrogen using the δD method. The equation is analogous to the previous one:

$$\delta D_{sample} = \left(\frac{\left(\frac{CH_3D}{CH_4}\right)_{sample}}{\left(\frac{CH_3D}{CH_4}\right)_{standard}} - 1 \right) \cdot 1000‰ \tag{2}$$

As a standard for the δD method, we utilized the Vienna Standard Mean Ocean Water (VSMOW).

S3. Leakage rate calculation for Oktoberfest

To calculate the methane leakage rate (r_{leak}) at Oktoberfest, the total mass of methane consumed at Oktoberfest 2019 ($\mathrm{M_{CH_4,total}}$) and the mass of methane leaking ($\mathrm{M_{CH_4,loss}}$) are related.

Knowing the total gas consumption of Oktoberfest 2019 is m_{gas} =185 000 $\mathrm{m^3}$, the density of CH_4 is $\rho_{\mathrm{CH4}} = 0.668\,\mathrm{kgm^{-3}}$ and the CH_4 share of the natural gas in Munich is on average about $r_{\mathrm{CH4}} = 96\%$ (SWM Infrastruktur GmbH und Co. KG, 2020), the total mass of methane consumed at Oktoberfest can be calculated as:

$$\begin{aligned} M_{\mathrm{CH_4,total}} &= m_{\mathrm{gas}} \cdot r_{\mathrm{CH4}} \cdot \rho_{\mathrm{CH4}} = \\ &= 1.85 \cdot 10^5 \mathrm{m^3} \cdot 0.96 \cdot 0.668 \frac{\mathrm{kg}}{\mathrm{m^3}} = \\ &= 1.186 \cdot 10^5 \mathrm{kg} \end{aligned} \tag{3}$$

To determine the CH_4 losses at Oktoberfest, the emission strength of Oktoberfest ($E_{\mathrm{Okt}} = 8.5\,\mu\mathrm{g(m^2s)^{-1}}$) is multiplied with the fugitives ratio $\mathrm{r_{fugitive}} = 88\%$, the festival area $\mathrm{a_{Okt}} = 3.45 \cdot 10^5\,\mathrm{m^2}$ and the duration t_{Okt}, assuming that the Oktoberfest operates 11 h per day and the emission is continuous throughout the day. Multiplying the flux rate by the area does not lead to any error. This is because the result of our multiple Gaussian plume model to determine emissions is a flux with unit $\mu g(s)^{-1}$. Just to allow comparison with other studies, we divided this number by the area of Oktoberfest to obtain a flux rate with unit $\mu g(m^2 s)^{-1}$. For the leakage rate calculation, we reversed this calculation, resulting in the Oktoberfest area having no effect on the mass of methane emitted.

$$
\begin{aligned}
M_{\mathrm{CH_4,loss}} &= E_{\mathrm{Okt}} \cdot r_{\mathrm{fugitive}} \cdot t_{\mathrm{Okt}} \cdot a_{\mathrm{Okt}} = \\
&= 8.5\,\frac{\mu\mathrm{g}}{\mathrm{m^2 s}} \cdot 88\% \cdot (16\,\mathrm{d} \cdot 11\,\frac{\mathrm{h}}{\mathrm{d}} \cdot 3600\,\frac{\mathrm{s}}{\mathrm{h}}) \cdot 3.45 \cdot 10^5\,\mathrm{m^2} = \\
&= 1.635 \cdot 10^3\,\mathrm{kg}
\end{aligned}
\tag{4}
$$

S4. Temporal development of energy usage at Oktoberfest

In the 30 years between 1990 and 2019, the average total energy consumption (electricity plus natural gas) of Oktoberfest was 17.4 ± 1.8 (1σ) Tera Joule (TJ) during the 16 to 18 days of the festivity. There was an increasing trend in total energy consumption (Figure S4), which was mainly driven by the increase in electricity usage (Figure S5a), with total electricity consumption increasing from 6.2 TJ in 1990 to about 10.2 TJ in 2019 (64% increase). Natural gas consumption has remained fairly constant over the past 30 years, with the most recent natural gas consumption in 2019 (7.4 TJ) actually being lower than in 1990 (7.7 TJ) (Figure S5a). At the same time, however, the share of renewable energies (in this case pure hydropower) in the electricity supply has increased

significantly, from 0% in 1990 to about 44% share in 2000 to full 100% hydropower supply since 2012 (Figure 4, right). This increased share of renewable energy resulted in cleaner electricity and a jump in estimated total CO_2eq emissions from electricity consumption in 2000 and in 2012. As a result, the carbon footprint of total natural gas consumption at Oktoberfest was smaller than that of total electricity consumption until 2011, after which electricity produced the smaller total carbon footprint (Figure S5c). Furthermore, the CO_2eq emission factors were higher for electricity than for natural gas (including leakage) only until 2002, due to the fossil fuel-based electricity supply of Oktoberfest (Figure S5d). After the share of green electricity continued to increase since 2000 until it reached 100% in 2012, CO_2eq emission factors of electrical energy consumed have decreased from 160 t to now 3.6 t CO_2eq/TJ of electricity consumption in 2019. In comparison, the carbon footprint of natural gas has been quite constant over the years, with a value of 71.7 t CO_2eq/TJ in 2019.

S5. Calculation of global methane leakage

To calculate methane leakage, we used methane emission data from the Methane Tracker datasets (International Energy Agency, 2022), which include methane emissions from different segments (gas pipelines, onshore/offshore gas/oil) and from different sources (fugitive or venting). We calculated the methane leakage rate using equation S1 as follows:

$$LeakageRate_{CH4} = \frac{Emissions_{CH4}}{Consumption_{CH4}} \cdot 100\% \tag{5}$$

Methane emissions are the sum of all fugitive and vented emissions obtained from the methane tracker dataset. Methane consumption data was taken from the BP energy statistics for 2019. Based on methane leakage rates from the IEA Methane Tracker,

values range from 0.02% (for the Netherlands) to 9.3% (for Venezuela) (see Figure S6). Most natural gas importing countries, such as Germany, France, Italy, etc., have much lower methane leakage rates compared to the countries they import from, such as Russia (4%) (see Figure S6). To account for these inconsistencies, the countries of origin and transit of gas would need to be identified for each country consuming natural gas and weighting factors applied to them. Since this calculation of the effective leakage rate for each country depends on too many unknown parameters, such as the time-varying proportions of gas origin, the type of transportation, the length of pipelines in transit countries, the comparability of data from different countries, etc., this approach would lead to large uncertainties and was therefore not used in this paper. Instead, to make our analysis robust, we calculated a distribution of all leakage rates at the country level to form an average value with a 90% confidence interval [0.22%, 5.35%] as upper and lower limits for the leakage rate. In this way, upstream, midstream, and downstream emissions are considered as an average value for all possible country combinations of gas origin, transport, and use.

S6. Temporal development of global emission factors

Depending on the types and shares of renewable (wind, hydropower, solar and geothermal/biomass) and non-renewable energy (coal, oil, natural-gas and nuclear) used for electricity generation (see Figures S7 and S8), the total emission factors for renewable and non-renewable electricity differ from country to country (see Figure S9). Although the emission factors of renewables also vary over time, these variations do not contribute significantly to the overall emission number, as emissions from non-renewable sources, with the exception of nuclear power, are generally much higher (e.g. 7.22 tCO_2eq/TJ for wind

energy vs. 246.67 tCO_2eq/TJ for electricity generated by coal; see Table 1). Only in France the emission factors for non-renewable and renewable electricity are in the same order of magnitude (see Figure S9), since France relies mainly (more than 70% throughout the last 20 years) on nuclear power as a non-renewable source for energy production (see Figure S7).

S7. Country comparison - phase transition plots

The emissions of natural gas versus electricity of these 25 countries for 2019 were examined using phase transition diagrams. Since our Oktoberfest results, as well as many other studies (Alvarez et al., 2012; Wigley, 2011; Pandey et al., 2019; Schneising et al., 2020; Weller et al., 2020), show that there is methane leakage in the upstream, midstream, and downstream natural gas process, we used the emission factor of natural gas, including the climate impact of leaking CH_4.

In these diagrams (see Figure S10), the climate friendliness of the accumulated non-renewable energy sources is indicated by the intersection of the white line with the x-axis. The farther to the left the intersection point is, the less carbon emissions are caused by non-renewable energy resources. One can see that, in addition to France, countries such as Belgium, Canada, Spain and the United Kingdom show comparable small non-renewable energy emissions, all due to a relatively high share of nuclear energy in electricity generation. Such a fact results in less renewable energy needed to reach the break-even point, where electricity and natural gas have the same carbon footprint (see dashed orange lines in Figure S10). In addition, the current shares of renewables for each country are shown as dashed green lines to see, how much effort is still needed to reach the break-even point.

References

Alvarez, R. A., Pacala, S. W., Winebrake, J. J., Chameides, W. L., & Hamburg, S. P. (2012, April). Greater focus needed on methane leakage from natural gas infrastructure. *Proceedings of the National Academy of Sciences*, *109*(17), 6435–6440. Retrieved 2021-06-02, from https://www.pnas.org/content/109/17/6435 (Publisher: National Academy of Sciences Section: Physical Sciences) doi: 10.1073/pnas.1202407109

Amponsah, N. Y., Troldborg, M., Kington, B., Aalders, I., & Hough, R. L. (2014). Greenhouse gas emissions from renewable energy sources: A review of lifecycle considerations. *Renewable and Sustainable Energy Reviews*, *39*(C), 461–475. Retrieved 2021-06-02, from https://ideas.repec.org/a/eee/rensus/v39y2014icp461-475.html (Publisher: Elsevier)

bp. (2020). Statistical Review of World Energy 2020. *bp Statistical Review of World Energy 2020*, *69*, 68. Retrieved 2021-01-06, from https://www.bp.com/content/dam/bp/business-sites/en/global/corporate/pdfs/energy-economics/statistical-review/bp-stats-review-2020-full-report.pdf

Chen, J., Dietrich, F., Maazallahi, H., Forstmaier, A., Winkler, D., Hofmann, M. E. G., ... Röckmann, T. (2020, March). Methane emissions from the Munich Oktoberfest. *Atmospheric Chemistry and Physics*, *20*(6), 3683–3696. Retrieved 2021-03-23, from https://acp.copernicus.org/articles/20/3683/2020/ (Publisher: Copernicus GmbH) doi: 10.5194/acp-20-3683-2020

Eurostat. (2021a). *Electricity prices for household consumers - bi-annual data (from 2007 onwards).* Retrieved 2021-10-29, from https://ec.europa.eu/eurostat/

databrowser/view/NRG_PC_204/default/table?lang=en

Eurostat. (2021b). *Gas prices components for household consumers - annual data.* Retrieved 2021-10-29, from https://ec.europa.eu/eurostat/databrowser/view/nrg_pc_202_c/default/table?lang=en

Landeshauptstadt München. (2019). *Ratsinformationssystem der Landeshauptstadt München* [text]. Retrieved 2021-10-29, from https://www.ris-muenchen.de/RII/RII/ris_fulltextsrch.jsp (Publisher: Landeshauptstadt München)

Landeshauptstadt München Redaktion. (2000). *Jahrtausend-Oktoberfest ohne Rekorde aber mit zufriedenstellendem Verkauf.* Retrieved 2021-10-29, from https://www.muenchen.de/rathaus/dam/jcr:0b8f5979-1919-45dc-913e-f7f6e1ac8a85/mb000703.pdf

Landeshauptstadt München Redaktion. (2020). *M-Statistik München - Historische Berichte.* Retrieved 2021-10-29, from https://www.mstatistik-muenchen.de/

oktoberfest.de Redaktion. (2019, October). *Die offizielle Oktoberfest-Bilanz 2019.* Retrieved 2021-10-29, from https://www.oktoberfest.de/magazin/oktoberfest-news/2019/die-offizielle-oktoberfest-bilanz-2019

Pandey, S., Gautam, R., Houweling, S., Gon, H. D. v. d., Sadavarte, P., Borsdorff, T., ... Aben, I. (2019, December). Satellite observations reveal extreme methane leakage from a natural gas well blowout. *Proceedings of the National Academy of Sciences*, *116*(52), 26376–26381. Retrieved 2021-06-02, from https://www.pnas.org/content/116/52/26376 (Publisher: National Academy of Sciences Section: Physical Sciences) doi: 10.1073/pnas.1908712116

Schneising, O., Buchwitz, M., Reuter, M., Vanselow, S., Bovensmann, H., & Burrows,

J. P. (2020, August). Remote sensing of methane leakage from natural gas and petroleum systems revisited. *Atmospheric Chemistry and Physics*, *20*(15), 9169–9182. Retrieved 2021-06-02, from https://acp.copernicus.org/articles/20/9169/2020/ (Publisher: Copernicus GmbH) doi: 10.5194/acp-20-9169-2020

SWM Infrastruktur GmbH und Co. KG. (2020). *Erdgasbeschaffenheit: Jahresmittel für 2019.* Retrieved 2021-08-09, from file:///C:/Users/ga42jel/AppData/Local/Temp/erdgasbeschaffenheit-jahresmittel-2019.pdf

Weller, Z. D., Hamburg, S. P., & von Fischer, J. C. (2020, July). A National Estimate of Methane Leakage from Pipeline Mains in Natural Gas Local Distribution Systems. *Environmental Science & Technology*, *54*(14), 8958–8967. Retrieved 2021-06-02, from https://doi.org/10.1021/acs.est.0c00437 (Publisher: American Chemical Society) doi: 10.1021/acs.est.0c00437

Wigley, T. M. L. (2011, August). Coal to gas: the influence of methane leakage. *Climatic Change*, *108*(3), 601. Retrieved 2021-06-02, from https://doi.org/10.1007/s10584-011-0217-3 doi: 10.1007/s10584-011-0217-3

Table S1. Emission factors EF_n used for electricity generation from different fuels, adopted from (Amponsah et al., 2014).

n	Fuel	Type	Emission factor (EF)
1	Coal	non-renewable	246.67 tCO_2eq/TJ
2	Oil	non-renewable	203.61 tCO_2eq/TJ
3	Natural gas	non-renewable	138.67 tCO_2eq/TJ
4	Solar	renewable	23.61 tCO_2eq/TJ
5	Geothermal/Biomass	renewable	11.39 tCO_2eq/TJ
6	Nuclear	non-renewable	8.05 tCO_2eq/TJ
7	Hydro	renewable	8.05 tCO_2eq/TJ
8	Wind	renewable	7.22 tCO_2eq/TJ

Table S2. Octoberfest statistics for the years 1990 to 2019. Data are adopted from (oktoberfest.de Redaktion, 2019) (for 2019), (Landeshauptstadt München, 2019) (for 2001 to 2018), (Landeshauptstadt München Redaktion, 2000) (for 2000) and (Landeshauptstadt München Redaktion, 2020) (for 1990 to 1998).

Year	Electricity (in kWh)	Gas (in m^3)	Water (in m^3)	RENE share (in %)	Duration (in days)	Visitors (in mio.)
2019	2,840,000	185,000	105,000	100	16	6.3
2018	2,925,157	200,937	107,090	100	16	6.3
2017	3,247,385	223,156	116,184	100	18	6.2
2016	2,708,001	197,790	111,565	100	17	5.9
2015	2,887,032	233,846	128,855	100	16	5.9
2014	3,007,610	225,902	129,606	100	16	6.3
2013	3,056,207	243,437	122,184	100	16	6.4
2012	2,730,083	220,915	114,612	100	16	6.4
2011	2,972,463	201,516	124,456	62	17	6.9
2010	3,050,370	228,110	123,854	62	17	6.4
2009	2,627,987	183,001	108,643	61	16	5.7
2008	2,630,676	244,295	105,756	61	16	6.0
2007	2,714,537	197,126	104,531	61	16	6.2
2006	2,961,629	198,489	107,641	60	18	6.5
2005	2,866,152	207,191	96,728	58	17	6.1
2004	2,439,799	198,000	88,023	56	16	5.9
2003	2,331,749	184,299	89,587	56	16	6.3
2002	2,721,470	188,489	90,370	53	16	5.9
2001	2,519,276	172,200	84,744	49	16	5.5
2000	2,645,618	203,602	95,221	44	18	6.9
1999	2,452,001	182,841	82,393	0	16	6.5
1998	2,344,720	205,655	80,505	0	16	6.5
1997	2,287,970	195,515	84,000	0	16	6.4
1996	2,174,561	217,026	86,700	0	16	6.9
1995	2,287,968	198,616	86,600	0	16	6.7
1994	2,351,794	198,456	73,594	0	17	6.6
1993	1,922,168	194,170	69,000	0	16	6.5
1992	N/A	N/A	N/A	0	16	5.9
1991	1,955,513	N/A	69,000	0	16	6.4
1990	1,731,190	194,170	65,000	0	16	6.7

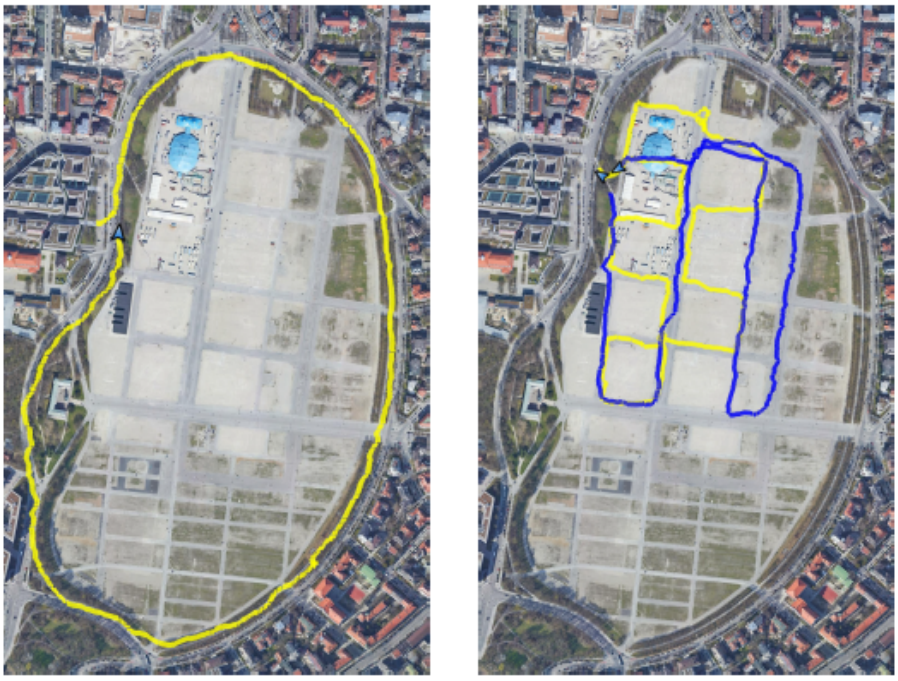

Figure S1. Illustration of the track around the perimeter of Oktoberfest (left; yellow) and the two different tracks on the site (right; yellow and blue). Map data are from ©Google, DigitalGlobe.

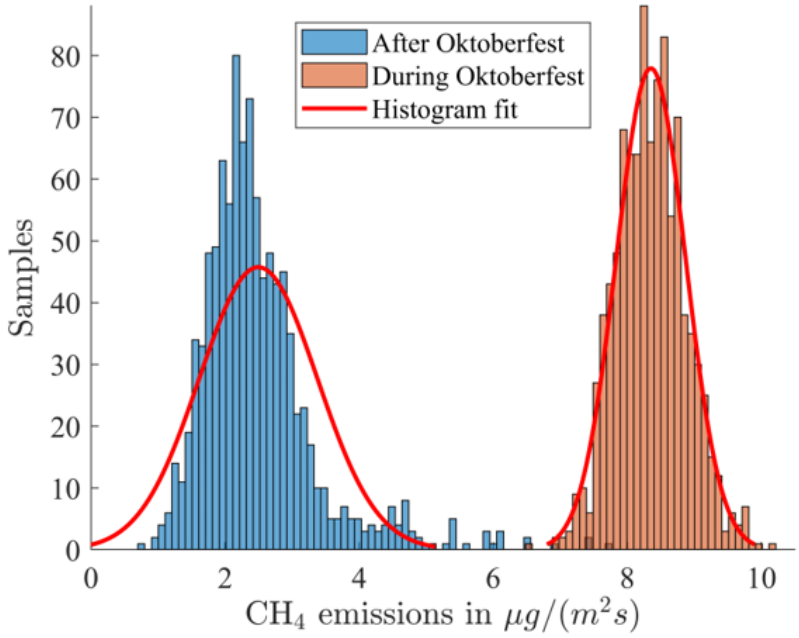

Figure S2. Distribution of total CH_4 emissions during (red) and after (blue) Oktoberfest 2019. The distributions were created by calculating the emission number 1000 times, with the input parameters wind speed, wind direction, measured CH_4 concentration, and modeled background concentration changed slightly in each iteration. For this purpose, these four input parameters were each modeled as independent Gaussian distributions (see Section 3.2 in (Chen et al., 2020)).

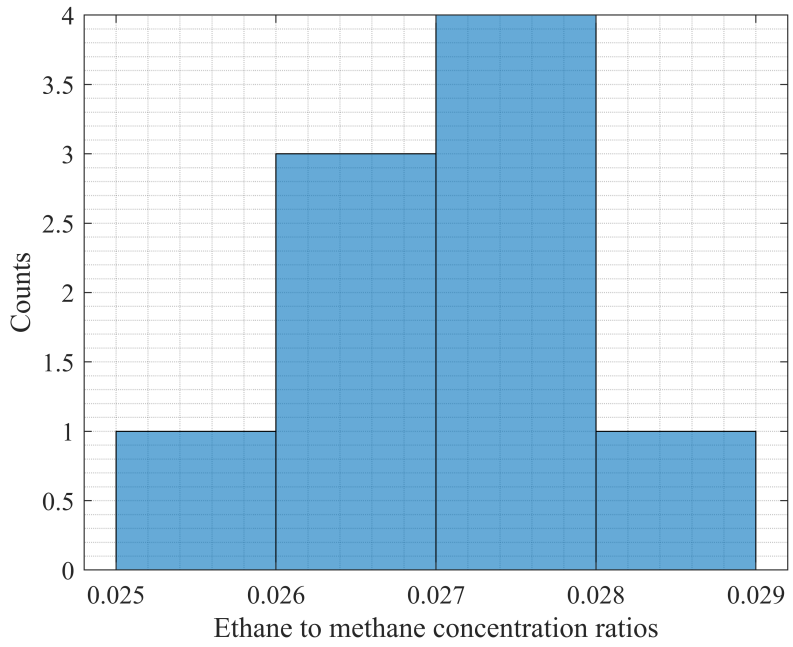

Figure S3. Distribution of the ethane to methane ratios measured inside the Oktoberfest tents. Since only nine ratios were determined, it is difficult to make a final conclusion about the nature of the distribution. However, the plot shows a Gaussian-like shape.

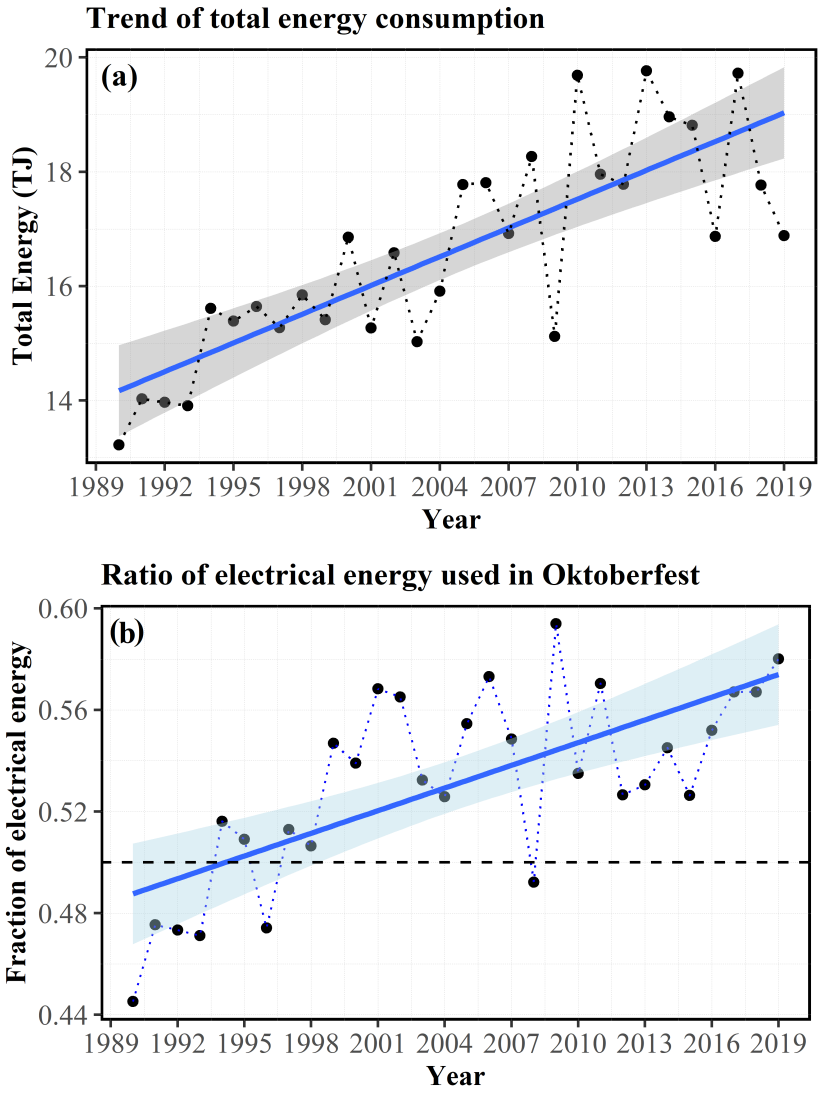

Figure S4. Top: trends in energy consumption at Oktoberfest. Bottom: fraction of electrical energy used at Oktoberfest from 1990 to 2019.

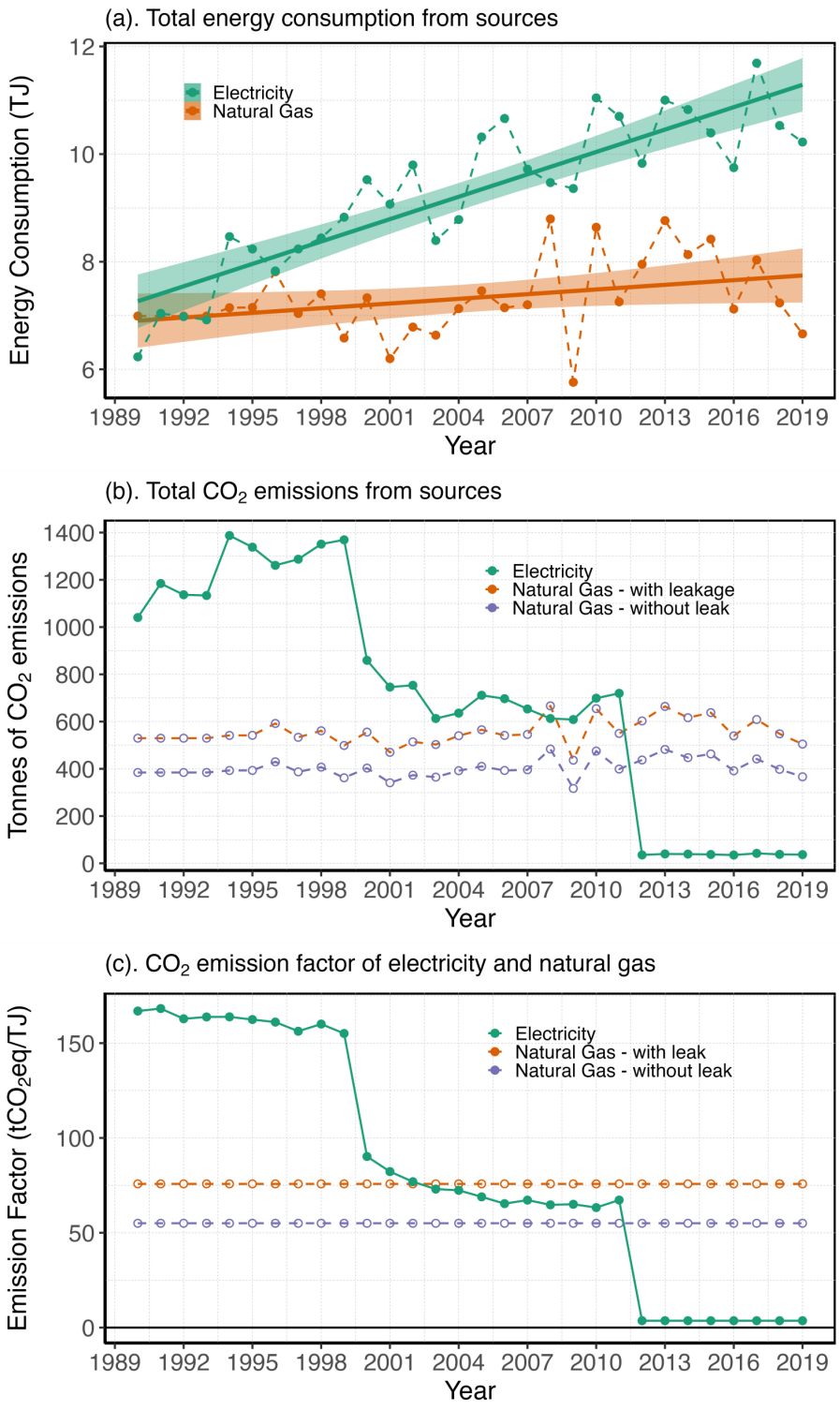

Figure S5. Energy consumption and emission statistics of Oktoberfest by electricity and natural gas sources from 1990 to 2019. (a) total energy consumption; (b) total CO_2 emissions from energy consumed; and (c) CO_2 emission factors for electricity (green), natural gas with 1.4% leakage rate (orange), and no leakage rate (purple).

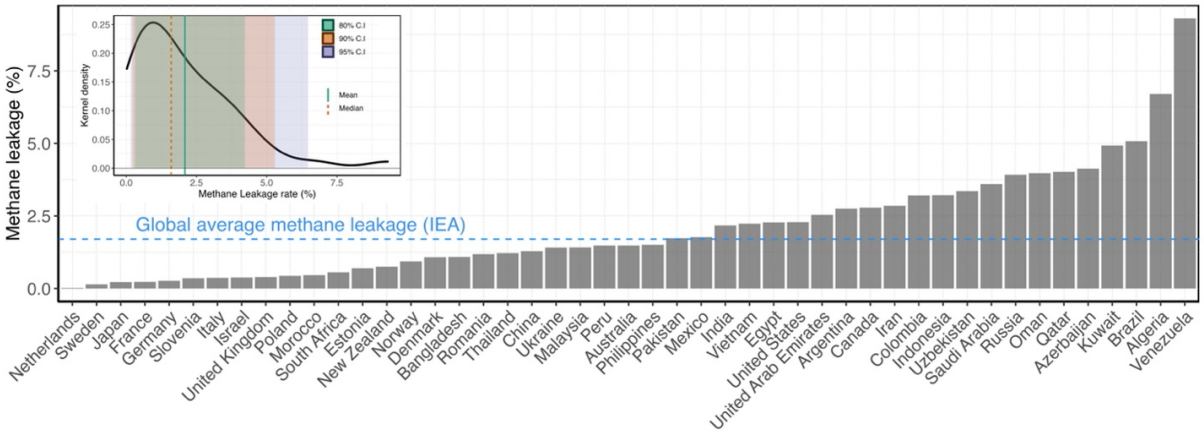

Figure S6. Calculated methane leakage rates for all studied countries based on the methane tracker dataset. The inset plot shows the distribution of methane leakage rates for all countries as kernel density. In addition, the 80%, 90%, and 95% confidence intervals (C.I.) are shown.

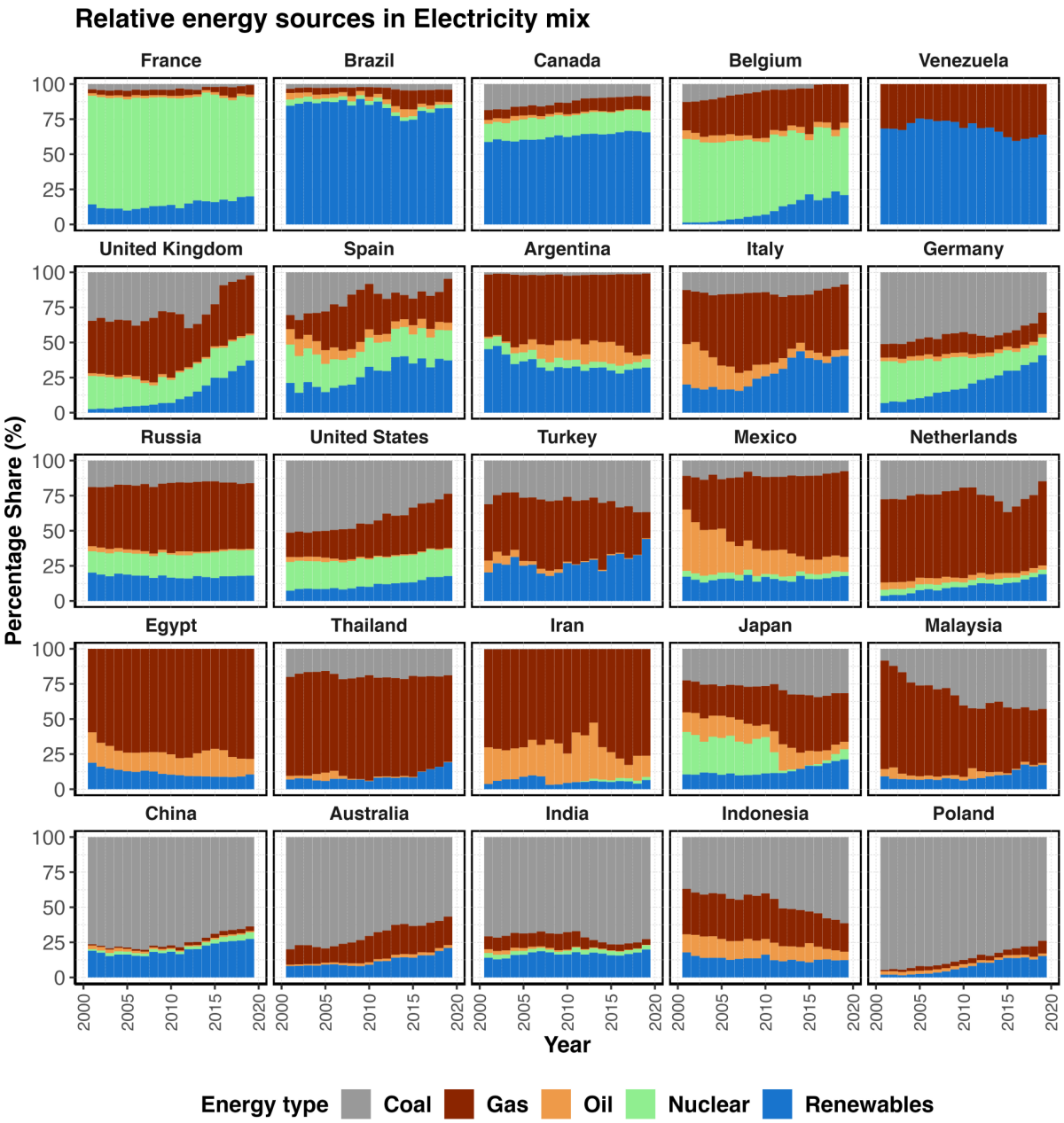

Figure S7. Relative share of the different types of energy sources (fossil fuel and renewable as colored bars) in electricity mix generation over the 30 years from 1990 to 2019 across 25 major natural gas consuming countries (20 years for Belgium, France and Venezuela). Data are adopted from (bp, 2020).

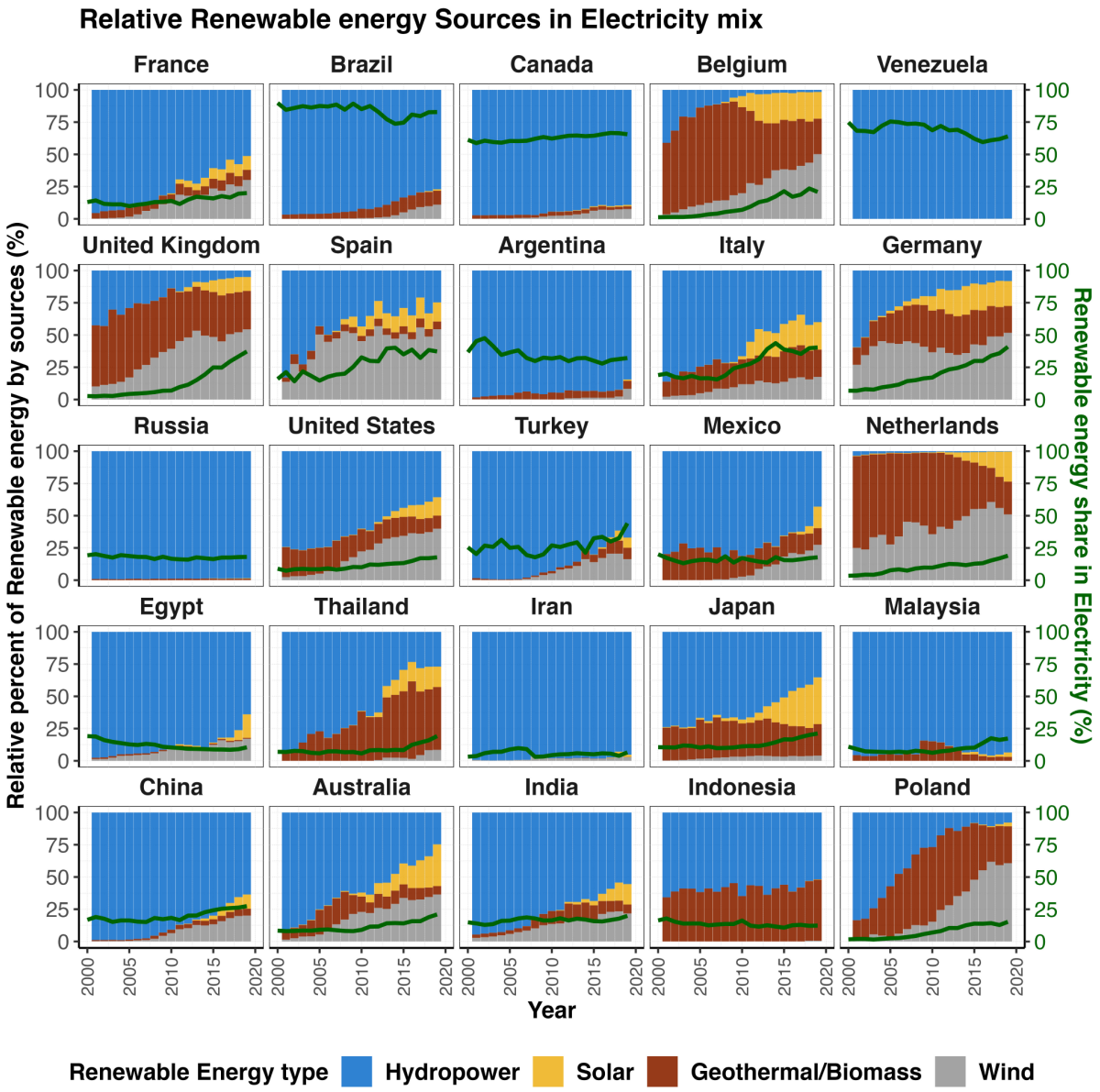

Figure S8. Relative share of the different types of renewable energy sources (colored bars) and share of renewable energy in total electricity consumption (in dark green line) over the 30 years from 1990 to 2019 across 25 major natural gas consuming countries (20 years for Belgium, France and Venezuela). Data are adopted from (bp, 2020).

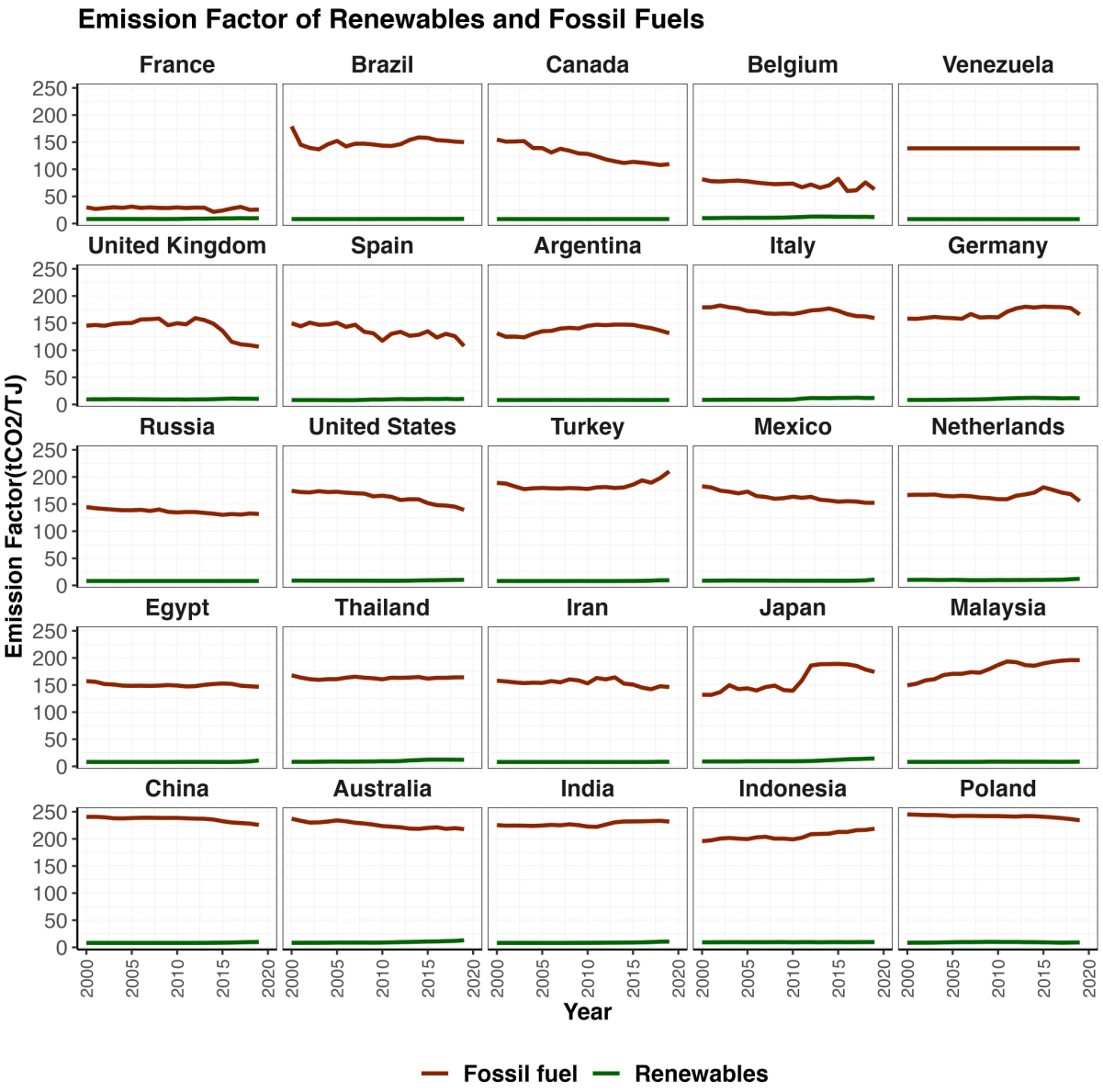

Figure S9. Emission factors of fossil fuel and renewable energy over the 30 years from 1990 to 2019 across 25 major natural gas consuming countries. Data are adopted from (bp, 2020).

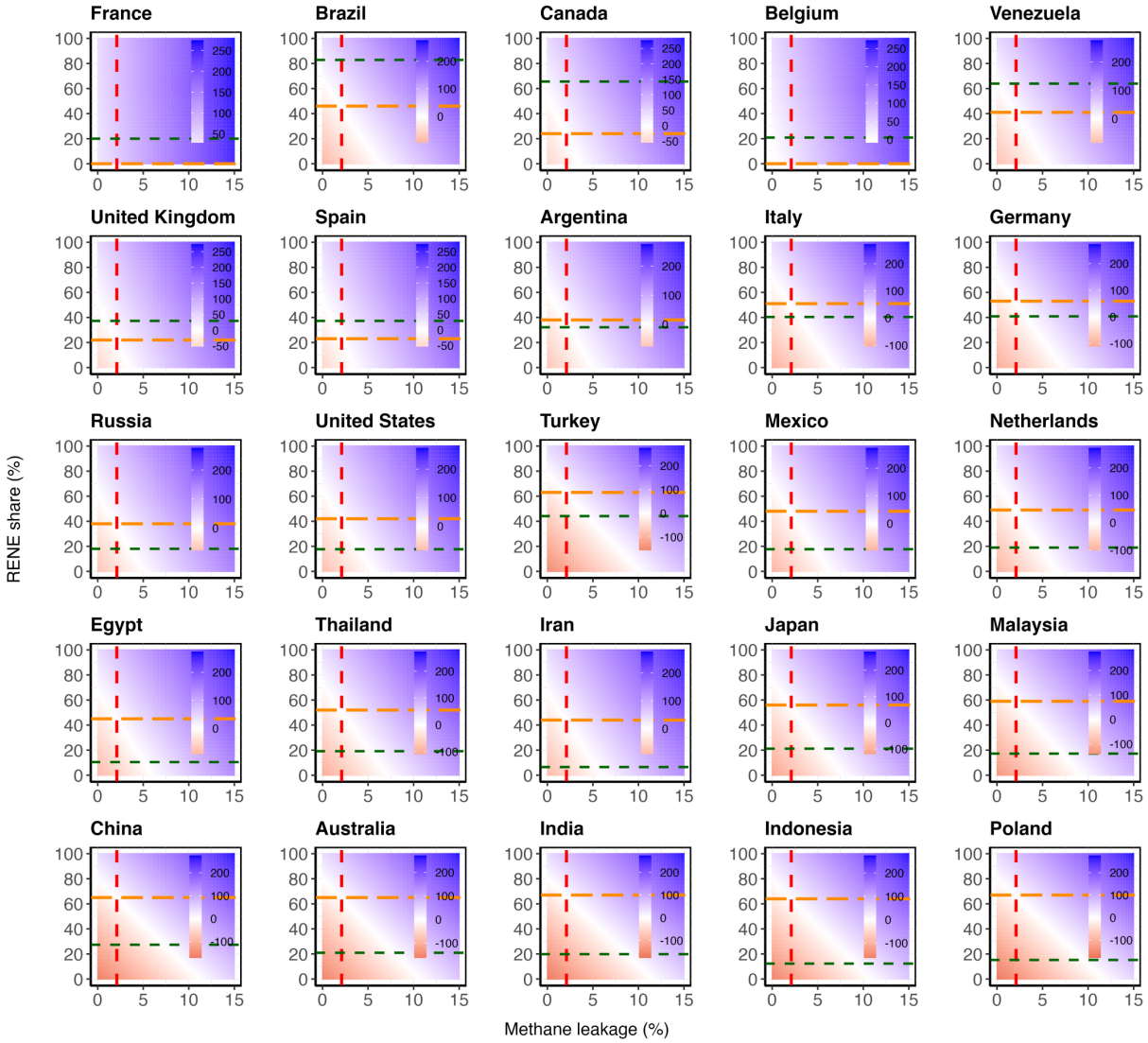

Figure S10. Phase transition plot for 25 countries based on electricity mix of 2019. The blue/red area represents where electricity/natural-gas is a better energy option. The vertical red line represents the mean methane leakage rate, whereas the horizontal dark green and orange dash line represents the current RENE share and break-even point where natural gas and electricity have the same carbon footprint.

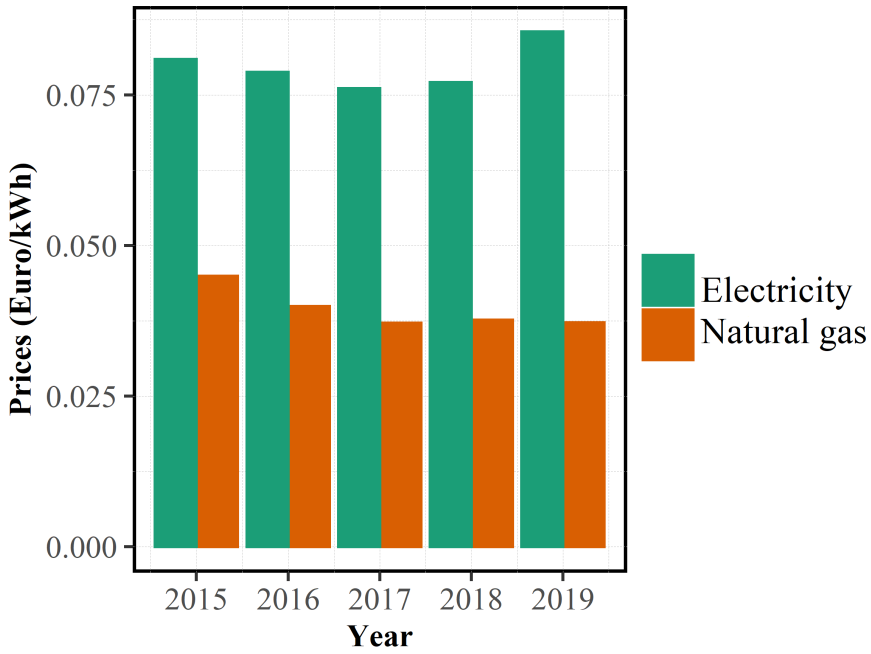

Figure S11. Development of the gas and electricity costs in Germany for 1 kWh of energy each. Data are adopted from (Eurostat, 2021a, 2021b).

Bibliography

[1] IPCC 2013, *Climate Change 2013: The Physical Science Basis. Contribution of Working Group I to the Fifth Assessment Report of the Intergovernmental Panel on Climate Change [Stocker, T.F., D. Qin, G.-K. Plattner, M. Tignor, S.K. Allen, J. Boschung, A. Nauels, Y. Xia, V. Bex and P.M. Midgley (eds.)]* Cambridge: Cambridge University Press, 2013, 1535 pp.

[2] World Health Organization, *Air Quality Guidelines: Global Update 2005 : Particulate Matter, Ozone, Nitrogen Dioxide, and Sulfur Dioxide*. World Health Organization, 2006, 497 pp., Google-Books-ID: 7VbxUdlJE8wC.

[3] IPCC 2006, "2006 IPCC Guidelines for National Greenhouse Gas Inventories, Prepared by the National Greenhouse Gas Inventories Programme, Eggleston H.S., Buendia L., Miwa K., Ngara T. and Tanabe K. (eds).", *IGES, Japan*, Jul. 1, 2006.

[4] IPCC 2019, "2019 Refinement to the 2006 IPCC Guidelines for National Greenhouse Gas Inventories, Calvo Buendia, E., Tanabe, K., Kranjc, A., Baasansuren, J., Fukuda, M., Ngarize, S., Osako, A., Pyrozhenko, Y., Shermanau, P. and Federici, S. (eds).", *IPCC, Switzerland*, 2019.

[5] G. Plant, E. A. Kort, C. Floerchinger, A. Gvakharia, I. Vimont, and C. Sweeney, "Large Fugitive Methane Emissions From Urban Centers Along the U.S. East Coast", *Geophysical Research Letters*, vol. 46, no. 14, pp. 8500–8507, 2019. DOI: https://doi.org/10.1029/2019GL082635.

[6] K. McKain, A. Down, S. M. Raciti, J. Budney, L. R. Hutyra, C. Floerchinger, S. C. Herndon, *et al.*, "Methane emissions from natural gas infrastructure and use in the urban region of Boston, Massachusetts", *Proceedings of the National Academy of Sciences*, vol. 112, no. 7, pp. 1941–1946, 2015.

[7] N. G. Phillips, R. Ackley, E. R. Crosson, A. Down, L. R. Hutyra, M. Brondfield, J. D. Karr, *et al.*, "Mapping urban pipeline leaks: Methane leaks across Boston", *Environmental Pollution*, vol. 173, pp. 1–4, Feb. 1, 2013. DOI: 10.1016/j.envpol.2012.11.003.

[8] R. B. Jackson, A. Down, N. G. Phillips, R. C. Ackley, C. W. Cook, D. L. Plata, and K. Zhao, "Natural Gas Pipeline Leaks Across Washington, DC", *Environmental Science & Technology*, vol. 48, no. 3, pp. 2051–2058, Feb. 4, 2014, Publisher: American Chemical Society. DOI: 10.1021/es404474x.

[9] M. E. Gallagher, A. Down, R. C. Ackley, K. Zhao, N. Phillips, and R. B. Jackson, "Natural Gas Pipeline Replacement Programs Reduce Methane Leaks and Improve Consumer Safety", *Environmental Science & Technology Letters*, vol. 2, no. 10, pp. 286–291, Oct. 13, 2015, Publisher: American Chemical Society. DOI: 10.1021/acs.estlett.5b00213.

[10] J. C. von Fischer, D. Cooley, S. Chamberlain, A. Gaylord, C. J. Griebenow, S. P. Hamburg, J. Salo, *et al.*, "Rapid, Vehicle-Based Identification of Location and Magnitude of Urban Natural Gas Pipeline Leaks", *Environmental Science & Technology*, vol. 51, no. 7, pp. 4091–4099, Apr. 4, 2017, Publisher: American Chemical Society. DOI: 10.1021/acs.est.6b06095.

[11] Z. D. Weller, J. R. Roscioli, W. C. Daube, B. K. Lamb, T. W. Ferrara, P. E. Brewer, and J. C. von Fischer, "Vehicle-Based Methane Surveys for Finding Natural Gas Leaks and Estimating Their Size: Validation and Uncertainty", *Environmental Science & Technology*, vol. 52, no. 20, pp. 11 922–11 930, Oct. 16, 2018, Publisher: American Chemical Society. DOI: 10.1021/acs.est.8b03135.

[12] Z. D. Weller, S. P. Hamburg, and J. C. von Fischer, "A National Estimate of Methane Leakage from Pipeline Mains in Natural Gas Local Distribution Systems", *Environmental Science & Technology*, vol. 54, no. 14, pp. 8958–8967, Jul. 21, 2020, Publisher: American Chemical Society. DOI: 10.1021/acs.est.0c00437.

[13] H. Maazallahi, J. M. Fernandez, M. Menoud, D. Zavala-Araiza, Z. D. Weller, S. Schwietzke, J. C. von Fischer, *et al.*, "Methane mapping, emission quantification, and attribution in two European cities: Utrecht (NL) and Hamburg (DE)", *Atmospheric Chemistry and Physics*, vol. 20, no. 23, pp. 14 717–14 740, Dec. 7, 2020, Publisher: Copernicus GmbH. DOI: 10.5194/acp-20-14717-2020.

[14] A. Karion, C. Sweeney, G. Pétron, G. Frost, R. M. Hardesty, J. Kofler, B. R. Miller, *et al.*, "Methane emissions estimate from airborne measurements over a western United States natural gas field", *Geophysical Research Letters*, vol. 40, no. 16, pp. 4393–4397, 2013. DOI: https://doi.org/10.1002/grl.50811.

[15] J. R. Roscioli, T. I. Yacovitch, C. Floerchinger, A. L. Mitchell, D. S. Tkacik, R. Subramanian, D. M. Martinez, *et al.*, "Measurements of methane emissions from natural gas gathering facilities and processing plants: measurement methods", *Atmospheric Measurement Techniques*, vol. 8, no. 5, pp. 2017–2035, May 7, 2015, Publisher: Copernicus GmbH. DOI: 10.5194/amt-8-2017-2015.

[16] A. L. Mitchell, D. S. Tkacik, J. R. Roscioli, S. C. Herndon, T. I. Yacovitch, D. M. Martinez, T. L. Vaughn, *et al.*, "Measurements of Methane Emissions from Natural Gas Gathering Facilities and Processing Plants: Measurement Results", *Environmental Science & Technology*, vol. 49, no. 5, pp. 3219–3227, Mar. 3, 2015, Publisher: American Chemical Society. DOI: 10.1021/es5052809.

[17] D. J. Zimmerle, L. L. Williams, T. L. Vaughn, C. Quinn, R. Subramanian, G. P. Duggan, B. Willson, *et al.*, "Methane Emissions from the Natural Gas Transmission and Storage System in the United States", *Environmental Science & Technology*, vol. 49, no. 15, pp. 9374–9383, Aug. 4, 2015, Publisher: American Chemical Society. DOI: 10.1021/acs.est.5b01669.

[18] M. Omara, M. R. Sullivan, X. Li, R. Subramanian, A. L. Robinson, and A. A. Presto, "Methane Emissions from Conventional and Unconventional Natural Gas Production Sites in the Marcellus Shale Basin", *Environmental Science & Technology*, vol. 50, no. 4, pp. 2099–2107, Feb. 16, 2016, Publisher: American Chemical Society. DOI: 10.1021/acs.est.5b05503.

[19] F. Bréon, G. Broquet, V. Puygrenier, F. Chevallier, I. Xueref-Remy, M. Ramonet, E. Dieudonné, *et al.*, "An attempt at estimating Paris area CO_2 emissions from atmospheric concentration measurements", *Atmospheric Chemistry and Physics*, vol. 15, no. 4, pp. 1707–1724, 2015.

[20] I. Xueref-Remy, E. Dieudonné, C. Vuillemin, M. Lopez, C. Lac, M. Schmidt, M. Delmotte, *et al.*, "Diurnal, synoptic and seasonal variability of atmospheric CO_2 in the Paris megacity area", *Atmospheric Chemistry and Physics*, vol. 18, no. 5, pp. 3335–3362, Mar. 2018. DOI: https://doi.org/10.5194/acp-18-3335-2018.

[21] B. K. Lamb, M. O. L. Cambaliza, K. J. Davis, S. L. Edburg, T. W. Ferrara, C. Floerchinger, A. M. F. Heimburger, *et al.*, "Direct and Indirect Measurements and Modeling of Methane Emissions in Indianapolis, Indiana", *Environmental Science & Technology*, vol. 50, no. 16, pp. 8910–8917, Aug. 16, 2016, Publisher: American Chemical Society. DOI: 10.1021/acs.est.6b01198.

[22] J. Kim, A. A. Shusterman, K. J. Lieschke, C. Newman, and R. C. Cohen, "The BErkeley Atmospheric CO_2 Observation Network: field calibration and evaluation of low-cost air quality sensors", *Atmospheric Measurement Techniques*, vol. 11, no. 4, pp. 1937–1946, Apr. 6, 2018, Publisher: Copernicus GmbH. DOI: 10.5194/amt-11-1937-2018.

[23] A. A. Shusterman, V. E. Teige, A. J. Turner, C. Newman, J. Kim, and R. C. Cohen, "The BErkeley Atmospheric CO_2 Observation Network: initial evaluation", *Atmospheric Chemistry and Physics*, vol. 16, no. 21, pp. 13 449–13 463, Oct. 2016. DOI: https://doi.org/10.5194/acp-16-13449-2016.

[24] B. Gioli, P. Toscano, E. Lugato, A. Matese, F. Miglietta, A. Zaldei, and F. P. Vaccari, "Methane and carbon dioxide fluxes and source partitioning in urban areas: The case study of Florence, Italy", *Environmental Pollution*, vol. 164, pp. 125–131, May 1, 2012. DOI: 10.1016/j.envpol.2012.01.019.

[25] C. Helfter, A. H. Tremper, C. H. Halios, S. Kotthaus, A. Bjorkegren, C. S. B. Grimmond, J. F. Barlow, *et al.*, "Spatial and temporal variability of urban fluxes of methane, carbon monoxide and carbon dioxide above London, UK", *Atmospheric Chemistry and Physics*, vol. 16, no. 16, pp. 10 543–10 557, Aug. 24, 2016, Publisher: Copernicus GmbH. DOI: 10.5194/acp-16-10543-2016.

[26] M. Menoud, C. van der Veen, B. Scheeren, H. Chen, B. Szénási, R. P. Morales, I. Pison, *et al.*, "Characterisation of methane sources in Lutjewad, The Netherlands, using quasi-continuous isotopic composition measurements", *Tellus B: Chemical and Physical Meteorology*, vol. 72, no. 1, pp. 1–20, Jan. 1, 2020. DOI: 10.1080/16000889.2020.1823733.

[27] X. Lu, S. J. Harris, R. E. Fisher, J. L. France, E. G. Nisbet, D. Lowry, T. Röckmann, *et al.*, "Isotopic signatures of major methane sources in the coal seam gas fields and adjacent agricultural districts, Queensland, Australia", *Atmospheric Chemistry and Physics*, vol. 21, no. 13, pp. 10 527–10 555, Jul. 14, 2021, Publisher: Copernicus GmbH. DOI: 10.5194/acp-21-10527-2021.

[28] M. Menoud, C. van der Veen, J. Necki, J. Bartyzel, B. Szénási, M. Stanisavljević, I. Pison, *et al.*, "Methane (CH_4) sources in Krakow, Poland: insights from isotope analysis", *Atmospheric Chemistry and Physics*, vol. 21, no. 17, pp. 13 167–13 185, Sep. 6, 2021, Publisher: Copernicus GmbH. DOI: 10.5194/acp-21-13167-2021.

[29] T. Röckmann, S. Eyer, C. van der Veen, M. E. Popa, B. Tuzson, G. Monteil, S. Houweling, *et al.*, "In situ observations of the isotopic composition of methane at the Cabauw tall tower site", *Atmospheric Chemistry and Physics*, vol. 16, no. 16, pp. 10 469–10 487, Aug. 19, 2016, Publisher: Copernicus GmbH. DOI: 10.5194/acp-16-10469-2016.

[30] V. Beck, H. Chen, C. Gerbig, P. Bergamaschi, L. Bruhwiler, S. Houweling, T. Röckmann, *et al.*, "Methane airborne measurements and comparison to global models during BARCA", *Journal of Geophysical Research: Atmospheres*, vol. 117, D15 2012. DOI: 10.1029/2011JD017345.

[31] R. Fisher, D. Lowry, O. Wilkin, S. Sriskantharajah, and E. G. Nisbet, "High-precision, automated stable isotope analysis of atmospheric methane and carbon dioxide using continuous-flow isotope-ratio mass spectrometry", *Rapid Communications in Mass Spectrometry*, vol. 20, no. 2, pp. 200–208, 2006. DOI: https://doi.org/10.1002/rcm.2300.

[32] S. D. Chamberlain, A. R. Ingraffea, and J. P. Sparks, "Sourcing methane and carbon dioxide emissions from a small city: Influence of natural gas leakage and combustion", *Environmental Pollution*, vol. 218, pp. 102–110, Nov. 1, 2016. DOI: 10.1016/j.envpol.2016.08.036.

[33] M. Zimnoch, J. Necki, L. Chmura, A. Jasek, D. Jelen, M. Galkowski, T. Kuc, *et al.*, "Quantification of carbon dioxide and methane emissions in urban areas: source apportionment based on atmospheric observations", *Mitigation and Adaptation Strategies for Global Change*, vol. 24, no. 6, pp. 1051–1071, Aug. 1, 2019. DOI: 10.1007/s11027-018-9821-0.

[34] D. Zavala-Araiza, D. R. Lyon, R. A. Alvarez, K. J. Davis, R. Harriss, S. C. Herndon, A. Karion, *et al.*, "Reconciling divergent estimates of oil and gas methane emissions", *Proceedings of the National Academy of Sciences*, vol. 112, no. 51, pp. 15 597–15 602, Dec. 22, 2015, ISBN: 9781522126119 Publisher: National Academy of Sciences Section: Physical Sciences. DOI: 10.1073/pnas.1522126112.

[35] D. T. Allen, V. M. Torres, J. Thomas, D. W. Sullivan, M. Harrison, A. Hendler, S. C. Herndon, *et al.*, "Measurements of methane emissions at natural gas production sites in the United States", *Proceedings of the National Academy of Sciences*, vol. 110, no. 44, pp. 17 768–17 773, Oct. 29, 2013, Publisher: National Academy of Sciences Section: Physical Sciences. DOI: 10.1073/pnas.1304880110.

[36] T. I. Yacovitch, S. C. Herndon, J. R. Roscioli, C. Floerchinger, R. M. McGovern, M. Agnese, G. Pétron, *et al.*, "Demonstration of an Ethane Spectrometer for Methane Source Identification", *Environmental Science & Technology*, vol. 48, no. 14, pp. 8028–8034, Jul. 15, 2014, Publisher: American Chemical Society. DOI: 10.1021/es501475q.

[37] T. I. Yacovitch, S. C. Herndon, G. Pétron, J. Kofler, D. Lyon, M. S. Zahniser, and C. E. Kolb, "Mobile Laboratory Observations of Methane Emissions in the Barnett Shale Region", *Environmental Science & Technology*, vol. 49, no. 13, pp. 7889–7895, Jul. 7, 2015, Publisher: American Chemical Society. DOI: 10.1021/es506352j.

[38] T. I. Yacovitch, B. Neininger, S. C. Herndon, H. D. van der Gon, S. Jonkers, J. Hulskotte, J. R. Roscioli, *et al.*, "Methane emissions in the Netherlands: The Groningen field", *Elementa: Science of the Anthropocene*, vol. 6, no. 57, D. Helmig and S. Schwietzke, Eds., Aug. 1, 2018. DOI: 10.1525/elementa.308.

[39] D. Crisp, H. R. Pollock, R. Rosenberg, L. Chapsky, R. A. M. Lee, F. A. Oyafuso, C. Frankenberg, *et al.*, "The on-orbit performance of the Orbiting Carbon Observatory-2 (OCO-2) instrument and its radiometrically calibrated products", *Atmospheric Measurement Techniques*, vol. 10, no. 1, pp. 59–81, Jan. 5, 2017, Publisher: Copernicus GmbH. DOI: 10.5194/amt-10-59-2017.

[40] A. Eldering, P. O. Wennberg, D. Crisp, D. S. Schimel, M. R. Gunson, A. Chatterjee, J. Liu, *et al.*, "The Orbiting Carbon Observatory-2 early science investigations of regional carbon dioxide fluxes", *Science*, Oct. 13, 2017, Publisher: American Association for the Advancement of Science. DOI: 10.1126/science.aam5745.

[41] F. M. Schwandner, M. R. Gunson, C. E. Miller, S. A. Carn, A. Eldering, T. Krings, K. R. Verhulst, *et al.*, "Spaceborne detection of localized carbon dioxide sources", *Science*, Oct. 13, 2017, Publisher: American Association for the Advancement of Science. DOI: 10.1126/science.aam5782.

[42] T. Yokota, Y. Yoshida, N. Eguchi, Y. Ota, T. Tanaka, H. Watanabe, and S. Maksyutov, "Global Concentrations of CO_2 and CH_4 Retrieved from GOSAT: First Preliminary Results", *Sola*, vol. 5, pp. 160–163, 2009. DOI: 10.2151/sola.2009-041.

[43] A. Kuze, H. Suto, M. Nakajima, and T. Hamazaki, "Initial Onboard Performance of TANSO-FTS on GOSAT", in *Advances in Imaging (2009), paper FTuC2*, Optical Society of America, Apr. 26, 2009, FTuC2. DOI: 10.1364/FTS.2009.FTuC2.

[44] E. A. Kort, C. Frankenberg, C. E. Miller, and T. Oda, "Space-based observations of megacity carbon dioxide", *Geophysical Research Letters*, vol. 39, no. 17, 2012.

[45] D. Crisp, "Measuring atmospheric carbon dioxide from space with the Orbiting Carbon Observatory-2 (OCO-2)", in *Earth Observing Systems XX*, vol. 9607, SPIE, Sep. 8, 2015, p. 960 702. DOI: 10.1117/12.2187291.

[46] D. Wunch, G. C. Toon, J. F. Blavier, R. A. Washenfelder, J. Notholt, B. J. Connor, D. W. Griffith, *et al.*, "The total carbon column observing network", *Philos Trans A Math Phys Eng Sci*, vol. 369, no. 1943, pp. 2087–112, 2011.

[47] M. Gisi, F. Hase, S. Dohe, and T. Blumenstock, "Camtracker: a new camera controlled high precision solar tracker system for FTIR-spectrometers", *Atmospheric Measurement Techniques*, vol. 4, no. 1, pp. 47–54, 2011. DOI: 10.5194/amt-4-47-2011.

[48] M. Gisi, "Setup of precise camera based solar tracker systems and greenhouse gas measurements using a modified portable spectrometer", PhD thesis, Karlsruhe, Karlsruher Institut für Technologie (KIT), Diss., 2012, 2012.

[49] F. Hase, M. Frey, M. Kiel, T. Blumenstock, R. Harig, A. Keens, and J. Orphal, "Addition of a channel for XCO observations to a portable FTIR spectrometer for greenhouse gas measurements", *Atmospheric Measurement Techniques*, vol. 9, no. 5, pp. 2303–2313, May 2016. DOI: https://doi.org/10.5194/amt-9-2303-2016.

[50] M. Frey, M. K. Sha, F. Hase, M. Kiel, T. Blumenstock, R. Harig, G. Surawicz, *et al.*, "Building the COllaborative Carbon Column Observing Network (COCCON): long-term stability and ensemble performance of the EM27/SUN Fourier transform spectrometer", *Atmospheric Measurement Techniques*, vol. 12, no. 3, pp. 1513–1530, Mar. 2019. DOI: https://doi.org/10.5194/amt-12-1513-2019.

[51] M. K. Sha, B. Langerock, M. Kiel, D. Dubravica, F. Hase, T. Borsdorff, A. Lorente, *et al.*, "Using the COllaborative Carbon Column Observing Network for validating space borne GHG sensors", presented at the IWGGMS-17, Jun. 17, 2021.

[52] J. Chen, C. Viatte, J. K. Hedelius, T. Jones, J. E. Franklin, H. Parker, E. W. Gottlieb, *et al.*, "Differential column measurements using compact solar-tracking spectrometers", *Atmos. Chem. Phys.*, vol. 16, no. 13, pp. 8479–8498, Jul. 12, 2016. DOI: 10.5194/acp-16-8479-2016.

[53] F. Hase, M. Frey, T. Blumenstock, J. Gro{\textbackslash}s s, M. Kiel, R. Kohlhepp, G. Mengistu Tsidu, *et al.*, "Application of portable FTIR spectrometers for detecting greenhouse gas emissions of the major city Berlin", *Atmospheric Measurement Techniques*, vol. 8, no. 7, pp. 3059–3068, 2015.

[54] X. Zhao, J. Marshall, S. Hachinger, C. Gerbig, M. Frey, F. Hase, and J. Chen, "Analysis of total column CO_2 and CH_4 measurements in Berlin with WRF-GHG", *Atmospheric Chemistry and Physics*, vol. 19, no. 17, pp. 11 279–11 302, Sep. 6, 2019, Publisher: Copernicus GmbH. DOI: 10.5194/acp-19-11279-2019.

[55] F. R. Vogel, M. Frey, J. Staufer, F. Hase, G. Broquet, I. Xueref-Remy, F. Chevallier, *et al.*, "XCO_2 in an emission hot-spot region: the COCCON Paris campaign 2015", *Atmospheric Chemistry and Physics*, vol. 19, no. 5, pp. 3271–3285, Mar. 13, 2019, Publisher: Copernicus GmbH. DOI: 10.5194/acp-19-3271-2019.

[56] M. V. Makarova, C. Alberti, D. V. Ionov, F. Hase, S. C. Foka, T. Blumenstock, T. Warneke, *et al.*, "Emission Monitoring Mobile Experiment (EMME): an overview and first results of the St. Petersburg megacity campaign 2019", *Atmospheric Measurement Techniques*, vol. 14, no. 2, pp. 1047–1073, Feb. 10, 2021, Publisher: Copernicus GmbH. DOI: 10.5194/amt-14-1047-2021.

[57] C. Viatte, T. Lauvaux, J. K. Hedelius, H. Parker, J. Chen, T. Jones, J. E. Franklin, *et al.*, "Methane emissions from dairies in the Los Angeles Basin", *Atmospheric Chemistry and Physics*, vol. 17, no. 12, pp. 7509–7528, Jun. 2017. DOI: https://doi.org/10.5194/acp-17-7509-2017.

[58] F. Toja-Silva, J. Chen, S. Hachinger, and F. Hase, "CFD simulation of CO2 dispersion from urban thermal power plant: Analysis of turbulent Schmidt number and comparison with Gaussian plume model and measurements", *Journal of Wind Engineering and Industrial Aerodynamics*, vol. 169, pp. 177–193, Oct. 1, 2017. DOI: 10.1016/j.jweia.2017.07.015.

[59] A. Butz, A. S. Dinger, N. Bobrowski, J. Kostinek, L. Fieber, C. Fischerkeller, G. B. Giuffrida, *et al.*, "Remote sensing of volcanic CO_2, HF, HCl, SO_2, and BrO in the downwind plume of Mt. Etna", *Atmospheric Measurement Techniques*, vol. 10, no. 1, pp. 1–14, Jan. 2017. DOI: https://doi.org/10.5194/amt-10-1-2017.

[60] F. Klappenbach, M. Bertleff, J. Kostinek, F. Hase, T. Blumenstock, A. Agusti-Panareda, M. Razinger, *et al.*, "Accurate mobile remote sensing of XCO_2 and XCH_4 latitudinal transects from aboard a research vessel", *Atmospheric Measurement Techniques*, vol. 8, no. 12, pp. 5023–5038, 2015.

[61] D. Jacob, *Introduction to atmospheric chemistry*. Princeton University Press, 1999.

[62] Sutton Oliver Graham and Simpson George Clarke, "A theory of eddy diffusion in the atmosphere", *Proceedings of the Royal Society of London. Series A, Containing Papers of a Mathematical and Physical Character*, vol. 135, no. 826, pp. 143–165, Feb. 1932. DOI: 10.1098/rspa.1932.0025.

[63] G. A. Briggs, "Diffusion estimation for small emissions. Preliminary report", National Oceanic, Atmospheric Administration, Oak Ridge, Tenn. (USA). Atmospheric Turbulence, and Diffusion Lab., TID-28289, May 1973. DOI: 10.2172/5118833.

[64] S. R. Hanna, G. A. Briggs, and R. P. J. Hosker, "Handbook on atmospheric diffusion", National Oceanic, Atmospheric Administration, Oak Ridge, TN (USA). Atmospheric Turbulence, and Diffusion Lab., DOE/TIC-11223, Jan. 1982. DOI: 10.2172/5591108.

[65] J. C. Lin, C. Gerbig, S. C. Wofsy, A. E. Andrews, B. C. Daube, K. J. Davis, and C. A. Grainger, "A near-field tool for simulating the upstream influence of atmospheric observations: The Stochastic Time-Inverted Lagrangian Transport (STILT) model", *Journal of Geophysical Research: Atmospheres*, vol. 108, D16 2003. DOI: 10.1029/2002JD003161.

[66] B. Fasoli, J. C. Lin, D. R. Bowling, L. Mitchell, and D. Mendoza, "Simulating atmospheric tracer concentrations for spatially distributed receptors: updates to the Stochastic Time-Inverted Lagrangian Transport model's R interface (STILT-R version 2)", *Geoscientific Model Development*, vol. 11, no. 7, pp. 2813–2824, Jul. 2018. DOI: https://doi.org/10.5194/gmd-11-2813-2018.

[67] C. D. Rodgers, *Inverse Methods for Atmospheric Sounding: Theory and Practice*. WORLD SCIENTIFIC, Jul. 2000. DOI: 10.1142/3171.

[68] J. Ray, J. Lee, V. Yadav, S. Lefantzi, A. M. Michalak, and B. van Bloemen Waanders, "A sparse reconstruction method for the estimation of multi-resolution emission fields via atmospheric inversion", *Geoscientific Model Development*, vol. 8, no. 4, pp. 1259–1273, Apr. 29, 2015, Publisher: Copernicus GmbH. DOI: 10.5194/gmd-8-1259-2015.

[69] Bundesamt für Justiz, *Neununddreißigste Verordnung zur Durchführung des Bundes-Immissionsschutzgesetzes*, (Verordnung über Luftqualitätsstandards und Emissionshöchstmengen - 39. BImSchV), Aug. 2, 2010.

[70] Y. Zhu, J. Chen, X. Bi, G. Kuhlmann, K. L. Chan, F. Dietrich, D. Brunner, *et al.*, "Spatial and temporal representativeness of point measurements for nitrogen dioxide pollution levels in cities", *Atmospheric Chemistry and Physics*, vol. 20, no. 21, pp. 13 241–13 251, Nov. 10, 2020, Publisher: Copernicus GmbH. DOI: 10.5194/acp-20-13241-2020.

[71] L. E. Mitchell, J. C. Lin, D. R. Bowling, D. E. Pataki, C. Strong, A. J. Schauer, R. Bares, *et al.*, "Long-term urban carbon dioxide observations reveal spatial and temporal dynamics related to urban characteristics and growth", *PNAS*, vol. 115, no. 12, pp. 2912–2917, Mar. 2018. DOI: 10.1073/pnas.1702393115.

[72] R. Hagemann, U. Corsmeier, C. Kottmeier, R. Rinke, A. Wieser, and B. Vogel, "Spatial variability of particle number concentrations and NOx in the Karlsruhe (Germany) area obtained with the mobile laboratory 'AERO-TRAM'", *Atmospheric Environment*, vol. 94, pp. 341–352, Sep. 1, 2014. DOI: 10.1016/j.atmosenv.2014.05.051.

[73] D. Hasenfratz, O. Saukh, C. Walser, C. Hueglin, M. Fierz, T. Arn, J. Beutel, *et al.*, "Deriving high-resolution urban air pollution maps using mobile sensor nodes", *Pervasive and Mobile Computing*, Selected Papers from the Twelfth Annual IEEE International Conference on Pervasive Computing and Communications (PerCom 2014), vol. 16, pp. 268–285, Jan. 1, 2015. DOI: 10.1016/j.pmcj.2014.11.008.

[74] M. Mueller, J. Meyer, and C. Hueglin, "Design of an ozone and nitrogen dioxide sensor unit and its long-term operation within a sensor network in the city of Zurich", *Atmospheric Measurement Techniques*, vol. 10, no. 10, pp. 3783–3799, Oct. 17, 2017, Publisher: Copernicus GmbH. DOI: 10.5194/amt-10-3783-2017.

[75] P. Schneider, N. Castell, M. Vogt, F. R. Dauge, W. A. Lahoz, and A. Bartonova, "Mapping urban air quality in near real-time using observations from low-cost sensors and model information", *Environment International*, vol. 106, pp. 234–247, Sep. 2017. DOI: 10.1016/j.envint.2017.05.005.

[76] O. A. M. Popoola, D. Carruthers, C. Lad, V. B. Bright, M. I. Mead, M. E. J. Stettler, J. R. Saffell, *et al.*, "Use of networks of low cost air quality sensors to quantify air quality in urban settings", *Atmospheric Environment*, vol. 194, pp. 58–70, Dec. 1, 2018. DOI: 10.1016/j.atmosenv.2018.09.030.

[77] K. R. Gurney, P. Romero-Lankao, K. C. Seto, L. R. Hutyra, R. Duren, C. Kennedy, N. B. Grimm, *et al.*, "Climate change: Track urban emissions on a human scale", *Nature*, vol. 525, pp. 179–181, 2015.

[78] S. Ladage, M. Blumenberg, D. Franke, A. Bahr, R. Lutz, and S. Schmidt, "On the climate benefit of a coal-to-gas shift in Germany's electric power sector", *Scientific Reports*, vol. 11, no. 1, p. 11 453, Jun. 1, 2021, Number: 1 Publisher: Nature Publishing Group. DOI: 10.1038/s41598-021-90839-7.

[79] K. Tanaka, O. Cavalett, W. J. Collins, and F. Cherubini, "Asserting the climate benefits of the coal-to-gas shift across temporal and spatial scales", *Nature Climate Change*, vol. 9, no. 5, pp. 389–396, May 2019, Number: 5 Publisher: Nature Publishing Group. DOI: 10.1038/s41558-019-0457-1.

[80] Y. Qin, R. Edwards, F. Tong, and D. L. Mauzerall, "Can Switching from Coal to Shale Gas Bring Net Carbon Reductions to China?", *Environmental Science & Technology*, vol. 51, no. 5, pp. 2554–2562, Mar. 7, 2017, Publisher: American Chemical Society. DOI: 10.1021/acs.est.6b04072.

[81] M. Fulton, N. Mellquist, and S. Kitasei, *Comparing Life Cycle Greenhouse Gas Emissions from Natural Gas and Coal*, Mar. 14, 2011.

[82] E. G. Nisbet, M. R. Manning, E. J. Dlugokencky, R. E. Fisher, D. Lowry, S. E. Michel, C. L. Myhre, *et al.*, "Very Strong Atmospheric Methane Growth in the 4 Years 2014–2017: Implications for the Paris Agreement", *Global Biogeochemical Cycles*, vol. 33, no. 3, pp. 318–342, 2019, _eprint: https://onlinelibrary.wiley.com/doi/pdf/10.1029/2018GB006009. DOI: 10.1029/2018GB006009.

[83] L. Heinle and J. Chen, "Automated enclosure and protection system for compact solar-tracking spectrometers", *Atmospheric Measurement Techniques*, vol. 11, no. 4, pp. 2173–2185, 2018. DOI: 10.5194/amt-11-2173-2018.

[84] F. Dietrich and J. Chen, "Portable Automated Enclosure for a Spectrometer Measuring Greenhouse Gases", presented at the EGU General Assembly 2018, Vienna, Austria: Copernicus Meetings, Apr. 9, 2018, EGU2018–16281–1. DOI: 10.13140/RG.2.2.11591.14248.

[85] F. Dietrich, J. Chen, B. Voggenreiter, P. Aigner, N. Nachtigall, and B. Reger, "MUCCnet: Munich Urban Carbon Column network", *Atmospheric Measurement Techniques*, vol. 14, no. 2, pp. 1111–1126, Feb. 11, 2021, Publisher: Copernicus GmbH. DOI: 10.5194/amt-14-1111-2021.

[86] B. Voggenreiter, "Development of a camera-based sensor system for detecting solar radiation", [unpublished thesis], Master's thesis, Technical University of Munich - Environmental Sensing and Modeling, Munich, Germany, Sep. 27, 2019.

[87] N. Hars, "Optimizing a Python software to fully automate measurements in the Munich permanent urban greenhouse gas column observing network", [unpublished thesis], Bachelor's thesis, Technical University of Munich - Environmental Sensing and Modeling, Munich, Germany, Mar. 1, 2021.

[88] D. Wunch, G. C. Toon, V. Sherlock, N. M. Deutscher, X. Liu, D. G. Feist, and P. O. Wennberg, "The Total Carbon Column Observing Network's GGG2014 Data Version", *Carbon Dioxide Information Analysis Center, Oak Ridge National Laboratory, Oak Ridge, Tennessee, USA*, vol. 10, 2015. DOI: 10.14291/tccon.ggg2014.documentation.R0/1221662.

[89] J. K. Hedelius, C. Viatte, D. Wunch, C. M. Roehl, G. C. Toon, J. Chen, T. Jones, *et al.*, "Assessment of errors and biases in retrievals of X_{CO2}, X_{CH4}, X_{CO}, and X_{N2O} from a 0.5 cm^{-1} resolution solar-viewing spectrometer", *Atmospheric Measurement Techniques*, vol. 9, no. 8, pp. 3527–3546, Aug. 2016. DOI: https://doi.org/10.5194/amt-9-3527-2016.

[90] N. Nachtigall, "Development of a Data Modeling Framework for Greenhouse Gas Emission Quantification Based on a Novel Atmospheric Dataset", [unpublished thesis], Master's thesis, Technical University of Munich - Environmental Sensing and Modeling, Munich, Germany, Oct. 19, 2020.

[91] M. Makowski, N. Nachtigall, F. Dietrich, D. H. Nguyen, and J. Chen. (2021). Extract retrieval data. https://github.com/tum-esm/extract-retrieval-data, (visited on 01/09/2022).

[92] P. Aigner, "Software Automation of EM27/SUN and Source Map Creation for Munich", [unpublished thesis], Master's thesis, Technical University of Munich - Environmental Sensing and Modeling, Munich, Germany, Sep. 9, 2016.

[93] Q. Tu, F. Hase, T. Blumenstock, R. Kivi, P. Heikkinen, M. K. Sha, U. Raffalski, *et al.*, "Intercomparison of atmospheric CO_2 and CH_4 abundances on regional scales in boreal areas using Copernicus Atmosphere Monitoring Service (CAMS) analysis, COllaborative Carbon Column Observing Network (COCCON) spectrometers, and Sentinel-5 Precursor satellite observations", *Atmospheric Measurement Techniques*, vol. 13, no. 9, pp. 4751–4771, Sep. 9, 2020, Publisher: Copernicus GmbH. DOI: 10.5194/amt-13-4751-2020.

[94] N. Humpage, H. Boesch, F. Dietrich, and J. Chen, "Testing an automated enclosure system for a ground-based greenhouse gas remote sensing spectrometer; application to the validation of Sentinel-5 Precursor carbon monoxide and methane", presented at the Copernicus Sentinel-5 Precursor Validation Team Workshop, Frascati (Rome), Italy, Nov. 12, 2019. DOI: 10.13140/RG.2.2.18535.80808.

[95] N. Humpage, H. Boesch, W. Okello, F. Dietrich, J. Chen, M. Lunt, L. Feng, *et al.*, "Greenhouse gas column observations from a portable spectrometer in tropical Africa", Jun. 5, 2020. DOI: 10.13140/RG.2.2.14528.97280.

[96] N. Humpage, H. Boesch, W. Okello, F. Dietrich, J. Chen, M. Lunt, L. Feng, *et al.*, "Greenhouse gas column observations from a portable spectrometer in Uganda", Copernicus Meetings, EGU21-10156, Mar. 3, 2021, Conference Name: EGU21. DOI: 10.5194/egusphere-egu21-10156.

[97] T. S. Jones, J. E. Franklin, J. Chen, F. Dietrich, K. D. Hajny, J. C. Paetzold, A. Wenzel, *et al.*, "Assessing urban methane emissions using column-observing portable Fourier transform infrared (FTIR) spectrometers and a novel Bayesian inversion framework", *Atmospheric Chemistry and Physics*, vol. 21, no. 17, pp. 13 131–13 147, Sep. 6, 2021, Publisher: Copernicus GmbH. DOI: 10.5194/acp-21-13131-2021.

[98] J. Chen, F. Dietrich, J. Franklin, T. Jones, A. Butz, A. Luther, R. Kleinschek, *et al.*, "Mesoscale Column Network for Assessing GHG and NOx Emissions in Munich", in *Geophysical Research Abstracts*, vol. 20, 2018, EGU2018–10192–2.

[99] F. Dietrich, J. Chen, B. Reger, A. Forstmaier, X. Bi, A. Luther, M. Frey, *et al.*, "First fully-automated differential column network for measuring GHG emissions tested in Munich", presented at the EGU General Assembly 2019, Vienna: Copernicus Meetings, Apr. 12, 2019, EGU2019–13 327. DOI: 10.13140/RG.2.2.26867.17441.

[100] J. Chen, F. Dietrich, H. Maazallahi, D. Winkler, A. Forstmaier, M. E. G. Hofmann, H. Denier van der Gon, *et al.*, "Investigations of Methane Emissions from the Munich Oktoberfest 2018", presented at the EGU General Assembly 2019, Vienna: Copernicus Meetings, Apr. 8, 2019, EGU2019–15485–1.

[101] J. Chen, F. Dietrich, S. Lober, K. Krämer, G. Legget, H. Denier van der Gon, I. Velzeboer, *et al.*, "Methane Emission Source Attribution and Quantification for Munich Oktoberfest", in *EGU General Assembly Conference*, Mar. 9, 2020, EGU2020–18 919. DOI: 10.5194/egusphere-egu2020-18919.

[102] J. Chen, F. Dietrich, H. Maazallahi, A. Forstmaier, D. Winkler, M. E. G. Hofmann, H. Denier van der Gon, *et al.*, "Methane emissions from the Munich Oktoberfest", *Atmospheric Chemistry and Physics*, vol. 20, no. 6, pp. 3683–3696, Mar. 27, 2020, Publisher: Copernicus GmbH. DOI: 10.5194/acp-20-3683-2020.

[103] F. Dietrich, J. Chen, B. Voggenreiter, and X. Zhao, "Greenhouse Gas Emission Estimate Using a Fully-automated Permanent Sensor Network in Munich", in *EGU General Assembly Conference*, vol. 20, Mar. 9, 2020, EGU2020–19 237. DOI: 10.5194/egusphere-egu2020-19237.

[104] J. Chen, F. Dietrich, A. Wenzel, N. Nachtigall, T. Jones, and J. Franklin, "Permanent Urban Column Network for Carbon Emission Monitoring in Munich", presented at the American Geophysical (AGU) fall meeting, B 108-0024, Nov. 20, 2020.

[105] F. Dietrich, J. Chen, A. Wenzel, M. Rißmann, A. Forstmaier, F. Klappenbach, X. Zhao, *et al.*, "Urban emission estimates and validation of satellite-measured urban GHG concentration gradients using MUCCnet data (Munich Urban Carbon Column network)", presented at the IWGGMS-17, Jun. 17, 2021.

[106] F. Dietrich, J. Chen, A. Wenzel, F. Klappenbach, X. Zhao, A. Forstmaier, M. Altmann, *et al.*, "Permanent urban carbon observations provided by the Munich Urban Carbon Column network (MUCCnet)", presented at the Annual TCCON/COCCON virtual meeting, Jun. 9, 2021.

[107] F. Dietrich, J. Chen, A. Wenzel, A. Forstmaier, F. Klappenbach, X. Zhao, N. Nachtigall, *et al.*, "Urban methane emission estimate using measurements obtained by MUCCnet (Munich Urban Carbon Column network)", Copernicus Meetings, EGU21-12210, Mar. 3, 2021, Conference Name: EGU21. DOI: 10.5194/egusphere-egu21-12210.

[108] F. Dietrich, J. Chen, A. Shekhar, S. Lober, K. Krämer, G. Leggett, C. van der Veen, *et al.*, "Climate Impact Comparison of Electric and Gas-Powered End-User Appliances", *Earth's Future*, vol. 11, no. 2, e2022EF002877, 2023. DOI: 10.1029/2022EF002877.

[109] A. Forstmaier, J. Chen, F. Dietrich, J. Bettinelli, H. Maazallahi, C. Schneider, D. Winkler, *et al.*, "Quantification of methane emissions in Hamburg using a network of FTIR spectrometers and an inverse modeling approach", *Atmospheric Chemistry and Physics Discussions*, pp. 1–33, Nov. 18, 2022, Publisher: Copernicus GmbH. DOI: 10.5194/acp-2022-710.

[110] J. Chen, F. Dietrich, A. Forstmaier, J. Bettinelli, H. Maazallahi, C. Schneider, T. Röckmann, *et al.*, "Multi-scale measurements combined with inverse modeling for assessing methane emissions of Hamburg", Copernicus Meetings, EGU22-11548, Mar. 25, 2022, Conference Name: EGU22. DOI: 10.5194/egusphere-egu22-11548.

[111] I. Super, S. N. C. Dellaert, A. J. H. Visschedijk, and H. A. C. Denier van der Gon, "Uncertainty analysis of a European high-resolution emission inventory of CO_2 and CO to support inverse modelling and network design", *Atmospheric Chemistry and Physics*, vol. 20, no. 3, pp. 1795–1816, Feb. 14, 2020, Publisher: Copernicus GmbH. DOI: 10.5194/acp-20-1795-2020.

[112] A. Lewis and G. Knowles, "Image compression using the 2-D wavelet transform", *IEEE Transactions on Image Processing*, vol. 1, no. 2, pp. 244–250, Apr. 1992, Conference Name: IEEE Transactions on Image Processing. DOI: 10.1109/83.136601.

[113] B. Zanger, J. Chen, M. Sun, and F. Dietrich, "Recovery of sparse urban greenhouse gas emissions", *Geoscientific Model Development*, vol. 15, no. 20, pp. 7533–7556, Oct. 17, 2022, Publisher: Copernicus GmbH. DOI: 10.5194/gmd-15-7533-2022.

[114] M. Rißmann, J. Chen, G. Osterman, X. Zhao, F. Dietrich, M. Makowski, F. Hase, *et al.*, "Comparison of OCO-2 target observations to MUCCnet – is it possible to capture urban X_{CO2} gradients from space?", *Atmospheric Measurement Techniques*, vol. 15, no. 22, pp. 6605–6623, Nov. 17, 2022, Publisher: Copernicus GmbH. DOI: 10.5194/amt-15-6605-2022.

[115] A. Shekhar, J. Chen, J. C. Paetzold, F. Dietrich, X. Zhao, S. Bhattacharjee, V. Ruisinger, *et al.*, "Anthropogenic CO_2 emissions assessment of Nile Delta using X_{CO2} and SIF data from OCO-2 satellite", *Environmental Research Letters*, vol. 15, no. 9, p. 095 010, Sep. 2020, Publisher: IOP Publishing. DOI: 10.1088/1748-9326/ab9cfe.

[116] M. Crippa, E. Solazzo, G. Huang, D. Guizzardi, E. Koffi, M. Muntean, C. Schieberle, *et al.*, "High resolution temporal profiles in the Emissions Database for Global Atmospheric Research", *Scientific Data*, vol. 7, no. 1, p. 121, Apr. 17, 2020, Publisher: Nature Publishing Group. DOI: 10.1038/s41597-020-0462-2.

[117] T. Oda, S. Maksyutov, and R. J. Andres, "The Open-source Data Inventory for Anthropogenic CO_2, version 2016 (ODIAC2016): a global monthly fossil fuel CO_2 gridded emissions data product for tracer transport simulations and surface flux inversions", *Earth System Science Data*, vol. 10, no. 1, pp. 87–107, Jan. 18, 2018, Publisher: Copernicus GmbH. DOI: 10.5194/essd-10-87-2018.

[118] C. D. Keeling, "The concentration and isotopic abundances of atmospheric carbon dioxide in rural areas", *Geochimica et Cosmochimica Acta*, vol. 13, no. 4, pp. 322–334, Jan. 1, 1958. DOI: 10.1016/0016-7037(58)90033-4.

[119] SWM Infrastruktur GmbH und Co. KG, *Erdgasbeschaffenheit: Monatsdurchschnitt September 2019*, 2019.

[120] H. Bovensmann, M. Buchwitz, J. P. Burrows, M. Reuter, T. Krings, K. Gerilowski, O. Schneising, *et al.*, "A remote sensing technique for global monitoring of power plant CO_2 emissions from space and related applications", *Atmospheric Measurement Techniques*, vol. 3, no. 4, pp. 781–811, Jul. 2010. DOI: 10.5194/amt-3-781-2010.

[121] E. Atherton, D. Risk, C. Fougère, M. Lavoie, A. Marshall, J. Werring, J. P. Williams, *et al.*, "Mobile measurement of methane emissions from natural gas developments in northeastern British Columbia, Canada", *Atmospheric Chemistry and Physics*, vol. 17, no. 20, pp. 12 405–12 420, Oct. 2017. DOI: https://doi.org/10.5194/acp-17-12405-2017.

[122] R. Nassar, T. G. Hill, C. A. McLinden, D. Wunch, D. B. A. Jones, and D. Crisp, "Quantifying CO_2 Emissions From Individual Power Plants From Space", *Geophysical Research Letters*, vol. 44, no. 19, pp. 10, 045–10, 053, 2017. DOI: 10.1002/2017GL074702.

[123] C. Kiemle, G. Ehret, A. Amediek, A. Fix, M. Quatrevalet, and M. Wirth, "Potential of Spaceborne Lidar Measurements of Carbon Dioxide and Methane Emissions from Strong Point Sources", *Remote Sensing*, vol. 9, no. 11, p. 1137, Nov. 2017. DOI: 10.3390/rs9111137.

[124] S. Lober, F. Dietrich, and J. Chen, "Computational Fluid Dynamics Model to Simulate Methane Dispersion at Oktoberfest", *Earth and Space Science Open Archive [preprint]*, Feb. 16, 2021, Publisher: Earth and Space Science Open Archive Section: Atmospheric Sciences. DOI: 10.1002/essoar.10506185.1.

[125] P. A. Durbin, "On the k-3 stagnation point anomaly", *International Journal of Heat and Fluid Flow*, vol. 17, no. 1, pp. 89–90, Feb. 1, 1996. DOI: 10.1016/0142-727X(95)00073-Y.

[126] A. Wenzel, J. Chen, F. Dietrich, S. T. Thekkekara, D. Zollitsch, B. Voggenreiter, L. Setili, *et al.*, "Stand-alone low-cost sensor network in the inner city of Munich for modeling urban air pollutants", Copernicus Meetings, EGU21-15182, Mar. 3, 2021, Conference Name: EGU21. DOI: 10.5194/egusphere-egu21-15182.

[127] D. Zollitsch, J. Chen, F. Dietrich, B. Voggenreiter, L. Setili, and M. Wenig, "Low-Cost Air Quality Sensor Network in Munich", in *EGU General Assembly Conference*, Mar. 9, 2020. DOI: 10.5194/egusphere-egu2020-19276.

[128] L. Setili, "Konzeptionierung und Aufbau eines NOx Messgerätes auf Basis eines elektrochemischen Sensors", [unpublished thesis], Diploma thesis, Technical University of Munich - Environmental Sensing and Modeling, Munich, Germany, Apr. 30, 2019.

[129] D. Zollitsch, "Development of an economical, portable and low-power NOx sensing device", [unpublished thesis], Master's thesis, Technical University of Munich - Environmental Sensing and Modeling, Munich, Germany, Aug. 13, 2019.

[130] A. Bigi, M. Mueller, S. K. Grange, G. Ghermandi, and C. Hueglin, "Performance of NO, NO_2 low cost sensors and three calibration approaches within a real world application", *Atmospheric Measurement Techniques*, vol. 11, no. 6, pp. 3717–3735, Jun. 2018. DOI: 10.5194/amt-11-3717-2018.

[131] D. Wunch, P. O. Wennberg, G. Osterman, B. Fisher, B. Naylor, C. M. Roehl, C. O'Dell, *et al.*, "Comparisons of the Orbiting Carbon Observatory-2 (OCO-2) X_{CO2} measurements with TCCON", *Atmospheric Measurement Techniques*, vol. 10, no. 6, pp. 2209–2238, Jun. 13, 2017, Publisher: Copernicus GmbH. DOI: 10.5194/amt-10-2209-2017.

[132] A. Luther, J. Kostinek, R. Kleinschek, S. Defratyka, M. Stanisavljević, A. Forstmaier, A. Dandocsi, *et al.*, "Observational constraints on methane emissions from Polish coal mines using a ground-based remote sensing network", *Atmospheric Chemistry and Physics*, vol. 22, no. 9, pp. 5859–5876, May 5, 2022, Publisher: Copernicus GmbH. DOI: 10.5194/acp-22-5859-2022.

[133] J. Turnbull, P. DeCola, K. Mueller, F. Vogel, A. Agusti-Panareda, D. Ahn, S. Baidar, *et al.*, "IG3IS Urban Greenhouse Gas Emission Observation and Monitoring Best Research Practices", *WMO GAW Report- No. 275*, 2022.

Publications

Journal publications

[J-1] J. Chen, F. Dietrich, H. Maazallahi, A. Forstmaier, D. Winkler, M. E. G. Hofmann, H. Denier van der Gon, *et al.*, "Methane emissions from the Munich Oktoberfest", *Atmospheric Chemistry and Physics*, vol. 20, no. 6, pp. 3683–3696, Mar. 27, 2020, Publisher: Copernicus GmbH. DOI: 10.5194/acp-20-3683-2020.

[J-2] F. Dietrich, J. Chen, A. Shekhar, S. Lober, K. Krämer, G. Leggett, C. van der Veen, *et al.*, "Climate Impact Comparison of Electric and Gas-Powered End-User Appliances", *Earth's Future*, vol. 11, no. 2, e2022EF002877, 2023. DOI: 10.1029/2022EF002877.

[J-3] F. Dietrich, J. Chen, B. Voggenreiter, P. Aigner, N. Nachtigall, and B. Reger, "MUCCnet: Munich Urban Carbon Column network", *Atmospheric Measurement Techniques*, vol. 14, no. 2, pp. 1111–1126, Feb. 11, 2021, Publisher: Copernicus GmbH. DOI: 10.5194/amt-14-1111-2021.

[J-4] G. Kuhlmann, K. L. Chan, S. Donner, Y. Zhu, M. Schwaerzel, S. Dörner, J. Chen, *et al.*, "Mapping the spatial distribution of NO_2 with in situ and remote sensing instruments during the Munich NO_2 imaging campaign", *Atmospheric Measurement Techniques*, vol. 15, no. 6, pp. 1609–1629, Mar. 21, 2022, Publisher: Copernicus GmbH. DOI: 10.5194/amt-15-1609-2022.

[J-5] A. Luther, R. Kleinschek, L. Scheidweiler, S. Defratyka, M. Stanisavljevic, A. Forstmaier, A. Dandocsi, *et al.*, "Quantifying CH_4 emissions from hard coal mines using mobile sun-viewing Fourier transform spectrometry", *Atmospheric Measurement Techniques*, vol. 12, no. 10, pp. 5217–5230, Oct. 1, 2019, Publisher: Copernicus GmbH. DOI: 10.5194/amt-12-5217-2019.

[J-6] A. Luther, J. Kostinek, R. Kleinschek, S. Defratyka, M. Stanisavljević, A. Forstmaier, A. Dandocsi, *et al.*, "Observational constraints on methane emissions from Polish coal mines using a ground-based remote sensing network", *Atmospheric Chemistry and Physics*, vol. 22, no. 9, pp. 5859–5876, May 5, 2022, Publisher: Copernicus GmbH. DOI: 10.5194/acp-22-5859-2022.

[J-7] M. Rißmann, J. Chen, G. Osterman, X. Zhao, F. Dietrich, M. Makowski, F. Hase, *et al.*, "Comparison of OCO-2 target observations to MUCCnet – is it possible to capture urban X_{CO2} gradients from space?", *Atmospheric Measurement Techniques*, vol. 15, no. 22, pp. 6605–6623, Nov. 17, 2022, Publisher: Copernicus GmbH. DOI: 10.5194/amt-15-6605-2022.

[J-8] A. Shekhar, J. Chen, J. C. Paetzold, F. Dietrich, X. Zhao, S. Bhattacharjee, V. Ruisinger, *et al.*, "Anthropogenic CO_2 emissions assessment of Nile Delta using X_{CO2} and SIF data from OCO-2 satellite", *Environmental Research Letters*, vol. 15, no. 9, p. 095 010, Sep. 2020, Publisher: IOP Publishing. DOI: 10.1088/1748-9326/ab9cfe.

[J-9] Q. Tu, F. Hase, T. Blumenstock, R. Kivi, P. Heikkinen, M. K. Sha, U. Raffalski, *et al.*, "Intercomparison of atmospheric CO_2 and CH_4 abundances on regional scales in boreal areas using Copernicus Atmosphere Monitoring Service (CAMS) analysis, COllaborative Carbon Column Observing Network (COCCON) spectrometers, and Sentinel-5 Precursor satellite observations", *Atmospheric Measurement Techniques*, vol. 13, no. 9, pp. 4751–4771, Sep. 9, 2020, Publisher: Copernicus GmbH. DOI: 10.5194/amt-13-4751-2020.

[J-10] J. Turnbull, P. DeCola, K. Mueller, F. Vogel, A. Agusti-Panareda, D. Ahn, S. Baidar, *et al.*, "IG3IS Urban Greenhouse Gas Emission Observation and Monitoring Best Research Practices", *WMO GAW Report- No. 275*, 2022.

[J-11] B. Zanger, J. Chen, M. Sun, and F. Dietrich, "Recovery of sparse urban greenhouse gas emissions", *Geoscientific Model Development*, vol. 15, no. 20, pp. 7533–7556, Oct. 17, 2022, Publisher: Copernicus GmbH. DOI: 10.5194/gmd-15-7533-2022.

[J-12] Y. Zhu, J. Chen, X. Bi, G. Kuhlmann, K. L. Chan, F. Dietrich, D. Brunner, *et al.*, "Spatial and temporal representativeness of point measurements for nitrogen dioxide pollution levels in cities", *Atmospheric Chemistry and Physics*, vol. 20, no. 21, pp. 13 241–13 251, Nov. 10, 2020, Publisher: Copernicus GmbH. DOI: 10.5194/acp-20-13241-2020.

Preprints

[P-1] A. Forstmaier, J. Chen, F. Dietrich, J. Bettinelli, H. Maazallahi, C. Schneider, D. Winkler, *et al.*, "Quantification of methane emissions in Hamburg using a network of FTIR spectrometers and an inverse modeling approach", *Atmospheric Chemistry and Physics Discussions*, pp. 1–33, Nov. 18, 2022, Publisher: Copernicus GmbH. DOI: 10.5194/acp-2022-710.

[P-2] S. Lober, F. Dietrich, and J. Chen, "Computational Fluid Dynamics Model to Simulate Methane Dispersion at Oktoberfest", *Earth and Space Science Open Archive [preprint]*, Feb. 16, 2021, Publisher: Earth and Space Science Open Archive Section: Atmospheric Sciences. DOI: 10.1002/essoar.10506185.1.

[P-3] X. Zhao, J. Chen, J. Marschall, M. Gałkowski, S. Hachinger, F. Dietrich, A. Shekhar, *et al.*, "Understanding greenhouse gas (GHG) column concentrations in Munich using WRF", *Atmospheric Chemistry and Physics Discussions*, pp. 1–30, May 17, 2022, Publisher: Copernicus GmbH. DOI: 10.5194/acp-2022-281.

Conference publications

[C-1] J. Chen and F. Dietrich, "Überwachung städtischer Schadstoff- und Treibhausgasemissionen mittels differentieller Säulenmessung", presented at the 53. Messtechnisches Kolloquium, Vienna, Austria, May 9, 2018.

[C-2] J. Chen and F. Dietrich, "Differential column network in Munich for greenhouse gas monitoring", presented at the 1st ICOS workshop on strategies to monitor greenhouse gases in urban environments, Helsinki/Hyytiälä, Finland, Jul. 3, 2019.

[C-3] J. Chen and F. Dietrich, "Erste Münchner Treibhausgas-Emissionszahlen unter Verwendung des differentiellen Säulennetzwerks", presented at the 54. Messtechnisches Kolloquium, Lübeck, May 28, 2019.

[C-4] J. Chen and F. Dietrich, "Methane investigations in Munich", presented at the United Nations CCAC Methane Science Studies - Urban Measurements Workshop, Paris, Nov. 15, 2019.

[C-5] J. Chen and F. Dietrich, "Munich EM-27 observations", presented at the OCO-2 science team meeting, Boulder, Colorado, Oct. 24, 2019.

[C-6] J. Chen and F. Dietrich, "Ground-based Remote Sensing", presented at the World Metereological Organization IG3IS workshop "Towards an International standard for Urban GHG Monitoring and assessment", Jun. 4, 2020.

[C-7] J. Chen, F. Dietrich, X. Bi, A. Forstmaier, and L. Setili, "Differential Column Sensor Network in Munich and Low-Cost NOx Sensor Development", presented at the Mid-term and 1st International Networking Workshop of the SmartAQnet Project, Munich, Germany, Dec. 4, 2019, p. 18.

[C-8] J. Chen, F. Dietrich, A. Forstmaier, J. Bettinelli, H. Maazallahi, C. Schneider, T. Röckmann, *et al.*, "Multi-scale measurements combined with inverse modeling for assessing methane emissions of Hamburg", Copernicus Meetings, EGU22-11548, Mar. 25, 2022, Conference Name: EGU22. DOI: 10.5194/egusphere-egu22-11548.

[C-9] J. Chen, F. Dietrich, J. Franklin, T. Jones, A. Butz, A. Luther, R. Kleinschek, *et al.*, "Mesoscale Column Network for Assessing GHG and NOx Emissions in Munich", presented at the EGU General Assembly 2018, Vienna, Austria: Copernicus Meetings, Apr. 18, 2018, EGU2018–10192–2.

[C-10] J. Chen, F. Dietrich, J. Franklin, T. Jones, and S. Wofsy, "Here comes the sun: A new carbon detective story", presented at the Symposium Celebration of Science and Times for Steven C. Wofsy, Harvard, Cambridge, Massachusetts, Jun. 23, 2018.

[C-11] J. Chen, F. Dietrich, M. Kiel, and G. Osterman, "Satellite validation and urban emission assessment using the Munich permanent urban GHG column observing network", presented at the NASA OCO-3/ OCO-2 validation group meeting, Oct. 6, 2020.

[C-12] J. Chen, F. Dietrich, L. Lan, X. Bi, A. Forstmaier, and L. Setili, "Greenhouse Gas Monitoring in Munich and Development of CO2 and NOx Sensors", presented at the German-Sino Symposium "Development of New Monitoring Strategies for the Investigation of Acute Air Pollution and Bioaerosol Episodes and Reducing Their Impacts on Human Health", Chengdu, China, Nov. 11, 2018.

[C-13] J. Chen, F. Dietrich, S. Lober, K. Krämer, G. Legget, H. Denier van der Gon, I. Velzeboer, *et al.*, "Methane Emission Source Attribution and Quantification for Munich Oktoberfest", in *EGU General Assembly Conference*, Mar. 9, 2020, EGU2020–18 919. DOI: 10.5194/egusphere-egu2020-18919.

[C-14] J. Chen, F. Dietrich, H. Maazallahi, D. Winkler, A. Forstmaier, M. E. G. Hofmann, H. Denier van der Gon, *et al.*, "Investigations of Methane Emissions from the Munich Oktoberfest 2018", presented at the EGU General Assembly 2019, Vienna: Copernicus Meetings, Apr. 8, 2019, EGU2019–15485–1.

[C-15] J. Chen, F. Dietrich, A. Wenzel, N. Nachtigall, T. Jones, and J. Franklin, "Permanent Urban Column Network for Carbon Emission Monitoring in Munich", presented at the American Geophysical (AGU) fall meeting, B 108-0024, Nov. 20, 2020.

[C-16] J. Chen, A. Wenzel, F. Dietrich, P. Aigner, X. Zhao, J. Gensheimer, A. Luther, *et al.*, "Integrated Measurements and Modeling Approach for Greenhouse Gas Emission Monitoring", presented at the ICOS Science Conference 2022, 2022.

[C-17] F. Dietrich and J. Chen, "Portable Automated Enclosure for a Spectrometer Measuring Greenhouse Gases", presented at the EGU General Assembly 2018, Vienna, Austria: Copernicus Meetings, Apr. 9, 2018, EGU2018–16281–1. DOI: 10.13140/RG.2.2.11591.14248.

[C-18] F. Dietrich, J. Chen, M. Kiel, and G. Osterman, "Fully Automated Permanent Sensor Network in Munich for GHG Satellite Validation", presented at the IWGGMS16, Jun. 4, 2020.

[C-19] F. Dietrich, J. Chen, B. Reger, A. Forstmaier, X. Bi, A. Luther, M. Frey, *et al.*, "First fully-automated differential column network for measuring GHG emissions tested in Munich", presented at the EGU General Assembly 2019, Vienna: Copernicus Meetings, Apr. 12, 2019, EGU2019–13 327. DOI: 10.13140/RG.2.2.26867.17441.

[C-20] F. Dietrich, J. Chen, B. Voggenreiter, and X. Zhao, "Greenhouse Gas Emission Estimate Using a Fully-automated Permanent Sensor Network in Munich", in *EGU General Assembly Conference*, vol. 20, Mar. 9, 2020, EGU2020–19 237. DOI: 10.5194/egusphere-egu2020-19237.

[C-21] F. Dietrich, J. Chen, A. Wenzel, A. Forstmaier, F. Klappenbach, X. Zhao, N. Nachtigall, *et al.*, "Urban methane emission estimate using measurements obtained by MUCCnet (Munich Urban Carbon Column network)", Copernicus Meetings, EGU21-12210, Mar. 3, 2021, Conference Name: EGU21. DOI: 10.5194/egusphere-egu21-12210.

[C-22] F. Dietrich, J. Chen, A. Wenzel, F. Klappenbach, X. Zhao, A. Forstmaier, M. Altmann, *et al.*, "Permanent urban carbon observations provided by the Munich Urban Carbon Column network (MUCCnet)", presented at the Annual TCCON/COCCON virtual meeting, Jun. 9, 2021.

[C-23] F. Dietrich, J. Chen, A. Wenzel, M. Rißmann, A. Forstmaier, F. Klappenbach, X. Zhao, *et al.*, "Urban emission estimates and validation of satellite-measured urban GHG concentration gradients using MUCCnet data (Munich Urban Carbon Column network)", presented at the IWGGMS-17, Jun. 17, 2021.

[C-24] N. Humpage, H. Boesch, F. Dietrich, and J. Chen, "Testing an automated enclosure system for a ground-based greenhouse gas remote sensing spectrometer", presented at the NCEO Annual Conference 2019, Nottingham, UK, Sep. 6, 2019. DOI: 10.13140/RG.2.2.18129.07521.

[C-25] N. Humpage, H. Boesch, F. Dietrich, and J. Chen, "Testing an automated enclosure system for a ground-based greenhouse gas remote sensing spectrometer; application to the validation of Sentinel-5 Precursor carbon monoxide and methane", presented at the Copernicus Sentinel-5 Precursor Validation Team Workshop, Frascati (Rome), Italy, Nov. 12, 2019. DOI: 10.13140/RG.2.2.18535.80808.

[C-26] N. Humpage, H. Boesch, W. Okello, F. Dietrich, J. Chen, M. Lunt, L. Feng, *et al.*, "Greenhouse gas column observations from a portable spectrometer in tropical Africa", Jun. 5, 2020. DOI: 10.13140/RG.2.2.14528.97280.

[C-27] N. Humpage, H. Boesch, W. Okello, F. Dietrich, J. Chen, M. Lunt, L. Feng, *et al.*, "Greenhouse gas column observations from a portable spectrometer in Uganda", Copernicus Meetings, EGU21-10156, Mar. 3, 2021, Conference Name: EGU21. DOI: 10.5194/egusphere-egu21-10156.

[C-28] N. Humpage, H. Boesch, W. Okello, F. Dietrich, J. Chen, M. Lunt, L. Feng, *et al.*, "Greenhouse gas column observations from an EM27/SUN portable spectrometer in Uganda", presented at the IWGGMS-17, Jun. 17, 2021.

[C-29] T. Jones, J. Franklin, J. Chen, C. Gately, F. Diertrich, and S. C. Wofsy, "Estimating Methane Emissions from Cities using Portable Ground-based Total Column Spectrometers", *AGU Fall Meeting Abstracts*, vol. 52, Dec. 14, 2018.

[C-30] F. Klappenbach, J. Chen, A. Wenzel, A. Forstmaier, F. Dietrich, X. Zhao, T. Jones, *et al.*, "Methane emission estimate using ground based remote sensing in complex terrain", Copernicus Meetings, EGU21-15406, Mar. 3, 2021, Conference Name: EGU21. DOI: 10.5194/egusphere-egu21-15406.

[C-31] F. Klappenbach, J. Chen, A. Wenzel, F. Dietrich, A. Forstermeier, X. Zhao, T. Jones, *et al.*, "Novel methane emission estimation method for ground based remote sensing networks", Copernicus Meetings, EGU22-10604, Mar. 25, 2022, Conference Name: EGU22. DOI: 10.5194/egusphere-egu22-10604.

[C-32] A. Luther, R. Kleinschek, J. Kostinek, M. Stanisavljevic, A. Dandocsi, A. Forstmaier, S. Defratyka, *et al.*, "Estimating coal mine methane emissions using ground-based FTIR spectrometry, WRF driven Lagrangian dispersion modelling, and a regularized inversion approach", Copernicus Meetings, EGU21-12751, Mar. 3, 2021, Conference Name: EGU21. DOI: 10.5194/egusphere-egu21-12751.

[C-33] A. Luther, J. Kostinek, R. Kleinschek, S. Defratyka, M. Stanisavljevic, A. Forstmaier, A. Dandocsi, *et al.*, "Quantifying CH4 emissions from coal-mine ventilation in the Upper Silesian Coal Basin (Poland) using COCCON spectrometers", Copernicus Meetings, EGU22-6488, Mar. 25, 2022, Conference Name: EGU22. DOI: 10.5194/egusphere-egu22-6488.

[C-34] A. Luther, N. Wildmann, M. Stanisavljević, J. Necki, J. Chen, F. Dietrich, A. Butz, *et al.*, "Towards verifying CH4 emissions from hard coal mines using mobile sun-viewing Fourier transform spectrometry", presented at the 8th International Symposium on Non-CO2 Greenhouse Gases (NCGG8), Jun. 12, 2019.

[C-35] B. Matthews, A. Watzinger, J. Chen, H. Schume, H. Sanden, F. Dietrich, and S. Leitner, "Introducing the Vienna Urban Carbon Laboratory (VUCL)", Copernicus Meetings, EGU21-12964, Mar. 3, 2021, Conference Name: EGU21. DOI: 10.5194/egusphere-egu21-12964.

[C-36] M. K. Sha, B. Langerock, M. Kiel, D. Dubravica, F. Hase, T. Borsdorff, A. Lorente, *et al.*, "Using the COllaborative Carbon Column Observing Network for validating space borne GHG sensors", presented at the IWGGMS-17, Jun. 17, 2021.

[C-37] F. Vogel, S. Ars, D. Wunch, J. Lavoie, R. C. Cruz, H. Maazallahi, T. Roeckmann, *et al.*, "Ground-based mobile measurements to track urban methane emissions from natural gas in twelve cities across eight countries", presented at the ICOS Science Conference 2022, 2022.

[C-38] M. Wenig, Y. Zhu, S. Ye, K. L. Chan, J. Chen, F. Dietrich, X. Bi, *et al.*, "Measuring Spatial and Temporal Patterns of Urban NO2 Concentrations by combining mobile and stationary DOAS instruments", Copernicus Meetings, EGU2020-7523, Mar. 9, 2020, Conference Name: EGU2020. DOI: 10.5194/egusphere-egu2020-7523.

[C-39] A. Wenzel, J. Chen, F. Dietrich, S. T. Thekkekara, D. Zollitsch, B. Voggenreiter, L. Setili, *et al.*, "Stand-alone low-cost sensor network in the inner city of Munich for modeling urban air pollutants", Copernicus Meetings, EGU21-15182, Mar. 3, 2021, Conference Name: EGU21. DOI: 10.5194/egusphere-egu21-15182.

[C-40] R. Winkler, I. Urbanova, V. Onderka, F. Dietrich, J. Chen, H. Maazallahi, M. Hofmann, *et al.*, "Gas leak detection and methane source attribution with a portable Battery-powered Cavity Ring-Down Spectrometer", presented at the Industrial Methane Measurement Conference 2019, Rotterdam, the Netherlands, May 22, 2019.

[C-41] X. Zhao, J. Chen, J. Marshall, M. Galkowski, C. Gerbig, S. Hachinger, F. Dietrich, *et al.*, "A semi-operational near-real-time Modelling Infrastructure for assessing GHG emissions in Munich using WRF-GHG", Copernicus Meetings, EGU2020-13164, Mar. 9, 2020, Conference Name: EGU2020. DOI: 10.5194/egusphere-egu2020-13164.

[C-42] X. Zhao, J. Chen, J. Marshall, M. Galkowski, C. Gerbig, S. Hachinger, J. Gensheimer, *et al.*, "Quantifying the impact of urban greenhouse gas emissions for Munich during the COVID-19 pandemic using WRF V3.9.1.1", Copernicus Meetings, EGU21-13431, Mar. 3, 2021, Conference Name: EGU21. DOI: 10.5194/egusphere-egu21-13431.

[C-43] D. Zollitsch, J. Chen, F. Dietrich, B. Voggenreiter, L. Setili, and M. Wenig, "Low-Cost Air Quality Sensor Network in Munich", in *EGU General Assembly Conference*, Mar. 9, 2020. DOI: 10.5194/egusphere-egu2020-19276.

Supervised and co-supervised theses

[T-1] M. Altmann, "Bayesian Inverse Modeling of Greenhouse Gas Emissions in Munich", [unpublished thesis], Master's thesis, Technical University of Munich - Environmental Sensing and Modeling, Munich, Germany, Apr. 30, 2020.

[T-2] N. Hars, "Optimizing a Python software to fully automate measurements in the Munich permanent urban greenhouse gas column observing network", [unpublished thesis], Bachelor's thesis, Technical University of Munich - Environmental Sensing and Modeling, Munich, Germany, Mar. 1, 2021.

[T-3] K. Krämer, "Big Data Analysis of Methane Emissions from the Oktoberfest 2019", [unpublished thesis], Master's thesis, Technical University of Munich - Environmental Sensing and Modeling, Munich, Germany, Sep. 23, 2020.

[T-4] S. Lober, "Methane Dispersion at the Oktoberfest Using CFD Simulations", [unpublished thesis], Master's thesis, Technical University of Munich - Environmental Sensing and Modeling, Munich, Germany, Mar. 13, 2020.

[T-5] D. Lu, "Automatic data analysis to determine greenhouse gas emissions in Munich", [unpublished thesis], Master's thesis, Technical University of Munich - Environmental Sensing and Modeling, Munich, Germany, Jan. 15, 2020.

[T-6] J. W. Maduawan, "Analysis of Greenhouse gas ratios from an urban column network in Munich", [unpublished thesis], Master's thesis, Technical University of Munich - Environmental Sensing and Modeling, Munich, Germany, Jun. 23, 2021.

[T-7] E. Miraglia, "Coupling of a UV/VIS spectrometer to a Fourier Transform Infrared Spectrometer for O3 and NO2 retrieval", [unpublished thesis], Master's thesis, Technical University of Munich - Environmental Sensing and Modeling, Munich, Germany, 2018.

[T-8] N. Nachtigall, "Development of a Data Modeling Framework for Greenhouse Gas Emission Quantification Based on a Novel Atmospheric Dataset", [unpublished thesis], Master's thesis, Technical University of Munich - Environmental Sensing and Modeling, Munich, Germany, Oct. 19, 2020.

[T-9] E. Özbas, "Building A Toxic Gas Measurement Sensor Circuit", [unpublished thesis], Bachelor's thesis, Technical University of Munich - Environmental Sensing and Modeling, Munich, Germany, Oct. 22, 2018.

[T-10] S. Pellegrino, "Web Scraping", [unpublished thesis], Engineering practice report, Technical University of Munich - Environmental Sensing and Modeling, Munich, Germany, Nov. 3, 2017.

[T-11] S. Pellegrino, "Measurement of Illuminance for Cloud Information", [unpublished thesis], Bachelor's thesis, Technical University of Munich - Environmental Sensing and Modeling, Munich, Germany, Jan. 24, 2018.

[T-12] B. Reger, "Automation of a protection housing for a spectrometer (PLC programming)", [unpublished thesis], Research internship report, Technical University of Munich - Environmental Sensing and Modeling, Munich, Germany, Nov. 9, 2018.

[T-13] M. Rißmann, "Development of a data visualization website for the Munich Urban Carbon Column Network", [unpublished thesis], Research internship report, Technical University of Munich - Environmental Sensing and Modeling, Munich, Germany, Mar. 1, 2021.

[T-14] M. Rißmann, "Validation and Application of Satellite Measurements of Atmospheric CO2", [unpublished thesis], Master's thesis, Technical University of Munich - Environmental Sensing and Modeling, Munich, Germany, Oct. 13, 2021.

[T-15] L. Setili, "Konzeptionierung und Aufbau eines NOx Messgerätes auf Basis eines elektrochemischen Sensors", [unpublished thesis], Diploma thesis, Technical University of Munich - Environmental Sensing and Modeling, Munich, Germany, Apr. 30, 2019.

[T-16] X. Z. Song, "Meteorological Data Analysis", [unpublished thesis], Master's thesis, Technical University of Munich - Environmental Sensing and Modeling, Munich, Germany, Apr. 1, 2021.

[T-17] H. Sun, "Further development of a Python software to fully automate a measurement system", [unpublished thesis], Master's thesis, Technical University of Munich - Environmental Sensing and Modeling, Munich, Germany, Dec. 5, 2019.

[T-18] M. Sun, "Compressive Sensing-based Greenhouse Gas Emission Estimate using Sensor Network in Munich", [unpublished thesis], Master's thesis, Technical University of Munich - Environmental Sensing and Modeling, Munich, Germany, Jun. 15, 2020.

[T-19] B. Voggenreiter, "Development of a camera-based sensor system for detecting solar radiation", [unpublished thesis], Master's thesis, Technical University of Munich - Environmental Sensing and Modeling, Munich, Germany, Sep. 27, 2019.

[T-20] A. Wenzel, “Implementation of UV/VIS spectrometer into the existing enclosure of an FTIR spectrometer”, [unpublished thesis], Research internship report, Technical University of Munich - Environmental Sensing and Modeling, Munich, Germany, Sep. 23, 2018.

[T-21] D. Winkler, “Big Data Analysis to Investigate Methane Sources at Oktoberfest”, [unpublished thesis], Bachelor’s thesis, Technical University of Munich - Environmental Sensing and Modeling, Munich, Germany, Jan. 11, 2019.

[T-22] B. Zanger, “Development of Inversion Models based on Sparse Estimation Methods”, [unpublished thesis], Master’s thesis, Technical University of Munich - Environmental Sensing and Modeling, Munich, Germany, Jan. 28, 2022.

[T-23] D. Zollitsch, “Development of an economical, portable and low-power NOx sensing device”, [unpublished thesis], Master’s thesis, Technical University of Munich - Environmental Sensing and Modeling, Munich, Germany, Aug. 13, 2019.